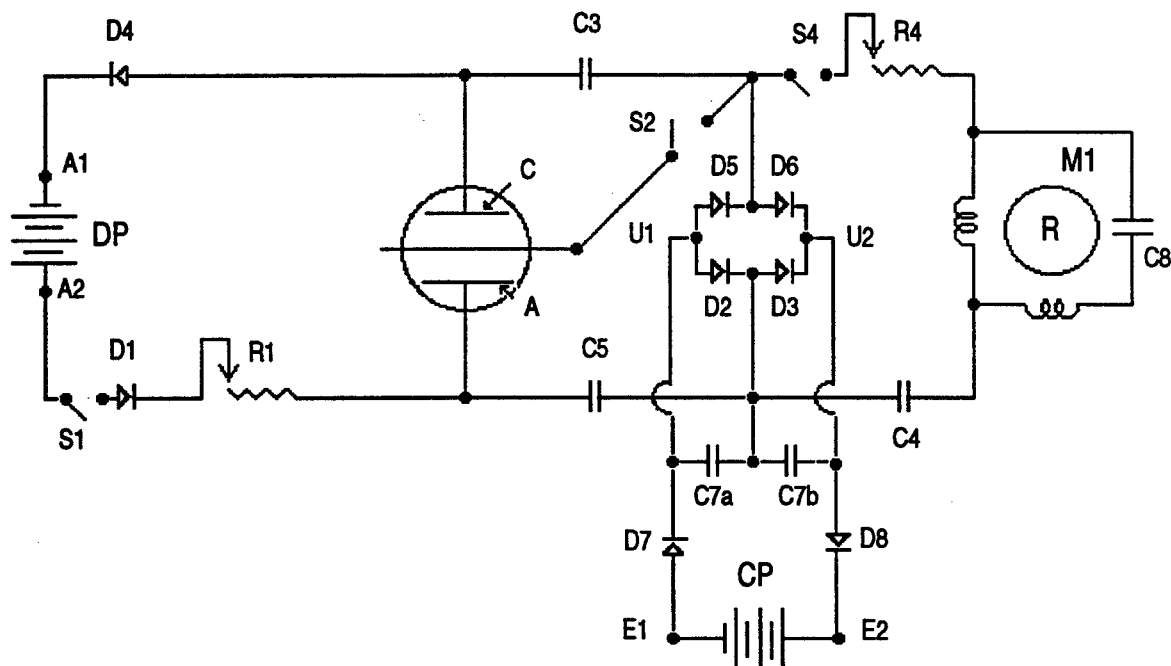




<p>(51) International Patent Classification ⁵ : H02M 7/48, H03K 3/04 H02P 7/26</p>	<p>A1</p>	<p>(11) International Publication Number: WO 94/09560 (43) International Publication Date: 28 April 1994 (28.04.94)</p>
<p>(21) International Application Number: PCT/CA93/00430 (22) International Filing Date: 13 October 1993 (13.10.93) (30) Priority data: 07/961,531 15 October 1992 (15.10.92) US 08/054,111 15 April 1993 (15.04.93) US (60) Parent Application or Grant (63) Related by Continuation US 08/054,111 (CIP) Filed on 15 April 1993 (15.04.93) (71)(72) Applicants and Inventors: CORREA, Paulo, N. [CA/CA]; CORREA, Alexandra, N. [CA/CA]; 42 Rockview Gardens, Concord, Ontario L4K 2J6 (CA).</p>	<p>(74) Agent: PARSONS, Richard, A., R.; Ridout & Maybee, Suite 2300, Richmond-Adelaide Centre, 101 Richmond Street West, Toronto, Ontario M5H 2J7 (CA). (81) Designated States: AT, AU, BB, BG, BR, BY, CA, CH, CZ, DE, DK, ES, FI, GB, HU, JP, KP, KR, KZ, LK, LU, MG, MN, MW, NL, NO, NZ, PL, PT, RO, RU, SD, SE, SK, UA, US, VN, European patent (AT, BE, CH, DE, DK, ES, FR, GB, GR, IE, IT, LU, MC, NL, PT, SE), OAPI patent (BF, BJ, CF, CG, CI, CM, GA, GN, ML, MR, NE, SN, TD, TG). Published <i>With international search report.</i></p>	

(54) Title: ENERGY CONVERSION SYSTEM



(57) Abstract

An energy conversion device includes a discharge tube which is operated in a pulsed abnormal glow discharge or interrupted vacuum arc discharge regime in a double ported circuit. A direct current source (DP) connected to an input port provides electrical energy to initiate emission pulses, and a current sink in the form of an electrical energy storage or utilization device (M1) connected to the output port captures at least a substantial proportion of energy released by collapse of the emission pulses.

FOR THE PURPOSES OF INFORMATION ONLY

Codes used to identify States party to the PCT on the front pages of pamphlets publishing international applications under the PCT.

AT	Austria	FR	France	MR	Mauritania
AU	Australia	GA	Gabon	MW	Malawi
BB	Barbados	GB	United Kingdom	NE	Niger
BE	Belgium	GN	Guinea	NL	Netherlands
BF	Burkina Faso	GR	Greece	NO	Norway
BG	Bulgaria	HU	Hungary	NZ	New Zealand
BJ	Benin	IE	Ireland	PL	Poland
BR	Brazil	IT	Italy	PT	Portugal
BY	Belarus	JP	Japan	RO	Romania
CA	Canada	KP	Democratic People's Republic of Korea	RU	Russian Federation
CF	Central African Republic	KR	Republic of Korea	SD	Sudan
CG	Congo	KZ	Kazakhstan	SE	Sweden
CH	Switzerland	LI	Liechtenstein	SI	Slovenia
CI	Côte d'Ivoire	LK	Sri Lanka	SK	Slovak Republic
CM	Cameroon	LU	Luxembourg	SN	Senegal
CN	China	LV	Latvia	TD	Chad
CS	Czechoslovakia	MC	Monaco	TG	Togo
CZ	Czech Republic	MG	Madagascar	UA	Ukraine
DE	Germany	ML	Mali	US	United States of America
DK	Denmark	MN	Mongolia	UZ	Uzbekistan
ES	Spain			VN	Viet Nam
FI	Finland				

- 1 -

ENERGY CONVERSION SYSTEM

This invention relates to energy conversion circuits utilizing discharge tubes operating in the pulsed abnormal glow discharge (PAGD) or vacuum arc discharge (VAD) regimes.

REVIEW OF THE ART

As the current passed through a gas discharge tube is increased beyond the levels at which normal glow discharge takes place, such normal gas discharge being characterized by a negative resistance characteristic leading to decreasing potential between the cathode and anode electrodes of the tube, a region of abnormal glow discharge is entered in which the negative resistance characteristic changes to a positive resistance characteristic leading to increasing potential between the electrodes. Typically this increased potential rapidly leads to breakdown into vacuum arc discharge between the electrodes, again characterized by a negative resistance characteristic. Accordingly, gas discharge tubes have been operated in the normal glow discharge or vacuum arc regimes in which stable operation can be achieved by adequate ballasting of the tube, the former regime being suitable for low current applications and the latter for high current. It is possible to utilize a normal glow discharge tube in a low frequency oscillator circuit by placing capacitance in parallel with the tube and in series with the ballast because such a tube is characterized by a comparatively high striking potential at which discharge is initiated, and a lower but still high extinction potential at which discharge ceases. Operation in such a mode with vacuum arc devices is difficult because, in order to turn off the device effectively, the arc must be extinguished or otherwise interrupted or diverted for long enough to disperse the intense ionization formed in its path.

- 2 -

Devices operating in the vacuum arc regime have other problems, particularly in terms of ensuring adequate electrode life. A further limitation of such devices is that the great difficulty in turning them off, except by
5 terminating current flow through the device for a finite period, limits their usefulness as control devices to rectification, current turn-on and low frequency alternating current applications.

The only prior art of which we are aware which
10 successfully exploits the abnormal glow discharge regime is the process described in U.S. Patent No. 3,471,316 (Manuel) issued October 7, 1969, which we understand is commercially utilized in forming organic coatings on metal cans. It
15 relies on the application of externally generated current pulses to force a discharge tube temporarily into the abnormal glow discharge region, the pulses being sufficiently short that no vacuum arc is established. There is no disclosure of any endogenous pulsed abnormal glow discharge, the apparatus is dependent upon an external pulse generator
20 to operate, and its utility is completely different from the present invention because it is a single ported device so far as electrical energy is concerned.

We are also aware that the use of vacuum arc discharge tubes has been proposed for the control of
25 inverters, as exemplified by U.S. Patent No. 4,194,239 (Jayaram et al), which discloses the use of atmospheric or vacuum arc discharge tubes in which the discharge is steered magnetically between multiple electrodes to provide a commutating effect. Such an arrangement acknowledges the
30 difficulty of extinguishing electrical arcs, and seeks to overcome the difficulty by instead switching a continuous discharge between electrodes by the use of externally applied magnetic fields.

Discharge tubes suitable for PAGD operation and
35 circuits incorporating them are described in our copending

International Patent Application PCT/CA93/00311.

It is known that there are anomalous cathode reaction forces associated with the cathodic emissions responsible for vacuum arc discharges, the origin and explanation of which have been the subject of extensive discussion in scientific literature, being related as it is to ongoing discussion of the relative merits of the laws of electrostatics as variously formulated by Ampere, Biot-Savart and Lorentz. Examples of literature on the subject are referenced later in this application.

SUMMARY OF THE INVENTION

The particular conditions which prevail in a discharge tube operated in the PAGD regime, in which a plasma eruption from the cathode is self-limiting and collapses before completion of a plasma channel to the anode gives rise to transient conditions which favour the exploitation of anomalous cathode reaction forces.

We have found that apparatus utilizing discharge tubes operated in a repeatedly initiated but discontinuous pulsed abnormal glow discharge or vacuum arc discharge regime, in a double ported circuit designed so that energy input to the tube utilized to initiate a glow discharge pulse is handled by an input circuit substantially separate from an output circuit receiving energy from the tube during collapse of a pulse, provides valuable energy conversion capabilities, and can effectively exploit the anomalous cathode reaction forces referenced above.

The invention extends to a method of energy conversion, comprising initiating repeated plasma eruptions of finite duration from the cathode of a discharge tube operating in a cathode emission-triggered abnormal glow discharge or vacuum arc discharge regime utilizing electrical energy from a source in a first circuit connected to said

- 4 -

discharge tube, and capturing electrical energy generated by the collapse of such eruptions in a second circuit connected to said discharge tube. In the cathode emission-triggered pulsed abnormal glow discharge regime, the pulse forming
5 function is autogenous to the discharge mechanism, whereas desired operation of a discharge tube in the VAD region requires the pulse to be formed externally.

The problems associated with the operation of vacuum arc devices are typically associated with the
10 establishment of a continuous channel of low resistance ionized plasma between the electrodes of a device operating in this mode, typically accompanied by intense heating of the electrodes. Such a channel is somewhat difficult to interrupt in rapid and predictable manner once established.
15 The pulsed abnormal glow discharge regime is characterized by no such continuous channel having been established, and predominantly cold-cathode auto-electronic emission rather than thermionic emission, these characteristics providing the ability to extinguish the discharge readily.

20 We have found that, by suitable design of a low pressure gas discharge tube, we can sufficiently inhibit transition from the abnormal glow discharge regime into the vacuum arc discharge regime that we can successfully exploit characteristics of the cathode emission-triggered pulsed
25 abnormal glow discharge regime to provide a device having valuable and controllable characteristics as a high power, pulse generator when fed from a current source. Such a pulse generator has useful applications in for example motor control and other applications requiring high current pulses.
30 It is a valuable characteristic that the autogenous pulse repetition frequency can be varied over a range, the extent of which itself varies according to the physical characteristics of the tube and the environment in which it is operated. According to circumstances, the frequency may
35 range as low as 0.1 pulses per second or range as high as 10^4

- 5 -

pulses, these figures being exemplary only and not limitative.

The purpose of the present invention is to provide
5 a means to operate electrically powered devices, including
alternating current machines, and in particular to derive
useful electrical energy and/or electromechanical work from
any vacuum discharge tube capable of sustaining a stable
cathode emission-triggered pulsed abnormal glow discharge
10 (PAGD) or repeatedly, a fully interrupted vacuum arc
discharge. The present invention provides a simple circuit
having at least two parallel arms: a pulse generator arm
containing the vacuum discharge and an energy recovery arm
which transduces electrical pulses into usable electrical or
15 mechanical energy. In the latter case, the electromechanical
device is integrated into a reactive load presenting a
capacitance in parallel with the tube. The present invention
was originally devised to work with specific cold cathode
vacuum tube pulse generators as disclosed in the above
20 referenced international application, using either diode or
triode connections, but the circuitry can be made to work
with any suitable vacuum device capable of sustaining
repeated high energy discharges as set forth above.

One advantage of using a spontaneous emission
25 self-pulsing device (i.e. operating in the PAGD regime) lies
in the fact that the speed of an AC motor and its torque can
be varied directly by altering any of the parameters that
affect pulse frequency. Two of these parameters, parallel
capacitance and applied, constant direct current, are of
30 particular usefulness, since when all other parameters are
the same, the rate of pulsed abnormal glow discharge,
controlling motor speed and torque, can be made to vary as a
function of increasing current applied to the cold cathode
device, for any given discharge capacitance employed. This
35 yields an extremely simple method of motor speed control,
particularly suited to drive synchronous and induction AC

- 6 -

motors from a starting DC supply, but also generally applicable to any motor, whether rotary or linear, whose speed or rate is dependent upon the frequency of a pulsed or alternating current. Rather than placing an alternating
5 current machine directly in the circuit containing the discharge tube, it may also be connected indirectly through a transformer or synchro-transmitter system.

The VAD regime has the advantage of transducing much greater peak and average currents than what is possible
10 with the PAGD regime for any given arrangement and conditions of operation of the vacuum tube (the plasma reactor). In the VAD regime, large output pulses are also observed at ignition, from an initial auto-electronic emission focus. However, as will be discussed, the extinction of the initial
15 emission focus is incomplete, with other foci of cathodic eruptions supervening and resulting in multiple, partial re-ignitions of the plasma. Subsequent cathodic emissions in the VAD regime thus lose the capacity to deliver the energy released by the discharge into the recovery arm of the
20 circuit, as the energy of the discharge is trapped in the intense plasma remaining in the gap, where the anomalous cathode reaction forces are damped or cancelled.

A solution to this difficulty is to use external
25 means to sever the VAD forcibly into a train of interrupted VADs, each discharge being made complete by switching off the arc. This may be accomplished in two basic ways: either by physically interrupting the discharge within the vacuum tube, or by utilizing an external circuit to form an intermittent
30 vacuum arc discharge, using any number of commutation techniques.

Further features of the invention will be apparent from the appended claims.

- 7 -

SHORT DESCRIPTION OF THE DRAWINGS

The invention is described further with reference to the accompanying drawings, in which:

Figure 1 is a graph illustrating the current to voltage relationship exhibited by a notional vacuum discharge tube;

Figure 2 is a graph illustrating the current to breakdown, extinction (PAGD) and sustaining (VAD) voltages of a particular vacuum discharge tube;

Figure 3 is a circuit diagram of a first embodiment of the invention, using a single phase permanent-split induction or synchronous capacitor motor connected in parallel with a pulse generator using a vacuum discharge tube configured either as a diode or as a triode;

Figure 4 is a circuit diagram of a second embodiment, employing two motors in series, and a triode connected vacuum tube pulse generator;

Figure 5 is a circuit diagram of a third embodiment, employing two motors in series, and two vacuum discharge tubes placed in series;

Figure 6 is a circuit diagram of a fourth embodiment, employing a two-phase motor, and two vacuum discharge tubes placed in series;

Figure 7 is a graph illustrating the results of tests using the first embodiment of the invention, using a permanent split capacitor induction motor, showing how motor speed in RPM varies with the total series value of the external capacitance placed in parallel with the vacuum discharge tube by the electromechanical arm of the circuit;

Figure 8 is a graph illustrating the synchronous RPM vs. pulses per second linear response, in the circuit of Figure 3, of a single phase, synchronous hysteresis capacitor motor for four different series capacitance values in the electromechanical arm of the circuit and the maximum pulse rates obtained for each combination;

Figure 9 is a graph showing the rotor blocked torque, measured by a rope and pulley method, of a single

phase, synchronous hysteresis capacitor motor in the circuit of Figure 3, as a function of the increasing direct current input resulting in increased pulse rate;

Figure 10 is a graph showing the rotor blocked torque, measured by a rope and pulley method, of a single phase, synchronous hysteresis capacitor motor both in the circuit of Figure 3 (as a function of increasing PAGD rate due to the increasing direct current applied to the circuit), and when run at AC line frequency of 60 Hz, torque being shown in each case as a function of the rms volts at the motor input;

Figure 11 is a graph exemplifying how the increasing pulse frequency of a PAGD discharge is related to the direct current applied to the tube in the circuit of Figure 1, accompanied by curves showing the potential applied to the tube and the power in watts drawn by the tube;

Figure 12 is a graph exemplifying variation in RPM, rms current drawn, input volts, and true and apparent power (watts and volt-amperes) of a synchronous motor in the circuit of Figure 1, and under the conditions of Figure 9;

Figure 13 is a graph showing the rms volts per pulse per second at various pulse rates for two different single phase capacitor motors (induction and hysteresis) utilized in the circuit of Figure 1;

Figure 14 shows in simplified form a variant of the circuit of Figure 3 in which the discharge tube is connected differently;

Figure 15 shows variation of applied DC current and the pulse AC rms currents characteristic of a low current PAGD regime, as a function of decreasing pressure, for a 128 cm² H34 aluminum plate pulse generator having a 5.5 cm gap length and being operated in the single or plate diode configuration of Figure 11A, at ~600 VDC.

Figure 16 shows variation of applied DC current and the pulse AC rms currents of a high current PAGD regime, as a function of the decreasing pressure, for a device identical to that of Fig. 1, and operated at the same potential.

- 9 -

Figure 17 shows the PAGD rate vs. pulse generator cathode temperature as a function of the time of continuous PAGD operation, for a pulse generator with 64 cm² plates having a 4cm gap distance, operated at VDC=555 (av) and
5 R1=600 ohms (see Fig.9).

Figure 18 shows PAGD frequency variation with time, for 18 successive one-minute spaced PAGD runs for a pulse generator with 128cm² plates, and a 5.5 cm gap distance, operated at VDC=560 (av) and R1=300 ohms.

10 Figure 19 shows variation of the PAGD frequency in pulses per minute (PPM) with increasing charge of a PAGD recovery charge pack (see Fig. 9), as measured in terms of the open circuit voltage following 15 minutes of relaxation after each one minute long PAGD run, repeated 18 times in
15 tandem, under similar conditions to Fig. 4.

Figure 20 shows volt amplitude variation of continuous PAGD at low applied current, as a function of decreasing air pressure, for a 128 cm² plate area device, gap length = 5 cm; (DCV at breakdown = 860).

20 Figure 21 shows volt amplitude variation of continuous PAGD at high applied current as a function of the decreasing air pressure, for a 128 cm² plate area device, gap length = 5 cm; (DCV at breakdown = 860).

Figure 22 is a schematic diagram of a first
25 experimental diode (without C6) or triode PAGD circuit.

Figure 23 is a schematic diagram of a preferred diode or triode PAGD circuit in accordance with the invention.

Figures 24A, 24B and 24C are fragmentary schematic
30 diagrams showing variations in the configuration of the circuit of Fig. 23.

Figure 25 is a modification of Figure 23, in which an electromagnetic machine, in the form of an electric motor, is connected into the circuit as an accessory
35 electromechanical arm.

Figure 26 shows a further development of the circuit of Figure 23, permitting interchange of driver pack

- 10 -

and charge pack functions.

Figure 27 shows open circuit voltage relaxation curves for battery packs employed in tests of the invention, respectively after pre-PAGD resistive discharge (DPT1 and CPT1), after a PAGD run (DPT2 and CPT2) and after post-PAGD resistive discharge (DPT3 and CPT3).

Figures 28A and 28B show resistive voltage discharge curves for two separate lead-acid gel-cell packs utilized respectively as the drive and the charge packs; load resistances employed were 2083 ohms across the drive pack (Fig. 32A) and 833 ohms across the charge pack (Fig. 32B).

Figure 29 shows resistive discharge slopes for a drive pack before and after a very small expenditure of power in providing energy input to a PAGD run; $R = 2083$ ohms.

Figure 30 shows resistive discharge slopes for a charge pack before and after capturing energy from the collapse of PAGD pulses in the same test as Fig. 28; $R = 833$ ohms.

Figure 31 shows resistive discharge slopes for a drive pack before and after a very small expenditure of power in providing energy input to a PAGD run in a further experiment; $R = 2083$ ohms.

Figure 32 shows resistive discharge slopes for a charge pack before and after capturing energy from the PAGD run of Fig. 31; $R = 833$ ohms.

Figure 33 shows an example of operational measurements taken videographically during a 10 second period for both the power consumption of the drive pack (PAGD input) and the power production captured by the charge pack (PAGD output); the two values are also related by the expression of percent breakeven efficiency.

Figure 34 shows variation of PAGD loaded voltage of a drive pack (in squares) compared with the PAGD charging voltage of the charge pack (in circles), during more than 1 hour of continuous PAGD operation.

Figures 35A and 35B are schematic plan and vertical sectional views of a discharge tube designed for the

- 11 -

production of interrupted vacuum arc discharges;

Figures 36 and 37 are electrical schematic diagrams of further embodiments of the invention utilizing a discharge tube operated in an interrupted VAD regime;

5 Figure 38 is an electrical schematic diagram of a converter circuit utilized to examine voltages and current during operation of the circuit in PAGD and VAD regimes;

10 Figures 39, 40, 41 and 42 are graphs showing variations of voltage and current with elapsed time in milliseconds at different points in the circuit of Figure 38 during PAGD and VAD respectively; and

Figure 43 is a circuit diagram of a further embodiment of the invention.

DESCRIPTION OF THE PREFERRED EMBODIMENTS

15 Throughout the following detailed description, the same reference numbers are used to denote identical elements present in related Figures.

The context of the invention in terms of vacuum discharge phenomena will first be discussed with reference to
20 Figures 1 and 2. Referring to Figure 1, which plots the potential between the principal electrodes of a vacuum discharge tube with increasing current, potential being shown on a linear but arbitrary scale of voltage, and current on a logarithmic scale in amperes, curve A, below its intersection
25 with curve B, represents a typical relationship between current and voltage for cold cathode discharges, including auto-electronic emissions, whilst curve B represents a typical relationship for thermionic glow discharges, including thermionic emissions. The high-current
30 intersection of the two curves at point E represents a transition into the vacuum arc discharge (VAD) region (curve C) with the establishment of a continuous low resistance plasma channel between the electrodes.

It will be noted that curve A exhibits, with

- 12 -

increasing current from very low levels, an initially rising voltage or "positive resistance" characteristic, through the Townsend discharge (TD) region, a flat characteristic through the constant discharge (CD) region, a falling voltage or
5 "negative resistance" characteristic through the transitional region discharge (TRD) and normal glow discharge (NGD) regions, to a minimum, before once again rising to a peak of F and then falling to an even lower minimum, equal to the sustaining voltage for a vacuum arc discharge, through the
10 abnormal glow discharge (AGD) region. The rising potential over the first portion of the AGD region is believed occasioned by saturation of the electrodes by the glow discharge, which causes the potential to rise until auto-electronic emission sets in allowing the potential to fall
15 again as the current rises further. In practice, the increasing interelectrode potential following saturation, and other factors such as electrode heating, leading to thermionic emission, will tend in conventional tubes to result in a premature transition from the AGD into the VAD
20 regime, following a curve similar to curve D shown in Figure 1.

The present invention relies in a presently preferred embodiment on the use of gas discharge tubes designed to avoid premature transition from the AGD to the
25 VAD regimes, and capable of being operated in a stable manner in that region of the characteristic curve of Figure 1 extending between points E and F. Referring now to Figure 2, which plots test results for just such a tube, constructed as described in International Application PCT/CA93/00311, and
30 shows, again on similar coordinates to Figure 1 (except that the potential units are defined), the extinction or sustaining potentials of the tube (the same information as plotted in Figure 1), together with the breakdown potential (i.e. the potential required to initiate the autoelectronic
35 discharge). It will be noted that the breakdown curve shows two discontinuous portions X and Y, corresponding to the

- 13 -

vacuum arc and abnormal glow discharge regimes respectively. The intersection of curve X, and curve Z representing the sustaining or extinction potential is illustrative of the difficulties inherent in extinguishing a vacuum arc
5 discharge, since an increase in current is accompanied by a decrease in breakdown voltage until it equals the VAD sustaining voltage which does not vary greatly in this region. On the other hand, the combination of a fairly high and constant breakdown voltage (curve Y) combined with an
10 extinction potential which rises with decreasing current in the region E-F (see Figure 1) of the pulsed abnormal glow discharge regime means that the pulsed abnormal glow discharge will be extinguished if the current source during the tube operation ceases to be able to sustain the
15 increasing current required to maintain the discharge as the potential between its electrodes drops, at some current below the intersection of curves X and Z.

If the effective internal resistance of the source is above some critical level, then as the current through the
20 tube rises, the proportion of the source potential developed across the tube will fall until it intersects the curve Z at a current below the intersection with curve X, at which point the abnormal glow discharge will self extinguish, and the current flow through the tube will drop abruptly until the
25 current through the tube combined with the potential between its electrodes again intersects the curve A in Figure 1. This permits reestablishment of a rising current through the tube traversing the abnormal glow discharge region as the potential across the tube rises to the peak F and then again
30 falls to a point short of E. Accordingly, under these circumstances, a pulsed abnormal glow discharge will be exhibited, accompanied by high amplitude current pulses through the tube. It should be understood that the curves of
35 Figure 1 are indicative of the static behaviour of a nominal discharge tube under particular current and voltage conditions, and are not fully indicative of the behaviour of

- 14 -

the tube under dynamic conditions in which tube current and inter-electrode potential vary with time, nor with changes of the many other factors which may influence tube behaviour. In particular, the plasma effects generated in various phases
5 of tube operation require finite time to form, reform or dissipate as the case may be, and in the case presently under consideration this time factor, combined with time constants of the external circuit in which the tube is placed, are determinative of the pulse frequency of the discharge.

10 The definition of any regime of electrical discharge in a vacuum is usually presented as dependent upon the major operational parameter being considered, i.e. upon the variation of direct current passing between the primary electrodes. For a given optimal vacuum (which must
15 necessarily be less than perfect) all gas electrical discharge regimes can be presented as dependent upon this parameter. Figure 1 is such a presentation and the peak that characterizes the abnormal discharge region means that within this region, as the applied current is increased linearly,
20 the resistance of the vacuum in the tube first increases with increasing current, only to subsequently decrease, still with increasing applied current, down to the minimum resistance value corresponding to the sustaining potential of a vacuum arc (which is somewhat above the ionization potential of the
25 gas, or in fact of the metal vapour, in the enclosure). As the transition from a normal glow discharge into a vacuum arc discharge is made either directly (in thermionic devices) or indirectly, in cold-cathode conditions, via an abnormal glow discharge that may be more or less precipitous, it is only in
30 the ideal diode and the ideal vacuum that both linear functions (corresponding to the regimes that have a sustaining potential) and nonlinear functions (corresponding to the transition regions, such as the TRD and the AGD) appear to depend exclusively upon the input current. In
35 fact, many factors affect the AGD, foremost amongst them, the presence of or absence of auto-electronic emission, pressure,

- 15 -

plate distance and plate area. Hence the peak in the curve of Figure 1 is an idealized view of events.

This said, we are left with the experimental observations and what they tell us. In this respect, auto-
5 electronic emissions characteristic of the pulsed abnormal gas discharge (PAGD) regime can be seen to emerge from the
10 NGD, as the current is increased beyond the point when the cathode glow has reached plate saturation.

The same effect occurs when the pressure is reduced
10 and the current is kept constant at a suitable level (neither too high nor too low, exact figures depending on other factors such as gap distance and plate area, etc.).

If the current is increased further, in either case, the cathode emission dependent PAGD regime fully
15 emerges (in other words, in pumpdown tests, the applied current also has to be sufficient). In this regime the plate is not so much saturated with a negative glow (which remains, but is attenuated), but exhibits local concentrations of the plasma that arise in a given area of the cathode as a
20 function of the auto-electronic emission mechanism. If the applied current is increased in steps, a stage is reached at which the extinction potential of the PAGD falls until it meets the minimum potential of an arc discharge, as demonstrated in Figure 2. With reference to Figure 1, this
25 means that the current-dependent variation of the PAGD in these devices passes from a high to a low extinction potential or from a high to a low electrical resistivity of the medium, and is thus localized on the descending slope of the peak in Figure 1. Expressed in terms of resistance
30 characteristics, the regime of the pulsed abnormal glow discharge spans, as a function of applied current, a subregion in which a positive resistance characteristic changes into a leading negative resistance characteristic. The pulsed regime of the AGD is only sustainable when the

- 16 -

intensity of the applied current is greater than that needed to rapidly saturate the plates (but not so great as to set up a VAD), the result being development of auto-electronic emission with its associated inverted cone-like discharge and
5 a residual glow of the entire cathode.

Each PAGD cycle begins as a singular emission and performs a cycle of functions whose electrical characteristics vary accordingly with time. During a charging process (which eventually leads to emission), the
10 plate potential rises to a maximum at F (see Figure 1), while being limited by the maximum virtual value of the applied current. Any substantial increase in the applied current is blocked by the insulating properties of the intervening
15 medium (as if a very large resistance characterized the device); in the discharge process, beginning with the initiation of auto-electronic emission at F, conditions for conduction across the vacuum are established and, as a consequence, the resistance characteristic of the device
20 becomes increasingly negative until the extinction potential is reached, at which point the glow discharge ceases. This endogenous on/off behaviour is exactly what characterizes the PAGD cycle.

Two boundary conditions arise. In the first case, the available current is not quite enough to sustain the
25 PAGD. In this instance, full escape from the NGD regime and the characteristics associated with its sustaining potential will not occur, while any heating of the cathode will eventually lead to the establishment of a semi-thermionic cathode glow. In the second instance, there is a risk of
30 degeneration into a thermionic glow discharge or a VAD if the available current is too high or sustained too long. This degeneration will set in during the second phase of the PAGD unit cycle, and may lower the resistance of the device to the point of constant conduction of current across the vacuum;
35 the result is that the auto-electronic emission is not

- 17 -

quenched, as spontaneously happens in the PAGD. Thereafter, extinction of the resulting VAD, which may be promoted by a variety of factors, is an unpredictable event; if the current is available, the arc will burn for as long as there is energy supplied and as long as there is cathode material available to consume. A VAD in no way resembles a regular, cyclic oscillator, which is the outstanding aspect of the PAGD. Whilst a vacuum arc discharge is, like the PAGD, an auto-electronic emission phenomenon characterized by intermittences (the apparent constancy of an arc is the result of the high frequency of these intermittences), such an arc does not of itself exhibit the regular or quasi-regular cyclical nature of the PAGD, nor its inherent current limiting characteristics.

In order that a stable pulsed abnormal glow discharge (PAGD) as discussed above may be obtained, the discharge to be utilized must be capable of repeated excursions into the region E to F of Figure 1. This entails that the tube be constructed so that, as the tube operates and the current through it rises, the potential across the tube can reach the peak F in Figure 1 and beyond, without the pulsed abnormal glow discharge degenerating into a vacuum arc discharge. This will be influenced, among other factors, by the extent of thermionic emission from the cathode which will itself be influenced by resistive heating of the electrodes and their work function, as well as by their separation and configuration, and the nature and pressure of gas within the tube, as well as the presence of auxiliary electrodes or probes. The influence of these various factors is extensively exemplified in the above referenced international application, which discloses tubes capable of sustaining PAGD. Whilst most embodiments of the present invention are described with reference to its use in connection with such tubes, it should be understood that the invention may be implemented utilizing any tube capable of sustaining a stable PAGD or a suitably interrupted VAD whether or not disclosed

- 18 -

in our earlier application.

The invention will first be described with reference to its utilisation in conjunction with electromagnetic machines.

5 Figure 3 shows a first exemplary embodiment of the invention operating in the examples described with a single phase permanent-split induction or synchronous capacitor motor having a rotor R, stator windings 15 and 16, and a capacitor 17. The motor is connected to terminals 13a and
10 13e and via capacitors 10 and 11 to the electrodes of a vacuum discharge tube 7, capable of producing cold cathode abnormal glow plasma pulses and constructed in accordance with the principles set forth in the parent application. Motors with other characteristics, such as single phase
15 capacitor-start induction motors, two-value (start and run) capacitor induction motors, repulsion-induction motors, repulsion-start induction-run motors, reluctance motors, universal motors, split phase motors, two-phase induction or synchronous motors (wired as single phase capacitor-run
20 motors), or single phase rotor input synchro-transformer generators could also be connected to the same terminals 13a and 13e.

As shown in Fig. 3, the voltage source may be either a line-fed DC power supply 1 (preferably constant
25 current), a DC generator 2 or a battery pack 3. The supply voltage and current may be controlled by using methods known to those skilled in the art, whichever source is used. With line fed power supplies it is preferred to control the DC output by varying the power input using the autotransformer
30 method. With a DC generator, the power output can be controlled directly by varying the speed of the generator. With a battery, simple control of input direct current and output pulse frequency from vacuum device 7 is best achieved with a variable series resistor 4. Diodes 5 and 6 prevent

- 19 -

transients from the pulse discharge from reaching the DC source.

The discharge tube 7 is shown in Fig. 3 connected in a diode configuration with cathode 8 placed between
5 rectifier 5 and capacitor 10 and the anode 9 placed between
rectifier 6 and capacitor 11, by virtue of a switch 22 being
turned off (position NC). When switch 22 is turned to
position 13a' so that an axial member 12 within the tube is
connected to the terminal 13a, the pulse frequency increases
10 by an amount depending on the parameters of the circuit as a
whole. In this configuration, the axial member of the pulse
generator lowers the breakdown potential and increases the
rate of discharge by adding its spontaneous emissions to
those of the cathode. The same result obtains when switch 22
15 connects axial member 12 to position 13e' instead, thus
joining it to terminal 13e.

The capacitors 10 and 11 are placed in parallel
with the reactive electrodes, with the motor 14 in series
between capacitors 10 and 11, but in parallel with either the
20 plates (diode configuration) or the axial member and the
cathode or anode (triode configurations) as the case may be.
For best results, it is desirable to have capacitances 10 and
11 disposed symmetrically in the circuit as shown in Fig. 3.
An unbalanced circuit results when one capacitor is absent,
25 and anode counter-emissions become frequent. Capacitance
values for discharge capacitors 10 and 11 are determined as
a function of the type of vacuum pulse device employed and
the nature and performance characteristics of the AC motor 14
chosen. If the capacitances are too small, the motor will
30 not start nor maintain rotation; if too large, the motor will
not turn smoothly or continuously, and spontaneous anode
counter-emissions may occur which will break the rotation of
the motor by reversing the direction of the electromagnetic
flux. The critical parameter is the total series value of
35 the capacitance placed in parallel with the pulse generating

- 20 -

device, and there is no need for the capacitances 10 and 11 to be identical; in fact it is preferred that there be a higher capacitance on the side of the cathode (capacitance 10) than on the anode side (capacitance 11) when the triode
5 configuration has the axial excitor member connected to 13a via switch 22 at position 13a', or the reverse when the axial member is connected to 13e.

The AC motor employed may, in general, be of any type. Split phase, single phase, or two phase AC motors, be
10 they universal, induction or synchronous types, having squirrel-cage, wound-type, eddy current, drag cup or hysteresis-type rotors, will all respond to the pulses generated in this circuit. Single phase, permanent-split capacitor, AC induction motors having squirrel-cage rotors
15 and single phase AC synchronous hysteresis capacitor motors are preferred. The latter, in particular, have the advantage of developing a nearly uniform torque from stationary or blocked rotor positions to synchronous speed as well as producing a smoother response to the pulsating nature of
20 single phase power (e.g. in a 60 Hz circuit, power is in fact delivered in pulses at 120 Hz) than that of other single phase motors. The motor 14 in Fig. 3 has its main winding coil 15 in parallel with the discharge tube and an auxiliary coil 16 connected in parallel with the main coil 15 via the
25 phase capacitor 17. This corresponds to the connection as a single phase AC permanent-split capacitor motor. To reverse the direction of the motor it is sufficient to switch the position of switch 18 from pole 19 to pole 20. If motor 14 were a suitable two phase AC induction or synchronous motor
30 wired as a permanent-split capacitor single phase motor, then the reversal obtained by switching 18 would provide an equal torque in either direction of rotor rotation of the motor. A less efficient start-up or phase displacement utilizes a resistance in place of capacitor 17, in a manner known in the
35 art. The resistance may be varied to alter the motor speed.

- 21 -

Replacement of pulse generator 7 by a suitable vacuum device, as diverse as a fluorescent light bulb (as a diode) or an hydrogen triode indicates that, despite the absence of desirable physical parameters identified in the parent application, any cold cathode operated vacuum tube device capable of sustaining pulsed abnormal glow discharges triggered by autoelectronic cathode emissions when operated in the abnormal glow discharge region, or of withstanding externally interrupted vacuum arc discharges, is capable of serving as the pulse-forming discharge tube in the circuit. By contrast, whilst discharge tubes operating in the normal glow discharge region can be used to form pulse generators, the mechanism is different and the power output would generally be too low to be useful in an electromechanical application.

Any inductive AC electromechanical device such as a relay solenoid or linear motor, may also be employed in place of motor 14 at terminals 13a and 13e, Fig. 3, to derive electromechanical work from the on and off switching action of the vacuum discharge tube 7 when operated in the pulsed abnormal glow discharge regime.

An advantage of the invention is that a constant current supply coupled to a suitable vacuum discharge tube can be used to obtain smooth rotary action from certain AC motors in an easily controllable fashion, without having recourse to a conventional inverter system in order to produce alternating current, and provides a simple means of frequency control. Whereas the main limitation imposed on the use of induction or synchronous AC motors is that they are essentially constant speed motors which can only vary their torque as a function of the magnitude of the AC voltage and current input (given that the frequency of the power supply cannot normally be changed), the present invention allows the torque and speed of an AC motor to be controlled by varying the DC voltage and current applied to any cold

- 22 -

cathode vacuum device 7 operated in the pulsed abnormal glow discharge regime as discussed above, as well as by varying the pulse rate of the PAGD by other means such as through the probe 12 in a device as described in the parent application.

5 Furthermore, the electromechanical force is developed from a nearly even sequence of discontinuous energy bursts, of controllable frequency, rather than continuous sinusoidal power pulses at a fixed frequency.

Figure 4 shows how two single phase permanent-split
10 capacitor AC motors 14a and 14b may be connected symmetrically in tandem, both placed in parallel with a single vacuum discharge tube 7, following the principles described above for Figure 3. Independently of whether the axial member 12 is or is not connected to junction 13b, a
15 capacitor 21 may be advantageously introduced between junctions 13b and junction 13c, to even out the rotation of the two motors, although it is not essential.

Figure 5 shows how two (or more) discharge tubes may be connected in series to drive two or more motors 14a
20 and 14b also in tandem, from the output of two or more vacuum devices 7 placed in series with each other. Connections 13a' and 13d' from axial members 12a and 12b, as well as capacitor 11 and its connection to 13b may be omitted and the circuit will still function. The circuit of Figure 5 will produce a
25 pulse sequence at the output from the second tube which is phase shifted with respect to that of the first tube, with further shifting as more tubes are added. It is thus possible to couple polyphase motors as shown in Figure 6, (showing a two phase motor) with a suitable capacitance 21
30 being introduced between junction 13b and junction 13c to control further the firing rate of the second vacuum device 7b. The addition of more tubes in series will further displace the phase of the pulse sequences in each successive device. Sufficient relative angular displacement of two
35 tube-generated pulse sequences can also be achieved by

- 23 -

introducing a suitable delay relay between points 23 and 24, at the cathode input to the second vacuum device.

In general, the pulse frequency developed by a discharge tube operated to produce PAGD in the circuits described will depend on several factors: some are circuit factors, such as the total discharge capacitance placed in parallel with the vacuum device, and the characteristics of the power supply (direct current and voltage values); others are physical factors, such as the pressure, the chemical nature of the gas fill and the field-emission work function of the cathode material and its composition and still others are geometrical or dimensional in nature, such as the interelectrode distance, the plate area and the parallel plate arrangement. All these factors are discussed in the parent application.

The following examples relate to tests of the circuit of Figures 3.

EXAMPLE 1

The circuit of Figure 3 was tested with a single phase squirrel cage induction motor, the capacitor 17 being $2\mu\text{Fd}$. The RPM of the rotor was measured with a stroboscopic tachometer to determine how it varied with the total series value of the external capacitances 10 and 11 (Fig. 3) placed in the electromechanical arm of the circuit, in parallel with the anode and the cathode of a discharge tube constructed as exemplified in the parent application, with 64 cm^2 plate area, 5.5 cm interelectrode distance and an air fill at 2 Torr. The tube was excited in a triode configuration (switch 22 at position 13a' and switch 18 at position 19, Fig. 3) by an AC line-fed DC power supply. The results are shown in Fig. 7. Provided that the capacitance is not too high or too low, other factors such as the frequency of the pulses generated by the vacuum device (which increases with decreasing parallel capacitance) and the type and characteristics of the

- 24 -

windings and of the rotor of the motor employed, have a greater influence on the motor speed.

EXAMPLE 2

The total value (internal to the power supply and external to it) of the capacitance placed in parallel with the discharge tube in the same triode configuration of the previous Example, in turn affects the maximum frequency of cathode emission-triggered abnormal glow discharge pulses produced, and the effective synchronous motor RPM, as shown in Fig. 8. This figure presents motor RPM as a function of the total series value of the external capacitances placed in the electromechanical arm of the circuit, and shows results obtained with a single phase hysteresis capacitor motor (rated as 10 VAC 1/10 Hp, with the auxiliary winding motor capacitance 17 having a value of 2.4 microfarad). These tests indicate that for any given AC motor there will be optimal values for the pulse rate produced by the discharge tube, and that this pulse rate will have a maximum value for any particular value of the total capacitance placed in parallel with the pulse generator, and specifically in the electromechanical arm of the circuit, and this capacitance itself will have an optimal value. Conversely, for any given motor characteristics, a pulse generator can be designed with optimized circuit or electrical, physical and geometrical parameters.

EXAMPLE 3

With a rope-and-pulley type of torque meter, the rotor-blocked torque developed by a synchronous hysteresis motor was tested using the circuit of Figure 3, and the same vacuum device as the previous two Examples. This type of motor was chosen because in an "ideal hysteresis" motor, the torque developed is constant at all speeds from standstill to synchronicity, locked rotor, pull-in and pull out torques being identical. Even though a single-phase capacitor-type hysteresis motor departs more from the ideal curve than a

- 25 -

polyphase hysteresis motor does, on account of the elliptically shaped rotating fields set up by a capacitor motor, most manufacturers make permanent-split capacitor single phase hysteresis motors with identical full-load and
5 locked rotor torques. We have utilized one such motor for our tests. Fig. 9 illustrates the range and mean of at least nine tests conducted at each of three different input direct currents into the pulse generator, the extinction voltage remaining relatively constant at about 330VDC, with the
10 results expressed as standstill torque in gm/cm developed related to the pulse rate of the pulse generator. The discharge tube was triode connected as described with reference to Fig. 3, and the total series value of the external parallel capacitance to the pulse generator was 36.6
15 microfarads. It is readily apparent that the torque developed is proportional to the pulse frequency as is desirable for the purposes of the present invention. The torque developed is also proportional to the voltage input into the motor (i.e. the tube output voltage) as is
20 exemplified in Fig. 10, where tests of the PAGD-induced torque (closed squares) obtained and measured under the same conditions described for Fig. 10, over the increasing frequency range of 11 to 45 PPS, are compared with tests of an AC 60Hz line sine wave generated torque (shaded circles),
25 as a function of the input volts into the motor from each source.

EXAMPLE 4

An example of the relationship of operational parameters involved in the performance of the circuit of Fig.
30 3 is shown in Figs. 11 and 12, using the same pulse generator device employed in the previous Examples 1 through 3 at an air pressure of 1.75 Torr, and using the same hysteresis motor as described in the previous Examples 2 and 3. The tests of Figs. 11 and 12 utilized a total series capacitance
35 for the external electromechanical arm of 7.9 μ fd (with reference to Fig. 3: capacitor 10=440 μ fd, capacitor

- 26 -

11=8 μ fd)). The same triode wiring of the plasma reactor was employed as in previous examples. Fig. 11 illustrates how the discharge rate of the pulse generator is controlled by the steep increase in applied DC amperes (open squares) while DC volts (closed squares) decrease to a near plateau as the pulse frequency reaches 40 pulse per second. Total wattage input to the discharge tube in the PAGD regime, at the output from the transformer secondary of the DC power supply, is shown in shaded squares. Fig. 12 shows the corresponding pulse output from the vacuum tube into the motor arm of the circuit and illustrates how the AC rms current (open squares), the AC rms voltage (open circles), the true and apparent power (respectively, solid and shaded circles) as well as the rpm (solid squares) of the synchronous hysteresis motor increase proportionately to the discharge rate of the pulse generator from 11 to 45 PPS. With reference to Fig. 3, the effect of the connection to the axial member 12 through the switch 22 is to promote, other conditions being equal, an increase in discharge frequency: at these tube input and output parameters changing from a diode to a triode configuration typically increases the maximum discharge rate from 30 to 43-45 PPS.

EXAMPLE 5

When a motor is wired as a single phase motor and connected to an adjustable frequency power source, the voltage applied to the motor stator terminals should change proportionately to the change in frequency in order to maintain the constant air-gap flux that permits the motor to develop its rated torque over its speed range. A provision is thus desirably made in the power source not only to maintain a volts to pulse rate relationship which is relatively constant over an operating range, but also to maintain it at a value suited to the motor. In the present invention this is easily accomplished by adjusting the total series capacitance in the electromechanical arm of the circuit to the set value of the operating motor for any given

- 27 -

input frequency range. Two such examples of volts per pulse per second curves as a function of PAGD frequency at the motor input are shown in Fig. 13, one (shaded circles) obtained with a squirrel cage induction motor (110VAC, 1/20 Hp, 2mfd auxiliary winding capacitance) and the other (open circles) with the same hysteresis motor used in the previous Examples 2 through 4. Total series capacitance values for the parallel electromechanical arm of the circuit were respectively 3 mfd (open circles) and 8 μ FD (shaded circles). In both instances shown, the volts per cycle value becomes constant with increasing frequency, reaching a plateau at around 25 PPS.

It should be understood that, using a suitable three or more phase transformer, and a vacuum discharge tube with three or more cathodes (or three or more discharge tubes), a higher cumulative pulse rate and a polyphase output may be obtained from the transformer. It should also be understood that, as shown in Figure 14, in some applications it may be advantageous to strap the plates 8a and 8b in parallel as cathodes 8a and 8b and use the axial member as an anode 9.

In the following embodiments, the recovery arm of the circuit is utilized to recover electrical energy.

For purposes of the experiments described below four aluminum H34 plate devices (one with 64 and three with 128cm² plate areas) and three aluminum (H200) plate devices (one with 64 and two with 128 cm² plate areas), with interelectrode gap lengths of 3 to 5.5 cm, were utilized at the indicated vacua, under pumpdown conditions and with either air or argon constituting the residual gas mixture. Some experiments were performed with the tubes under active evacuation, at steady-state conditions, while others utilized sealed devices enclosing the desired residual gas pressures.

- 28 -

The circuit designs utilized in the various experiments to be described are set out further below, and represent further developments and extensions of the circuits already described above.

5 Large banks of 12V, 6Ah lead-acid gel cells (Sonnenschein (trade mark) A212/6S) were utilized either as power sources (designated as drive packs) or as accumulators of the energy (referred to as charge packs) captured by the test circuits. Charge packs made of rechargeable 9V NiCad or
10 of nominally nonrechargeable C-Zn or alkaline batteries were also utilized.

PAGD emission areas were determined by metallographic examination of a series of craters produced by PAGDs in clean H34 cathodes, under a metallurgical Zeiss
15 (trade mark) standard 18 microscope equipped with an epi-fluorescent condenser, very high power apochromatic objectives and a 100W mercury lamp. For best results a focusable oblique source of light (12V halogen) was also added to the incident light.

20 Following our low and high applied current studies on PAGD production as set forth in the above referenced international application, we noticed that the AC rms value of the component associated with each abnormal glow discharge pulse varied nonlinearly with the magnitude of the applied
25 current. Originally, we noted the existence of a current induced shift of the entire PAGD region upward in the pressure scale: while the PAGD regime became more clearly defined as the applied constant DC was increased, the pressure required to observe the PAGD also increased two to
30 three orders of magnitude. In the course of these rarefaction studies we found that, at applied currents of 1mA or less, the input AC rms value (e.g. at R9, Fig.38) of the different waveforms associated with the consecutive regimes of the discharge (TRD->NGD->AGD+PAGD) was, by more than half

- 29 -

log, inferior to the value of the applied DC current, during the first two regimes (TRD and NGD) and reached a value equivalent to the applied current with the onset of spontaneous PAGD, at pressures <0.1 Torr (see Fig. 15);

5 however, in the downward pressure tail of the PAGD regime (down to $3 \cdot 10^{-3}$ Torr in the example given), the AC rms current component of each PAGD decreased with decreasing pressure. In stark contrast, at high applied currents of ~ 500 mA, and aside from the high current-induced upward shift in pressure

10 of the PAGD regime (to the point that the compression of the pre-PAGD regimes on the pressure scale results in their being suppressed, as was the case in the present example), the AC rms component associated with each pulse (see closed circles, Fig. 16) is, from onset of the discharge at about 8 Torr,

15 significantly greater in magnitude than the value of the applied current (open circles, Fig. 16). Under the conditions described, the distribution of the field current associated with each pulsed abnormal glow discharge approached (on a linear Y axis; not shown) an unimodal

20 gaussian distribution with the pressure peak at about 1 Torr, and a corresponding observed maximum of $7.5 \times$ higher AC rms values than the applied DC values. But even these input AC rms current values did not compare with the large emission currents of 100 to >200 A registered at the collector of the

25 plasma reactor (see our co-pending application PCT/CA93/00311, and Figs. 38 to 42 ahead).

The PAGD frequency is affected by several factors, namely: the magnitude of the parallel discharge capacitance, the value of the negative pressure for the relevant vacuum

30 PAGD range, the magnitude of the applied potential, the magnitude of the applied direct current, the interelectrode gap distance and the area of the parallel plate electrodes. We have already described how the wiring configuration (plate diode versus triode) affects the PAGD frequency by adding

35 autoelectronic emissions from the axial electrode, to those emissions from the plate. The following data indicates the

- 30 -

specific effect of the above factors upon PAGD frequency.

In the data presented in Table 1, control of the PAGD frequency parameter for the circuit shown in Figure 26 is by a ballast resistance R1 within a specific range of interest (about 800-150 ohms, for Table 1 experimental conditions), and this in turn increases the applied current which, at "high current" values (ie >100 mA, as for Table 1 conditions), will drive the PAGD frequency up, as previously reported in the '863 application.

10 Another variable that interacts with the PAGD frequency is the molecular nature of the residual gas: Table 2 shows the differential frequency response of air with a halogen quencher, argon. It is apparent that argon produces much higher rates of AGD pulsation for the same range of negative pressure, for the same "broken in" cathode, than
15 does the air mixture. (All these measurements were taken at cathode support-stem temperatures of 35°C.)

Time of operation is also a variable affecting the frequency and operating characteristics of the cathode, as it becomes expressed by the passive heating of the electrodes, particularly the cathode, an effect which is all the more pronounced at the higher pressures and at the higher frequencies examined. Utilizing the triode configuration, the pulse rate (solid squares) of a PAGD generator with 64cm² plates can be seen (see Fig. 17) to decrease with time T, in minutes, at a negative pressure of 0.8 Torr, from 41 PPS to the operating plateau of 6 PPS within 15 minutes of continuous operation, as the temperature (open circles) of the cathode support increased from 19 to ~44°C. As the
25 temperature plateaus at ~51±1°C, so does the pulse rate at 6 PPS, for the remaining 48 minutes of continuous operation.
30

However, in order to confirm this time-dependent heating effect and threshold, we also performed the same

- 31 -

experiment, utilizing the same circuit and the same negative air pressure, with twice as large a cathode area (128cm^2 , which should take nearly twice as long to heat), being operated for 18 one-minute long continuous periods equally spaced apart by 15 minutes of passive cooling, with the cathode stem always at 19.7 to 21°C , room temperature at the start of each period. The results surprised us, inasmuch as they showed that for a larger area tube which takes longer to heat to the same temperatures at comparable rates of PAGD triggering, one could observe a much earlier frequency reduction (by half, within the first 5 minutes or periods of interrupted functioning) in the absence of any significant heating effect ($<1.5^\circ\text{C}$) of the cathode (see Fig. 18 which plots pulses per second against run time T in minutes). Repetition of these experiments has led us to conclude that, as shown in Fig. 19, which plots pulses per second against charge pack open circuit voltage 15 minutes, after the variable responsible for this repeatedly observed reduction in the PAGD frequency, (when the PAGD operation sequence is periodic), is the state of charge/discharge of the battery pack (the charge pack) at the output of the triode circuit in question: the PAGD PPM rates in Fig. 19 decrease rapidly with the steepest rate of charging of the charge pack and the fastest recovery rate of its open circuit voltage; above a given state of charge, when the open voltage of the charge pack climbs more slowly ($>340\text{V}$), in a log fashion, the PPM rate stabilizes at its plateau values.

Confirmation of the importance of the charge pack in the PAGD function of the present circuitry here considered, comes from the fact that the size (the number of cells) and the intrinsic capacitance of the charge pack affect the PAGD frequency dramatically (see Table 3): increasing the charge pack size of 29 cells to 31, by 7% leads to a 10-fold reduction in frequency; further increases in the number of charge pack cells extinguishes the phenomenon. On the upper end of the scale, this effect

- 32 -

appears to be tied in to restrictions that it places on the ability of the larger charge packs to accept the discharge power output once the charge pack voltage exceeds the PAGD amplitude potential. All of these measurements were
5 conducted with the same 128cm² plate PAGD generator, at a pressure of 0.8 Torr and in the triode configuration (see Fig. 23).

Other factors can also affect the frequency: the motion of external permanent magnetic fields oriented
10 longitudinally with the interelectrode gap, external pulsed or alternating magnetic fields, external electrostatic or electromagnetic fields, and the presence of a parallel capacitative, capacitative-inductive or self-inductive arm in the circuit, such as we have described for our
15 electromechanical PAGD transduction method described above.

Analysis of the modulation of PAGD amplitude is simpler than that of its frequency, because fewer factors affect this parameter: (1) magnitude of the applied
20 potential, (2) interelectrode gap distance and (3) the negative pressure, for "low" applied currents. As the magnitude of the applied potential itself is limited by the gap and the pressure, to the desired conditions of breakdown, the important control parameter for the PAGD amplitude is the
25 pressure factor. This is shown in Figs. 20 and 21, respectively for "low" (5mA) and "high" (~500mA) applied currents and for the same plate diode configuration of a H34 Al 128cm² plate PAGD generator (5cm gap), in a simple single ported circuit; it is apparent that both positive and
30 negative components of the amplitude of these pulses in the oscillograph, are a function of the pressure, but the maximum cut-off limit of our equipment, for the negative component (at 240 volts for the "low" current experiment and at 120 volts for the "high" current), precluded us from measuring
35 the peak negative voltage of these pulses. However, rms measurements of the pulse amplitude at the plates and DC

- 33 -

measurements at the circuit output to the charge pack indicate that the negative component increases with decreasing pressure to a maximum (420 volts in the example at 0.08 Torr), for a given arrangement of potential and gap distance; no pressure-dependent bell shape variation of the pulse amplitude, as that seen for the positive component at "high" applied currents (Fig. 21) is observed with the negative amplitude component. For the typical range of 0.8 to 0.5 Torr, the rms value for pulse amplitude varies from 320 to 480 volts, for a 5.5cm gap distance and applied DC voltages of 540 to 580. PAGD amplitude is a critical factor for the design of the proper size of the charge pack to be utilized in the optimal circuit.

The circuits to be described differ substantially from those used in the methods of electromechanical transduction of AGD plasma pulses described above. Whereas this electromechanical coupling (capacitive and self-inductive) directly utilizes the AGD pulses inverted from the DC input by the vacuum generator, the purpose of the development that led to the presently described experiments was to capture efficiently, in the simplest of ways, most of the pulse energy as electrical energy in a closed circuit, so that power measurements for the energy transduction efficiency of the observed endogenous pulsation could be carried out. Ideally, comparative DC power measurements would be performed at both the input and output of the system, taking into account the losses generated across the components; this would obviate the measurement problems posed by the myriad of transformations implicit in the variable frequency, amplitude, crest factor and duty-cycle values of the PAGD regime, and necessitated some form of rectification of the inverted tube output. From the start our objective was to do so as simply as possible. Early circuits utilizing half-wave rectification methods coupled in series to a capacitive arm (for DC isolation of the two battery packs), with the charge pack CP (the battery pack receiving the

- 34 -

captured charge) also placed in series, showed marginal recoveries of the energy spent at the PAGD generator input. Attempts at inserting a polar full-wave rectification bridge led, as shown in Fig. 22, to the splitting of the parallel capacitor into capacitors C3 and C5, at the rectification bridge input, and capacitor C4 in series with both C3 and C5 capacitors, all three being in a series string in parallel with the PAGD generator. Under these conditions a DC motor/generator could be run continuously in the same direction at the transversal output (U1 and U2) of the bridge; but if this inductive load was replaced with a battery pack CP (charge recovery pack), either the parallel capacitor C4 had to remain in the circuit, for the diode configuration or, less desirably, a further capacitor C6 could replace C4 and connect one electrode, preferably the cathode C, to the axial member of the discharge tube T, thus resulting in a first triode configuration as actually shown in Fig. 22. Energy recovery efficiencies of the order of 15 to 60% were obtained utilizing C6 in this manner, but measurements of the potential and currents present at the output from the rectifier bridge were substantially lower than those obtained using optimal values of C4. Effectively, under these conditions, much of the power output from the tube was never captured by the output circuit formed by the second, right hand arm of the system and, being prevented from returning to the drive pack DP by diodes D1 and D4, was dissipated and absorbed by the interelectrode plasma, electrode heating and parasitic oscillations.

Solutions to this problem were explored using the circuit shown in Figure 23, which still maintains the necessary communication link for the quasi-sinusoidal oscillation of the capacitatively stored charges at the input and outputs of the rectification bridge, but integrated the functions of capacitor C4 into the single rectification circuit, in the form of an asymmetric capacitative bridge C7a and C7b placed transversally to the capacitative bridge

- 35 -

formed by C3 and C5 and in parallel with the charge pack CP at the output from the rectification bridge formed by D5, D6, D2, and D3. This second capacitative bridge is so disposed as to have its centre point connected to the anode A through
5 capacitor C5. If the axial member of the tube T were to connect to the junction of D2 and D3 instead of at the junction D5-D6, the function of bridge C7a and C7b would be connected to the cathode C through capacitor C3. The capacitative bridge is insulated from the charge pack whose
10 voltage it stabilizes, by rectifiers D7 and D8, which also prevent leakage of charge across C7a and C7b. The anode and cathode oscillations generated by the electrostatic charge transduction through C3 and C5 into the poles of the charge
15 bridge, at the outputs from the rectification bridge, of which the oscillation has to become split between the bridge inputs into half-waves, for electrostatic transduction and full wave rectification to occur. In fact, under these conditions, removal of the C7 bridge will suppress the PAGD
20 phenomenon, unless other circuit variables are also altered. The transversal bridge is thus an essential piece of this novel circuit. Variations in the circuit as shown in Fig. 27 were then studied, the first two being selectable utilizing switch S2 (Fig.23).

25 The presence of the capacitative bridge effectively reduces the dynamic impedance of the charge pack CP so that the output circuit approximates to a characteristic in which it presents a very high impedance to the tube T at potentials below a certain level, and a very low impedance at potentials
30 above that level.

With this modified circuit, more effective recovery of the energy produced by collapse of the PAGD pulses is possible with more effective isolation from the input circuit utilized to trigger the pulses. Under these conditions, the
35 energy captured by this circuit at the output, is not

- 36 -

directly related to that utilized in triggering the pulses from the input. The attainment of this condition critically depends on the appropriate sizing of the C3 and C5 capacitances and on the large capacitance of the transversal
5 bridge being able to transfer the output energy from the tube T into the charge pack CP. We have found, as will be shown below, that the large peak pulse currents released by collapse of the PAGD pulses released more energy than is used to trigger them, and these findings appeared to tally with
10 other observations (abnormal volt-ampere characteristics and anomalous pulse currents, etc.) associated with the anomalous cathode reaction forces that accompany the auto-electronic emission-triggered PAGD regime. Experiments so far indicate that the power output can be increased proportionately to the
15 series value of C3, C5 and the two identical C7 capacitors.

The circuits shown in Figure 24 represent various ways of connecting the plasma reactor in the circuit of Figure 23: Figure 24A, a plate diode; Figure 24B, triode; and Figure 24C

20 The circuits of Figures 23 and 24 can be integrated with electromechanical recovery as described above, as shown in Figure 25, in which a part of the energy recovered can be shunted by the switch S4 into an induction motor M1 having a rotor R, to a degree determined by the adjustment of
25 potentiometer R4 and the value selected for C4.

The circuit of Figure 25 can be further developed as exemplified in Fig. 26 to include configurations which provide switching permitting interchange of the functions of charge packs and the drive packs, it being borne in mind that
30 the nominal potential of the drive pack must be substantially higher than that of the charge pack, the former needing to exceed the breakdown potential of the tube at the beginning of a PAGD cycle, and the latter to be less than the extinction potential.

- 37 -

Figure 26 essentially represents a duplication of the circuit of Figure 28, with the output from the two reactors being placed in series, the two circuits however sharing two identical battery packs BP1 and BP2, and being provided with a six pole two way switch, the contact sets of which are identified as S1, S2, S3, S4, S5 and S6. When the contacts are in position A as shown, battery pack BP1 acts as a drive pack for both circuits which may be commutated by electronic switches, with the upper half (as shown) of the battery pack BP2 forming the charge pack for the upper circuit, and the lower half forming the charge pack for the lower circuit. When the pack BP1 is at least partially discharged, the switch is thrown so that contacts move to position B, which reverses the function of the battery packs thus allowing extended operation of the motors in each circuit each time the switch is thrown.

Based on the manufacturer's data, and using current values within the range of our experimentation as discussed in the next sections, an optimal discharge cycle for a fully charged 6.0Ahr battery pack at 0.300A draw is 20 hours, as claimed by the manufacturer, and this corresponds to a cycling between 100% (12.83V/cell open circuit and load short voltage) and <1% (10.3V/cell load voltage) of the battery's absolute charge capacity. Even though the discharge mechanism is a time cumulative process with a logarithmic action, the discharge can, within 4 to 5 hour time segments (or periods with 20-25% of the full range), be regarded as practically linear with time. This trait, or linearization of the discharge slope, becomes more marked with advancing age and decreasing absolute storage capacity of the cells.

The proportionality between open circuit voltage and the percentage of residual relative capacity for these cells when new (uncycled and not yet aged) is uniform over 98% of the permissible charge capacity withdrawal; in practice this translates into a slope that becomes steeper

- 38 -

with time, while the absolute storage capacity diminishes. In turn, this decreasing absolute capacity of the cells results in shorter load discharge times and their further linearization.

5 A circuit in general accordance with Fig. 23, employed in the studies reported in this and the following sections, utilizes a drive pack of 46*12V Lead acid gel-cells each with a 6.0Ah rating, and a charge pack with 28 or 29*12V identical cells. The charge pack was cycled anywhere from
10 11.2V to 12.8V/cell (open circuit voltages), within the proportional region of the relative capacity slope, to yield a capacity increment in the order of 50% (eg. from 20 to 70%), anywhere within the range of 2 to 100% of its total charge capacity, assumed for now as invariant. The charging
15 process, hereinafter referred to as a PAGD run, took about 20-30 minutes under optimal conditions. The drive pack typically consumed, in the same period of time, 4 to 11% of its initial total capacity, its open circuit voltage typically falling 0.1 to 0.2 V per cell after a PAGD run,
20 within the open circuit range of 12.8V/cell (100% relative capacity) and 11.2V/cell (~2%). At the 100% capacity benchmark, the drive pack would theoretically have $20\text{h} * 46\text{cells} * 12.83\text{V/cell} * 0.3\text{A} = 3.5\text{KWh}$, and the charge pack, for example, $20\text{h} * 29 * 12.83\text{V/cell} * 0.3\text{A} = 2.2\text{KWh}$. Since the
25 capacity per cell is linear with the open circuit voltage within the proportional range, as claimed by the manufacturer, we projected the open circuit voltage intercepts on the manufacturer's proportional curve in order to determine the residual percentage of the total relative
30 capacity and the standard hours of operation left, from any experimental open circuit voltage measurements.

Three pulse generators (2*128cm² and 1*64cm² plate areas) were employed in these studies; they were operated in PAGD runs at 1-120 pulse/second rates, within a negative
35 pressure range of 0.2 to 0.8 Torr and with applied direct

- 39 -

currents of 0.2 to 0.6A.

Both drive and charge packs utilized cells which were bought new at the same time and had initial charge values of 12.4 to 12.55V/cell (open circuit). These
5 batteries are capable of energy densities of 33-35 Whr/kg. However, the experiments shown in Table 4 are selected from a series that spanned nearly 12 months, beginning 6 months after purchase; hence, loss of absolute storage capacity by the batteries had occurred in the intervening time, as a
10 function of both age and charge/discharge cycle life.

Measurements of the open voltage of either drive (D) or charge (C) (see column 2, Table 4) packs for 8 separate experiments, all utilizing the triode configuration, were performed before (b) and after (a) a PAGD run (see
15 columns 3 and 4), at either 15 or 30 minutes (see column 26) of the open circuit voltage relaxation after a PAGD run was terminated. Corresponding open circuit voltages per cell are shown in column 5, and the percentages of the predicted total relative charge capacity resulting from the intercepts on the
20 manufacturer's proportional curve are shown in column 6, Table 4. Equivalent maxima for the theoretical hours of operation left are shown in column 7, the percentage change in relative capacity arising as a consequence of either charge pack charge capture (capacity gained) or of drive pack
25 output (capacity lost) is shown in column 8. Translating the intercepts into power units yields the values shown in column 9, Table 4, for total kWh left in each pack before and after PAGD production, those shown in column 10 for the actual power gained and lost during the periods of operation
30 (presented in column 12) and those shown in column 13 for the power predicted to be gained or lost per hour of PAGD production. On the basis of the experimental open voltage values and their intercepts, the predicted net kWh values per hour of PAGD energy production (after deduction of measured
35 losses) and the corresponding experimental breakeven

- 40 -

efficiencies (where breakeven=100%) are presented, respectively, in columns 14 and 15. The PAGD frequency per second is shown in column 11; the number of 12V cells, in column 16; the tube ID, in column 17; the cathode (and anode) area (s), in column 18; the plate material, in column 19; the input ballast utilized (R1, Fig. 23), in column 20; the size of each capacitor (C3 or C5) of the tube output bridge, in column 21; the size of each capacitor (C7a or C7b) of the transversal capacitative bridge, in column 22; the status of S4 and thus, of the parallel and auxiliary electromechanical arm (see Fig. 25), in column 23; the negative air pressure in column 24; the gap distance between the plates, in column 25; and columns 27,28 and 29, show the status of the elements of the switched on parallel electromechanical arm of the circuit- the parallel C4 capacitor, the motor input resistor R4 and the motor revolutions per minute (measured stroboscopically), respectively.

From these figures of Table 4, and utilizing the data for the two first examples shown, we calculated the predicted performance of the system based on the open voltage measurements. In the first example, where the system was run continuously without interruption, the charge pack increased the percentage of its total capacity by 43% (a two-fold increase in capacity) and, during the same period, the driver pack decreased the percentage of its total capacity by 7% (a ~10% decrease in capacity relative to the percentage of residual total capacity at the start, ie. 77%) (cp. columns 6 and 8, Table 4). Subtracting the predicted initial total energy (0.835KWh) available to the charge pack before the experimental run (first line of column 9, Table 4) from the predicted total energy (1.823KWh, second line of column 9) available to the charge pack after the PAGD charge run, gives us the total energy gained by the charge pack: 0.988 KWh (column 10) in 21.5 minutes (column 12) of continuous PAGD performance. Conversely, subtracting the predicted final total energy (2.4 KWh) available to the driver after the

- 41 -

experimental run (fourth line of column 9, Table 4) from the predicted total energy (2.66KWh, third line) available to the driver before the PAGD charge run, gives us the total energy lost by the drive pack: 0.26KWh in 21.5 minutes. If we
5 divide the total available energy gained by the charge pack, by the total energy lost by the drive pack, we obtain a surplus factor of 3.9x, or 388% of the breakeven point (column 15). The same values result from dividing the charge pack % of total capacity gain by the drive pack % of total
10 capacity lost, and then downscaling this value by multiplying it by the typical scale factor for the two packs, $29/46 = 0.63x$.

In an analogous fashion, we analyzed the results for the second example shown in Table 5. Here, the charger
15 increased the percentage of its total capacity by 45.5% (a 22.75 fold increase in estimated total relative capacity) and, during the same period, the driver decreased the percentage of its predicted total capacity by 7% (a ~17.5% decrease in capacity relative to the percentage of residual
20 total capacity at the start, ie. 40%). By dividing the predicted total available energy gained by the charge pack (0.962KWh/18 minutes) by the expected total energy lost by the driver pack (0.246KWh/18 minutes) we obtain a surplus factor of 3.9x, or 391% of the breakeven point. This
25 corresponds to an interrupted, total sequential run of 18 minutes, each minute-long run being separated by a cooling and voltage relaxation period of 15 minutes before the next run is carried out, at an average PAGD frequency of 61 PPS.

30 Analysis of the remaining results illustrates how a number of PAGD controlling parameters interact to determine conditions for effective maintenance of a PAGD regime. The lower gain and higher loss per unit time registered for the third run of Table 4, which results in the lower breakeven
35 efficiency of 230% and a smaller net power production rate than before (power estimates of 1.396 kWh/h of PAGD operation

- 42 -

vs 2.387kWh/h, for the second run, Table 5) illustrate, for example, the combined effect of lowering the pressure (0.8 to 0.7 Torr) and running the PAGD continuously (the heating effect), both of which depress the PAGD frequency. The
5 fourth run of Table 5 identifies the continuous performance of a "broken in" softer grade of aluminum (column 19), having a lower work-function (as determined from the higher PAGD frequency spectrum) than the harder H34 plates of the previous examples, and shows that, despite the series value
10 of the total capacitance being higher (5,333 mfd vs 4,030 mfd for runs one through three), and despite the higher vacuum (0.2 Torr), the lower work-function results in a higher frequency; however, even though this run registers a predicted higher breakeven efficiency (310%) than the
15 previous experiments, these conditions result in a 4/5-fold lower estimate of net power produced, when compared to the previous three PAGD runs.

PAGD runs 5 and 6, Table 5, illustrate the effect of switching on the auxiliary electromechanical arm of the
20 circuit shown in Figure 28. Increasing the amount of charge capacitatively shunted into the electromechanical arm by higher C4 values (column 27), and increasing the current that feeds the squirrel cage induction motor utilized by lowering R4 (column 28), results in a power capture by the charge pack
25 that registers an energy loss (predicted to be 96% efficient, falling short 4% of breakeven recovery), as most of the tube output power is spent in the electromechanical arm and its motor effect. Furthermore, under the conditions of maximum electromechanical action, the drain imposed on the drive pack
30 becomes considerable (see loss in columns 10 and 13), even if the C3 and C5 values are reduced, column 21, Table 5). These runs also illustrate how the motor appears to function as an electrical induction generator having rpm values much higher than the synchronous values prescribed by
35 the frequency of the PAGD (column 29, Table 5).

- 43 -

The extremely large breakeven efficiency of PAGD run 5, Table 5, indicates that with selected values of C4 and R4, it is possible to operate the motor in the auxiliary arm and still accumulate excess energy from the PAGD production
5 in the charge pack.

Runs 7 and 8 illustrate results obtained for 64cm² plates, and a shorter interelectrode gap distance, for two pressures (0.8 and 0.5 Torr), the device being open to a rotary pump manifold in the first instance and sealed from
10 the pump, in the second case. Despite the lower vacuum, the higher pulse frequency (32 vs 5PPS) and breakeven efficiency (906% vs 289%) registered by run 8 when compared to run 7, are a consequence of the method of run 8, which was interrupted systematically by 5 passive cooling periods, as
15 in the case of run 2, whereas run 7 was continuous. This again resulted in higher average PAGD frequencies (at lower pressures), a predicted two-fold greater gain and a predicted two-fold smaller loss (columns 13 and 14) for run 8.

Fig. 27 shows curves representing the slopes of
20 the open circuit relaxation voltages, which are linear with the log of time T in minutes elapsed from cessation of discharge, for both drive and charge packs, in the same run 8 set out in Table 5. The experiment in its entirety consisted of preliminary resistor-loaded measurement
25 discharges and their corresponding open circuit voltages from the moment of cessation of the resistive discharge (illustrated, respectively, by the open squares of DPT1 for drive pack relaxation time 1, and by the open circles of CPT1 for charge pack relaxation time 1), followed by their
30 relaxation rates in the wake of the PAGD production (the hatched squares of DPT2 for drive pack relaxation time 2, and the hatched circles of CPT2 for charge pack relaxation time 2), and finally, by the relaxation rates from the final resistor-loaded measurement discharges (the black squares of
35 DPT3 for drive pack relaxation time 3, and the black circles

- 44 -

of CPT3 for charge pack relaxation time 3). Discharge resistances were 833 ohms for the charge pack, and 2083 ohms for the drive pack in all cases, corresponding to resistors R3 and R2, respectively, of Fig. 26. This methodology will be examined in greater detail below. It is apparent that, after every load period, be this resistive (CPT1, DPT1, CPT3 and DPT3) or due to PAGD operation (DPT2), the relaxation slope is positive; as shown from slopes CPT1 and DPT1, the log time proportionality of the open circuit voltage relaxation, under these conditions, tends to plateau after ~30 minutes. The exception to this general behaviour lies in the voltage relaxation slope CPT2, which is negative and reflects the charge accumulation occurring in the charge pack and obtained by capture of energy produced during PAGD operation, triggered by the energy drawn from the drive pack during load time 2.

As a first approximation of electrical power generated and consumed by the energy conversion system of the invention, the previous open circuit voltage method is of significance in showing the basic trends involved in interaction of the operating parameters. However, in all likelihood, it overestimates the actual values of electrical power consumed and generated, for a variety of reasons. First, it assumes that the relative capacity scale of the batteries in the drive and charge packs is an absolute charge capacity scale with an invariant maximal charge retention, which it is not; in fact, the absolute charge capacity is itself a variable subject to several factors, such as the cycle life, overcharging or undercharged conditions, cell age, residual memory and the rate of charge and discharge. Hence, the inference of a uniform time scale on the basis of the open circuit voltage/capacity intercepts may not be warranted. Finally, it does not integrate the open voltage decrease over time, and utilizes the specification load current as the average current over time.

- 45 -

In order to obviate these problems, we resorted to other measurement methods.

Direct, instantaneous measurements of the voltage and current characteristics of the PAGD production and capture phenomena being discussed were performed during PAGD runs for diverse sets of conditions. In Table 5 we show these results for two PAGD generators having an identical electrode area (128cm^2) and connected to electrical energy capture circuits of three separate configurations as set forth in Figs. 24A, 24B and 24C and column 2, Table 5. In the configuration of Fig. 24C, or double diode configuration, both electrode plates act as cathodes and the axial member as the anode collector (experiments 1-4, for the H220 device and 13-14, Table 5, for the H34 device). In the configuration of Fig. 27B, or triode configuration, one plate acts as the cathode, the axial member as an auxiliary cathode and the other plate as a collector (experiments 5-9, Table 5). In the configuration of Figure 24A or single (plate to plate) diode configuration, the axial member is disconnected, and the polarity of the plates remain as in the triode configuration (experiments 10-12). All measurements were taken after 1 minute of PAGD operation of the devices, which were, at the start of each run, at room temperature. All cathodes had been previously broken in with $>2 \times 10^6$ AGD pulses. The open circuit voltage of the charge pack was, for all cases, at 359 to 365 volts, before each test. The direct measurements of the PAGD input and output DC voltages and currents were obtained as statistical means of 10 second long measurements, and at no time did the standard error of the plate voltage mean exceed 35 volts.

The air pressure within the tube during these tests is shown in column 3, Table 5, the drive pack DC voltage (X), in column 5, the DC voltage across the plates (Y), in column 6, the drive pack output current (PAGD input current), in column 7, and the drive pack total watts output

- 46 -

is shown in column 8. Columns 9 and 10 show the PAGD voltage (PAGD $V = (X-Y)$) and the value of the PAGD extinction field in V/cm. The recovery values (ie the PAGD output energy) found at the U1-U2 output (Fig. 26), are shown in columns 11 to 13, 5 as the charge pack's E1-E2 input DC voltage, amperage and power (in watts), respectively. The calculated resistance of the entire circuit is given in column 14, the registered PAGD frequencies in column 16, and running conditions in columns 17 to 18. The breakeven efficiency obtained by direct 10 comparison of the electrical power figures for the drive and charge packs, respectively, is given in column 15. This assumes, for purposes of a generalization of power production rates over time, that the quasi-instantaneous, direct measurements here obtained can be translated to outputs 15 obtained per unit time, and thus into direct Watt-hour measurements.

Data from runs 1 through 4 demonstrate that, at these PAGD frequencies, there is no difference between using fast switching (32 nanoseconds) MUR 860 diodes, or regular 20 40HFR-120 silicon diodes, in the rectification bridge of the electrical energy capture circuit, and that the PAGD frequency varies as a function of decreasing air pressure.

Runs 5 to 14 show that, in general, for the same tube, the single and double diode configurations are the most 25 efficient, for the same pressure, the diode configuration typically yields ~1.5-2x larger breakeven efficiencies (cp runs 10-11 and 13-14, with runs 5-9, Table 7). The largest accumulations of power are also registered in the diode mode(s). This trend appears to be a function of the much 30 lower cathodic work-function of the aluminum plates, than of the tungsten of the axial member utilized as an auxiliary cathode in the triode configuration. A feature of the data from these 14 different runs is the consistent excess power outputs (column 15, Table 7) and their narrower range (218 to 35 563%), when compared to those observed with the previous two

- 47 -

methods of experimental analysis.

Run 12, Table 7, shows that the switching on of the electromechanical arm can be performed without entailing a power loss in the PAGD capture circuit, as previously found for run 5, Table 5, utilizing the open circuit voltage method. In fact, with $C4=8\mu F$ and $R4=500\text{ohms}$, the AC induction motor behaves as an electrical flywheel (eg. 2800-3000 rpm for 10 PPS inputs), while the electrical energy capture circuit still registers a sizeable excess electrical power production (compare runs 11 and 12, Table 7). Runs 13 and 14 illustrate how the charge pack's state of charge and its inherent capacitance affects both the PAGD frequency and the power producing efficiency of the entire system: as the charge pack is reduced from 29 to 19 cells, the PAGD generator adjusts by reducing its frequency by an order of magnitude and, while the charge pack input current is greater than before, the drive pack loss becomes still larger and the breakeven efficiency much lower (by $>1/2$, from 563% to 228%). This is because the circuit must translate the naturally larger PAGD amplitude over and above the charge pack potential, into a larger surplus of output current, and in this process becomes less efficient.

If the first measurement method employed (the open circuit method) had to make too many theoretical assumptions about the system's performance under load conditions and hence about its effective charge capacity, in the second method just described, theoretical assumptions were avoided except that, in these measurements, the actual performance of a given battery over time (time of delivery and time of capture) was also ignored; no account is taken of the time-dependent modulation of the PAGD frequency, as effected by certain of the parameters analyzed, namely the charge pack state of charge, the method of sequencing the PAGD runs (continuous vs interruption sequences) and its concomitant heating effects, and the state of charge (load voltage and

- 48 -

current capacity) of the drive pack. Simple and extensive resistive measurement of power lost by the drive pack, and identical extensive measurement of the power gained by the charge pack, for the same experiment and the same singular
5 time of PAGD production, were performed repeatedly to corroborate the previous two approaches. For this purpose, all experiments were designed as a continuous series of sequential phases:

1) before a PAGD run, a resistive discharge was measured
10 across either pack over periods of 1 to 3 hours (utilizing the DP and CP resistances previously reported in the open voltage section) and followed by a 15 to 30 minute open circuit voltage relaxation;

2) then, the PAGD runs were performed, either
15 continuously or as interrupted, composite sequences, and the corresponding open circuit relaxation voltage(s) were measured, after the cessation of the integral PAGD run;

3) finally, resistive discharge measurements, obtained
20 under identical conditions to those recorded before the PAGD run, were carried out for either pack, followed by concomitant battery voltage relaxation rate measurements.

Under these experimental conditions, exact power measurements could be taken from an analysis of the actual battery discharge curves before and after the PAGD run.
25 Based on a comparison of the curve trends of the pre-run resistive discharge of the drive pack with those of the post-run resistive discharge, the effective power drawn (E_c) from the withdrawable power capacity of the drive pack incurred during a PAGD run, was ascertained. This represents
30 the power consumption during the run, and the experimental value thus recorded constitutes the actual power figure that must be matched for breakeven ($\#$) to occur. Hence, the breakeven value equals, by definition, the electrical energy input to the system. Similarly, a comparison of the charge
35 pack pre-run and post-run resistive discharge curve trends identified the effective power (E_p) added to the withdrawable

- 49 -

capacity of the charge pack. This quantity represents the electrical energy recovered during the run. The relation for the two quantities is expressed by the breakeven efficiency (BE=#%) equation:

5 $\# \% = E_p / E_c * 100$

If the breakeven efficiency is less than #%=100, then the apparatus registers a net loss in electrical energy in the CP with respect to the DP. Conversely, if #%>100, then there is a net gain in electrical energy in the CP, as
10 compared to that lost in the DP. For purposes of this analysis, a limit to the minimum withdrawable capacity was placed, from experiment and in agreement with the load current curves of the manufacturer, at 115W for the driver pack (average current of 0.250A, minimum current of 0.230A),
15 and at 90W for the charge pack (average current of 0.375A, minimum current of 0.334A), as a function of both their total cell size (respectively, 46:29) and the difference in the resistive loads employed for the discharge measurements. All cathodes had been broken in, as described before.

20 The results obtained with this fourth method, for six selected experiments with three diverse types of devices (using different electrode plate areas, gap lengths, and electrode work-functions), configured both in the triode or the (single) diode (e.g. Fig. 24B) arrangements, at the
25 indicated pressures, are presented in Table 6. In all cases, a net excess of combined battery pack charge, expressed as electrical watt hours, is registered (columns 8 and 10, Table 8) and the breakeven efficiencies are all >100% (column 10). Experimental groups #1 and #2 again demonstrate that, for the
30 same cathode, the interrupted PAGD sequence method of group #2 (1 minute of PAGD function, followed by a 15 minute relaxation, and so on) yields a higher breakeven efficiency because of the lower losses registered with this minimal plate heating method (column 10, Table 8). Group #3, Table
35 8, shows that the PAGD power production efficiency is also

- 50 -

higher for a lower work-function cathode material (H220 vs H34), being subjected to PAGD auto-electronic conditions at a 4-fold lower pressure than the control groups #1 and #2; however, the lower pressure depresses the frequency and, together with the interrupted PAGD sequencing method, it also lowers the loss, causing an actually much larger breakeven value than registered for the previous two groups. Groups #4 and 5 exemplify the dual effect of lowering both the plate area and the gap distance: the former affects the PAGD event frequency, whereas the latter affects the PAGD amplitude, and thus the capture efficiency of the charge pack. Despite a cathodic work-function practically and operationally identical to that of groups # 1 and 2, these smaller plate area and shorter gap devices utilized in groups #4 and 5, yield 3- to 6-fold lower net power outputs, as well as lower breakeven efficiencies, than the former groups, at the same pressure. Finally, group #6 exemplifies the results obtained for the plate diode configuration, where the frequency is lower (no triggering role for the axial member), and a higher loss leads to the lower breakeven efficiency, comparable to that of the lower area and shorter gap groups #4 and 5.

In order to verify the duration lengths of discharge curves employed in these analyses and experimentally establish the actual charge capacity of the battery packs, calibration resistive discharges, between the maximum charge state and the minimum limits chosen, were performed for each pack with their respective discharge resistances R2 and R3 (see Fig. 23). These discharge calibration curves were plotted for half maximal charge values shown in Figures 28A and 28B, which plot the rate of discharge in DC watts W against time T in minutes. From the curve produced, we have determined the total half-charge capacities of each battery pack to be 1.033 kWh (100%=2.066 kWh) for the drive pack and 660 Wh (100%=1.320 kWh) for the charge pack. Based upon the corresponding maximal (100%) capacity values, we determined the actual percentages of the

- 51 -

relative charge capacities shown in column 5, Table 8, which correspond to the experimental values obtained. We also noted that the curves plotted showed two quite distinct time linear slopes, the slope of the delivery of power per time unit steepening very markedly at the approach to the limits of the permissible withdrawable capacity, occurring at 115W into R2, and 90W into R3.

The pre-PAGD run and post-PAGD run, drive and charge pack discharge curves corresponding to groups #3 and #6, respectively for triode and plate diode configurations, in Table 6, are shown in Fig. 29 (drive pack) and Fig. 30 (charge pack), for group #3, and in Fig. 31 (drive pack) and Fig. 32 (charge pack), for group #6. In all cases, the open symbols represent the pre-PAGD run resistor discharge curves, whereas the closed symbols represent the post-PAGD run resistor discharge curves. The diagonally hatched areas represent power lost in pre-PAGD resistive discharge, the cross hatched area power left in the drive pack after PAGD run and lost in the post-PAGD resistive discharge, and the horizontally hatched area the power gained by the charge pack in the PAGD run and lost in the post-PAGD resistive discharge. In Figures 29 and 31, the narrow area to the right of the cross-hatched area represents power lost during the PAGD. The vertically hatched area in Figure 32 represents power left before the PAGD run. Each Figure plots either drive pack (Figs. 29 and 31) or charge pack (Figs. 30 and 32) DC watts W before and after the PAGD run against time T in minutes.

As a further check on these values, a videographic, frame analysis of measurements for the singular power simultaneities occurring at both ends of the system (drive and charge packs) was performed for various 10 second samples of diverse PAGD runs. A typical example is shown in Figure 33, which plots watts W against time TS in seconds for a sample of the PAGD run designated as #6 in Table 6.

- 52 -

Whereas the drive pack DC wattage spent as input to PAGD production (closed circles) varied from 36.6 to 57.82 watts, by a factor of 1.6x, the DC wattage entering the charge pack as captured PAGD output (open circles) varied more pronouncedly by a factor of 2.7x, from 146.4 to 399.6 watts (all meters were in the same selected ranges of voltage and current) with the semi-periodic, intermittent character of each singular emission, though within specific, ascertainable ranges for both amplitude and current outputs. Assimilation of the singular behaviour of the PAGD in this sample, by a statistical treatment of its variation (n=64), indicates that the operational breakeven efficiency (filled squares) observed during this sampled period lies at $485.2\% \pm 18\%$ with projected 48.3Wh drive pack loss and 221.7Wh charge pack gain. This matches rather closely the observed 483% breakeven efficiency, and the 37.7Wh loss as well as the 182.2 kWh gain for the overall PAGD run reported in group#6, Table 6, and indicates how close are the values obtained by the operational and extensive resistive discharge power measurement methods employed.

Finally, an example of the correlation between the drive pack PAGD load voltage VDC and the charge pack PAGD charging voltage, as a function of the duration T in minutes of the intervening PAGD run between resistive discharge measurements, is shown in Fig. 34, for the PAGD run corresponding to group #4, Table 6.

Using the same pulse generator with H200 AL 128cm² plates, in a double diode configuration, and the same circuit values (but with CP = 23 cells), three experiments were conducted at different PAGD frequencies, as a function of varying air pressure. Analysis of driver pack losses and charge pack gains by the extensive load discharge measurement method, as described before, led to the determination of the gross and net gains (respectively, without and with losses included) per pulse, in milliwatt-hour, for each frequency,

- 53 -

as well as of the gross and net power gains per second of PAGD operation. The results are shown in Table 7. Even though the gross and net gains of power per pulse were observed to increase with decreasing frequency, the gross
5 power gain per unit time increased with increasing frequency. However, this last trend does not necessarily translate into a higher net gain per unit time, because the losses in the driver pack (not shown) also increase significantly with PAGD frequency. These losses are in all probability related to
10 more energy retention by the plasma at higher frequencies when plasma extinction becomes incomplete. We expect net gains to reach optimal thresholds for any given type of circuit configuration set of values and pulse generator dimensions.

15 Certain additional observations made during experiments with the double diode configuration of Figure 23A may assist in understanding of the invention.

1) Replacing residual air with argon gas leads to higher PAGD frequencies, for example with a 128cm² H200 AC
20 plate pulse generator in the double diode configuration (V = 575). At 1 Torr, the pulsation rate went from 20 PPS in air to 1300-400 PPS in argon. With 29*12v cells in the charge pack, input currents ceased to flow into it. Under these conditions, the tube potential across the plates decreased
25 and the drop across the input resistor increased. The value of $E(=V/d)$ became smaller (gap size = 3 cm from plate to axial anode collector), as the extinction voltage decreased.

2) With frequencies of 400 PPS, the currents flowing into the charge pack fell to zero. Replacing a fast-
30 recovery type HFR 120 (1200v, 40A) diode bridge by a type MUR 860 (600v, 16A) diode bridge had no effect. When the amplitude of plate potential oscillations falls below the potential of the charge pack, there is also a tendency to produce arc discharges. For output currents from the vacuum
35 pulse generator to enter the charge pack, the number of cells must be reduced so that the potential of the charge pack is

- 54 -

low enough to admit the transduced currents. A reduction from 29 to 23 cells allowed currents of 250 mA to enter the CP, and further reduction to 19 cells doubled these currents (per polarity arm).

5 3) Our observations show that it suffices under these conditions (CP=19 cells) to increase the vacuum, so that the frequency decreases, and the plate potential and the charge pack input currents increase. At 0.1 Torr, the currents reached 1A D.C. per plate, and at 0.05 Torr, 2A D.C.

10 The interconnection between these factors indicates that the extinction voltage is a function of the PAGD frequency: the higher the PAGD frequency, the lower the extinction voltage, until empirical (in distinction from predicted) VAD field values are reached. As a consequence,
15 the operation of the energy converter system in the PAGD regime requires the start voltage of the charge pack to be adjusted, by varying the number of cells composing it, so that it lies below the lowest extinction voltage of the PAGD, for any given geometry and gap distance.

20 Secondly, as the ion plasma is made more rarefied, the frequency of the emissions decreases, but the peak values of the output voltage and current per pulse increase. The slower the PAGD and the more rarefied the atmosphere, the higher is the output energy produced by the system relative
25 to the input energy.

 Autographic analysis of PAGD-induced cathode craters in H34 plates was performed, and their average inner diameter and maximal depth were determined. Similar studies were performed for PAGD-induced craters in Alzak (trade mark)
30 plates. The secondary craters characteristically found in Alzak plates, along fracture lines irradiating from the main crater, are absent in H34 plates; instead, in H34 plates, one observes a roughened surface surrounding the emission crater, quite distinct from the original rough aspect of the pulled

- 55 -

finish of these hardened aluminum plates. Also unlike the Alzak main craters, the H34 craters often have a convex center occupied by a cooled molten metal droplet, whereas the Alzak craters had a concave, hollowed out aspect.

5 Eventually, as the pitting resulting from PAGD cathodic emissions covers the entire cathode, the metallic surface gains a very different rough aspect from its original appearance. In this process, craters from earlier metal layers become progressively covered and eroded by subsequent

10 emissions from the same cathode. Altogether different is the surface deposition process occurring at the anode; here, the surface appears to become more uniform, through the mirroring and possibly abrasive actions of cathode jets. Macroscopically, with increased periods of PAGD operation,

15 the anode surface appears cleaner and more polished.

With the data obtained by the metallographic method of crater measurement, we estimated the volume of metal ejected from the cathode, by assuming that the crater represents a concavity analogous to a spherical segment

20 having a single base ($1/6\pi * H [3r^2 + H^2]$, where H is the height of the spherical segment and r the radius of the sphere), while disregarding the volume of the central droplet leftover from the emission. The following are mean \pm SEM crater diameters (D), crater depths (H) and maximum volumes (V) of

25 extruded metallic material for two types of aluminum cathodes, Alzak and H34 hardened aluminum, subject to a high input current PAGD:

- 1- Alzak: D-0.028cm \pm 0.003; H-0.002cm \pm 0.0002;
V-6.2*10⁻⁷cm³;
- 30 2- H34: D-0.0115cm \pm 0.0004; H-0.0006 \pm 0.0001;
V-3.1*10⁻⁸cm³;

Accordingly, utilizing plates composed of either material with 3mm of thickness, and thus with a volume of 38.4cm³ per plate and considering that only 2/3rds of the

- 56 -

cathode shall be used (a 2mm layer out of the 3mm thickness), the total number of pulses per plate total (TLT) and partial (PLT) lifetimes is theoretically:

- 1- Alzak: TLT: $6.2 \cdot 10^7$ pulses; PLT: $4.1 \cdot 10^7$ pulses;
- 5 2- H34: TLT: $1.2 \cdot 10^9$ pulses; PLT: $8.1 \cdot 10^8$ pulses.

Typically, an H34 device can produce ~ 0.25 kWh per 10,000 pulses (though we estimate this to be just one fifth of its possible maximum if C3 and C5 values are increased). The corresponding value for a PLT is thus a minimum of
10 1.0MWh/Alzak cathode and of 20MWh/H34 cathode. As the cathode for each combination is only 66.7% consumed, the vacuum pulse generator may continue to be used in a reverse configuration, by utilizing the other plate in turn as the cathode; thus, the estimated minimal values become,
15 respectively, 2.0MWh/Alzak pulse generator and 40MWh/H34 pulse generator. The same rationale applies for the double diode configuration of Figure 24C.

We have in the foregoing examples created a two-ported system for the production of the singular discharge
20 events which we have identified as an autogenous pulsatory abnormal glow discharge regime where the plasma discharge is triggered by spontaneous electronic emissions from the cathode. We have examined the functioning of this two-ported system in order to determine what were the electrical power
25 input and output characteristics of a sustained PAGD regime. Despite the observed variations in net power and breakeven efficiencies measured by the three different methods employed (open voltage measurements, operational power measurements and resistor discharge measurements), all methods indicate
30 the presence of an anomalous electrical transduction phenomenon within the vacuum pulse generator, such as can result in the production at the output port of electrical energy measured and directly captured which is greater than would be anticipated having regard to the electrical energy

- 57 -

input at the input port. With the most accurate of the methods employed we have found typical PAGD power production rates of 200 Wh per hour of PAGD operation, and these may reach >0.5 kWh values.

5 Our systematic approach demonstrates that the most frequently employed method of measuring the charge capacity of batteries by the open voltage values is the least reliable approach for the determination of the actual net power lost or gained by the battery packs used in the system. When
10 compared to other methods, it overestimates net power consumed and produced by up to 10 fold, as well as it distorts the breakeven efficiencies, particularly at the extremes of operation. All this results from the grossly diminished (50-60% of manufacturer's theoretical estimate)
15 effective charge capacity of the lead acid gel cells employed, as determined experimentally, when compared to the theoretical maximal charge capacity values that serve as scale for the open voltage measurements. In other words, the effective energy density of the batteries during these
20 experiments was in fact approximately half of the manufacturer's estimated 30Wh/kg.

 Under these actual conditions of battery performance, the second and third methods (respectively, operational and extensive resistor discharge measurements) of
25 power consumption and production proved to be the best approach to measure both PAGD electrical power input and output, as the results of both methods matched each other closely, even though the former is a statistical treatment of simultaneous events and the latter is a real time integration
30 of their cumulative effects on the battery packs.

 The main advantage of the third method is that it effectively takes into account the actual time performance of the batteries comprised by the overall PAGD production and capture system we have described. As such, the method may

have the main disadvantage of reflecting more the limitations of the batteries employed (their high rate of degradation of the absolute value of total effective charge capacity, and limited efficiency in retaining charge derived from
5 discontinuous input pulses) than indicating the actual power output. There are a number of possibilities for fine tuning of the system introduced by the present work, beginning with the utilization of secondary batteries or other charge storage or absorption devices (e.g. flywheels) that have less
10 variable or more easily predictable actual charge capacity. In this respect, there are two major shortcomings to the batteries used to form the drive and charge packs; (1) their significant memory effect and (2) their design for constant, rather than discontinuous, DC charging. Recently developed
15 Nickel Hydride batteries are an example of an electrostatic charge-storage system that lacks a substantial charge memory effect, and experimental batteries are being developed currently for higher efficiency intermittent charging methods. Electrostatic charge retention systems having
20 higher energy densities, better charge retentivities and insignificant memory effects will probably be more efficient at capturing and holding the energy output by the circuit. In practical embodiments of the invention, effectiveness in charge utilization will be more important than measurability,
25 and any device that will use the energy effectively whilst presenting an appropriate back EMF to the system may be utilized.

The effect of the performance characteristics of the drive and charge packs is only one amongst many
30 parameters affecting operation of the invention. As shown by our extensive investigation of the diverse PAGD phenomenon the recovery of energy from it by electromechanical transduction as described with reference to Figures 3-14 above, or electrostatic capture as described with reference
35 to Figures 14-34, the factors involved in modulating the frequency, amplitude and peak current characteristics of the

- 59 -

PAGD regime are complex. Manipulation of these factors can improve electrical energy recovery, or reduce it or even suppress PAGD. We have so far noted numerous factors that affect PAGD frequency and some amongst those that also affect
5 the PAGD amplitude. Aside from these factors, the circuit parameters of the output port portion of the circuit, in addition to the nature and chemical characteristics of the battery cells already discussed, the charge potential of the charge pack, and the effective values of the parallel and
10 transversal capacitance bridges can all influence the results achieved. Certain factors however have a radical effect on PAGD operation, such as the gap distance and the charge pack potential. Too small a gap distance between the cold emitter (cathode) and the collector will reduce the energy recovery.
15 The potential presented by the charge pack must be less than the voltage amplitude developed by the PAGD, as specified by a given gap distance at a given pressure. Too large a charge pack size with respect to PAGD amplitude and the gap length will preclude PAGD production (and the concomittant cathode
20 drop) or result in extremely low PAGD frequencies. In brief, the energy absorption rate and the counter potential presented by the charge pack or other energy utilization device are important factors in the operation of the circuit as a whole, and should either be maintained reasonably
25 constant, or changes should be compensated by adjustments in other operating parameters (as is typical of most power supply circuits).

Since our test results indicate that the electrical power output of the circuit can be greater than the
30 electrical power input to the circuit, the circuit clearly draws on a further source of energy input. Whilst we do not wish to be confined to any particular theory of operation, the following discussion may be helpful in explaining our observations. These observations have been discussed in some
35 detail so that the phenomenon observed can be reproduced, even if the principles involved are not fully understood.

- 60 -

We have identified a novel, cold-cathode regime of vacuum electrical discharge, which we have termed the pulsed abnormal glow discharge (PAGD) regime. This regime, which occupies the abnormal glow discharge region of the 5 volt-ampere curve of suitable discharge tubes, has the singular property of spontaneously pulsing the abnormal glow discharge with an auto-electronic emission mechanism, in a fashion which is endogenous to the tube and its circuit environment that constitutes a vacuum pulse generator device, 10 when it is operated under the conditions we have identified. In fact, when stimulated with continuous direct current, in such conditions, such a circuit responds with spontaneous abnormal glow discharge pulses that enable effective segregation of input and output currents. We have 15 demonstrated electrically, metallographically, oscillographically and videographically, how the pulsed discontinuity results from a self-limiting, autoelectronic cathode emission mechanism that results in repeated plasma eruptions from the cathode under conditions of current 20 saturation of the cathode glow. The auto-electronic triggering mechanism of the PAGD regime is thus akin to that of the high-field emission mechanism thought to be responsible for vacuum arc discharges (VAD regime). However, under the PAGD conditions we have defined, this mechanism is 25 found to operate in the pre-VAD region at very low field and low input average direct current values, with very large interelectrode distances and in a self-limiting, repetitive fashion. In other words, the PAGD regime we have identified has mixed characteristics: its current versus potential 30 (abnormal glow) discharge curve is not only distinct from that of a vacuum arc discharge, but the electrical cycle of the PAGD regime itself oscillates back and forth within the potential and current limits of the abnormal glow discharge region, as a function of the alternate plasma generation and 35 collapse introduced by the discontinuous sequencing of the auto-electronic emission process. Accordingly, the intermittent presence of the abnormal glow, as well as the

- 61 -

observed segregation of the current flows, are due to the diachronic operation of these spontaneous cathode emission foci. The micro-crater and videographic analyses of the PAGD have demonstrated the presence of an emission jet at the
5 origin of each pulse, a phenomenon which VAD theory and experiment has also identified. Metallic jets originating at the cathode spots of VADs have been known to present velocities up to, and greater than 1000m/sec.

In light of the above, the energy graft phenomenon
10 we have isolated would have to be operated, at the micro-event scale, by the interactions of the cathode emission jet with the vortex-formed impulse-transducing plasma in the interelectrode space. Several aspects can be approached in terms of the complex series of events that
15 constitute a complete cycle of operation, on a micro-scale. There are interactions within the cathode, interactions at the cathode surface, interactions between the emission jet and the plasma globule close to the cathode, and finally, interactions of the resulting electron and ion distributions
20 in the interelectrode plasma, within parallel boundaries.

In general, in the presence of an electrical field, the distribution of potential near the cathode forms a potential barrier to the flow of electronic charge, as this barrier is defined by the energy that the most energetic
25 electrons within the metal, the Fermi energy electrons, must acquire before freeing themselves from the cathode surface potential to originate an emission jet. Before any free electrons become available for conduction in the space adjoining the cathode, they must cross the boundary posed by
30 the potential barrier. With a weak applied field, classical electron emission from a metal can only occur if an energy practically equal to the work-function of the metal is imparted in addition to the Fermi energy. Under thermionic conditions of emission, the heating of the cathode provides
35 the needed energy input. However, the cold-cathode

- 62 -

Fowler-Nordheim quantum-field emission theory predicted the existence of a finite probability for an electron to tunnel through the potential barrier, when the applied field is high. Cold-cathode electron emissions are thus possible, 5 under these conditions, at practically Fermi energy levels, as the high field would catalyze the tunnelling through the potential barrier by Fermi energy electrons. The exact localization of the emission would then depend on the randomized fluctuations of high fields at the cathode, which 10 would be produced by positive space charges sweeping in proximity to it. For most purposes, this theory has been the working hypothesis of the last 60 years of field emission studies, which have centered upon the VAD mechanism, despite the fact that observed field gradients are evidently 15 inadequate to explain breakdown as a function of the theoretical high field mechanism. The Fowler-Nordheim theory has therefore suffered major revisions and additions, mostly to account for the fact that it postulates, as a condition for cold-cathode field emission in large area electrodes, the 20 presence of enormous fields ($>10^9\text{V/m}$) and extremely low work functions, neither of which are borne out by experimental VAD investigations. Some researchers have found that the breakdown responsible for the VAD field emission is promoted by Joule heating and vaporization of microscopic emitter 25 tips, and that this requires a critical current density (10^{12}A/cm^2), while others emphasized that this explanation and these thresholds did not hold for large area emitters and that a space charge effect of concentrating the ion distribution near the cathode promoted breakdown under these 30 circumstances, when the field reached a critical value; large field enhancement factors (>1000 -fold) have been postulated to explain the discrepancy between theoretical predictions and experimental findings regarding the critical breakdown field values, and others have demonstrated how this critical 35 field value effectively varies with work-function and electrode conditioning.

- 63 -

The PAGD regime and its self-extinguishing auto-electronic emission mechanism stands as an exception to the high field emission theory as it currently stands with all its modifications, especially given that in this phenomenon we are confronted with a cathode emission that spontaneously occurs across the large gaps in large plate area pulse generators, at very low field values (down to $<1 \cdot 10^4 \text{V/m}$), as shown above. Moreover, a Fowler-Nordheim plot (in the form $\text{Log}_{10} (I/V^2)$ vs $1/V$) of the PAGD volt-ampere characteristic exhibits a positive slope, rather than the Fowler-Nordheim negative slope characteristic of VAD field emission. However, current density values obtained from correlations of autographic analysis of the cathode with an analysis of event-oscillograms (peak pulse currents), indicates that the PAGD current density J may reach values of 10^5 to 10^7A/m^2 during the emission process (the larger Alzak craters have an associated lower J value), values which, at the upper end, do not reach the 10^9A/m^2 current density threshold required by the Fowler-Nordheim theory. Considering these two distinct observations with regards to field strength and current density, we have to admit the existence of a low field, large area cold-cathode auto-electronic emission endowed with high current densities, which is not predicted by current field emission theory.

Unlike the typical VAD regime, the PAGD is neither a high frequency oscillation, nor does it occur in a random fashion. It constitutes a semi-regular, quasi-coherent, periodic energy transduction which cycles between cathode drop limits that are higher by a factor of 2-15 than typical vacuum arc cathode drops. The intermittent cathode emission responsible for the low frequency, pulsed behaviour of the abnormal glow, is also self extinguishing and self-starting, under the conditions we have defined. Furthermore, we have also identified a novel and unexpected dependency in the PAGD regime, of the periodic pulse rate upon the cathode area. This indicates the presence of field emission control

- 64 -

parameters heretofore unsuspected. It is likely that field fluctuations of the polarized pre-breakdown field is responsible for eliciting the particular localizations of the auto-electronic emission foci, as well as what concentrates, the distorted field energy needed for electron surface release. In this sense, external, electrical or magnetic field fluctuations (eg. motion of static charges or of constant magnetic fields) induced by us at pre-breakdown potentials, provoked PAGD emissions and electrical breakdown at these levels.

In general, VAD studies have shown that, for large area electrodes, microgeometry, adsorbed gas layers and gas impurity contents of the cathode play a role in modulating field emission. In our PAGD studies, the interactions at the cathode surface and across the cathode potential drop are clearly modulated by: (1) the nature of residual gases, as shown by our air vs Argon studies; (2) their pressure, (3) electrode conditioning, (4) work-function and (5) cumulative pulse count, amongst others.

The plasma, in leak-controlled or sealed low pressure PAGD devices, has both residual gas and metallic vapor substrates. In devices initially closed at high to very high vacua (diffusion pump pressures), the major residual substrate, whose presence increases with time of operation, is the metallic vapor released from the cathode and not impacted onto the envelope walls or the anode. It has been previously shown for externally (magnetically or electrostatically) pulsed plasma accelerators, that the amount of residual gas or vapor left in the interelectrode space diminishes with increasing number of consecutive discharges and a growing amount of electrode-insulator absorption of gas. The effect of such removal of residual gas or vapor is to decrease the vacuum of a sealed envelope. With high vacuum sealed PAGD generators we have observed that prolonged operation and sputter-induced mirroring of the

- 65 -

envelope causes a progressive disappearance of the discharge, as the voltage potential needed to trigger it also increases. At the thermocouple, low frequency pulsed abnormal glow discharges can also be seen to increase the vacuum significantly. These results suggest instead the presence of a pumping mechanism in the PAGD which is somewhat analogous to that of sputter ion pumps, where collision of ionized gas molecules with the cathode is responsible for the sputtering of cathode material that either combines with the gas substrate ('gettering' action) or 'plasters over' inert gas molecules onto the anode (a process known as 'ion burial'). These are the two basic pressure reducing actions of sputtered getter atoms, in ion pumps. However, in ion sputter pumps, the initiation of the cycle is a function of the presence of high velocity electrons in the high field plasma of the glow discharge, which are necessary to ionize the gas substrate molecules; also, the getter material typically has too high a work-function for field emission. Hence, the sputtering is due to the secondary impact of plasma positive ions at the cathode, after plasma ionization has occurred in the interelectrode space. Altogether different is the mechanism of spontaneous, primary electron emission from the cathode, which is characteristic of the low field PAGD: here, the sputtering is caused by the electronic emission itself and attendant metallic vaporization processes. By artificially confining the firing foci to a part of the cathode, we have shown in the single diode configuration how the PAGD induced sputtering is associated with the cathode autoelectronic emission mechanism, rather than with the abnormal cathode glow per se, given the localization of sputtering onto the emission region of the plate, despite its overall cathode glow saturation.

These observations would thus seem to corroborate the hypothesis of a progressive vacuum increase with the cumulative number of emitted pulses, were it not for the fact that experiments performed with leak controlled devices

- 66 -

(reported here and in previous studies) show that, when the negative pressure is maintained by balanced leak admission of air or argon, pulse rates still decrease with cumulative pulse count, and do so neither as a function of an increase
5 in vacuum, nor as a function of envelope mirroring (unless this is so extensive as to establish envelope conduction), but rather as a function of processes (generally referred to as conditioning) inherent to the electrodes, specifically, to the cathode. We have further shown that, for such altered
10 emitter states, the pressure of the vessel must be increased, not because of an increasing vacuum (precluded by the controlled gas leak), but because of the effect that residual gases may have in modulating the low field PAGD emission.

PAGD electrode conditioning is a cathode-dominant
15 process resulting from the cumulative emission of high numbers of pulses by a cathode, and has been shown to be a factor independent of the nature and pressure of the residual gas and partially reversible only by operation with reversed plate polarity, unlike reports of copper cathode-dominant
20 conditioning. It is thought that electrode conditioning and the accompanying increase in VAD breakdown potential are due to the progressive adsorption of residual gases, though cathode-dominant conditioning processes, such as subjecting the vacuum gap to consecutive discharges, have been shown to
25 correlate the decrease in plasma impulse strength with electrode outgassing of absorbed or adsorbed gases. Moreover, given the pitting action of crater formation at the cathode by the PAGD regime, and, as we shall see below, the metallic plating of the anode, the PAGD cathode-dominant
30 process of conditioning we have observed with respect to decreased pulse frequency and increase in potential, suggests that the apparent increase in cathode work function is not due to gas adsorption or absorption. These processes are more likely to occur on the plated anode. It is likely that,
35 given the observed PAGD pressure reducing effect caused by the cathodic jet, a certain outgassing of the cathode is in

- 67 -

fact occurring during PAGD function. One might also expect that the anode, if plated by sputtering atoms, would increase its gas content in the formed surface film. However, controlled leak experiments suggest instead that some other
5 type of alteration of the cathode work function is occurring, which is, as we shall examine below, independent of the adsorbed gas state of the electrodes, as well as independent of the PAGD ion pump-like effect. Nonetheless, even at the level of the anode, the PAGD sputtering action may have
10 contradictory effects: it may impact interelectrode gap molecules onto the collector, as well as release, by ionic bombardment and vaporization, gases adsorbed to, or contaminating the anode. If we assume that gas adsorption by impact on the collector is the predominant mechanism, one
15 could explain the increase in the number of breakdown sites per unit time, as observed by us for a reversed anode, if the number of PAGD breakdown sites depended on the quantity of adsorbed gases, eg oxygen, on the cathode being tested. Recovery of the cathode work-function would depend on the
20 electronic charge recovery of the positively charged, adsorbed or occluded gas layer at the cathode- either by reversal or as a function of time of inactivity. The surface film theory of 'electrical double layer formation at the cathode' in fact contended that 'low field flash over' is a
25 photocathodic effect dependent upon the presence of a glowingly positively polarized gaseous film at the cathode; this film would lower the cathode emissivity by decreasing the field between the cathode surface and the leading edge of the cathode glow, across the cathode drop. However, even
30 though the surface film theory of 'electrical double layer formation at the cathode' predicts the lowering of the emission breakdown potential and the increase in 'flash over' rate when the electrodes are reversed - as the anode would have acquired a surface charge capable of affecting the
35 breakdown potential, it acknowledges nevertheless, that the anodic surface charge hardly explains the observed intensity of the polarization effects observed in flash over. Moreover

- 68 -

non-reversed, conditioned cathodes retained their lower PAGD frequencies in a time independent manner, for as long as reversal was avoided (excluding a PAGD frequency recovery effect due to plate cooling, which may be as short as 15 minutes). PAGD conditioning was independent of idle time and increased with cumulative pulse count. Moreover, the AGD pulses are not UV photocathodic Townsend discharges, liberating secondary electrons via positive ion impact at the cathode. Nor could photocathodic emissions generate currents of the magnitude observed in the PAGD. Lastly, the PAGD discharge and breakdown thresholds appear to be unaffected by UV, though they may be somewhat depressed by visible light, and the emission mechanism in the PAGD is the primary process.

Removal or flattening of protuberances and tips from the emitting cathode by the action of the discharge, is a process also thought to play a role in hardening the cathode or increasing its field emission work-function. However, this explanation may not be adequate for the PAGD emission process, if we consider our metallographic findings of a smoothing action of the discharge at the collector. This then could not explain how a cathode partially recovers its work function after its utilization as a collector. In fact, it would appear that the flattened, smoother, plated, mirrored and cleaner surfaces subjected to PAGD bombardment are the explanation for the observed increased emission ability of re-reversed cathodes: mirrored Alzak surfaces emit at higher frequencies than do dull H34 and H220 surfaces; new, polished surfaces emit at a higher frequency than do pitted, broken in surfaces; anode surfaces, never before utilized as cathodes but subjected to prolonged PAGD action, emit at higher frequencies when employed as cathodes, than do new, identical cathode surfaces; and ex-cathodes, employed for prolonged periods as anodes, regain a higher emission frequency upon re-use as cathodes. The better PAGD emission performance of smoother cathodes, compared with the worse VAD

- 69 -

emission performance of the same, when pitted cathodes (lacking protuberances) are used, requires explanation.

Rakhovsky has put forth a VAD model for cathode spots, that distinguishes between Type I spots (quickly moving spots, far from steady state and responsible for crater formation), and Type II spots (quasi-stationary and near steady-state, but leaving an itinerant track with no sign of crater formation). Whereas the former would obey the Fowler-Nordheim requirement for high fields ($>10^9\text{V/m}$), the latter could hardly be expected to do so with typical arc voltage drops in the order of 10V. Once again, autographic analysis of the PAGD emission aspect indicates mixed characteristics: the PAGD cathode spot is a hybrid. It behaves as an intermittent instability that leaves single (eg. in H34) or clustered (eg. in Alzak) craters, which are both qualities of Type I cathode spots; and it exists under low field conditions ($<10^5\text{V/m}$), with cathode drops of 20 to 150V, in a quasi-coherent mode, leaving an itinerant track of successive craters when operating at the higher frequencies, all of which are properties approaching those of a VAD Type II cathode spot. Furthermore, the macroscopically visible metal sputtering (due to the explosive action of the PAGD emission phenomenon) occurring at the upper end of the permissible DC current input scale, and the presence of large solidified molten metal droplets in and around the craters, suggest models which have been proposed for explosive electronic emission. Explosion models propose that the creation of a residual plasma ball in front of a microprotuberance provokes the large potential drop at the prospective emission focus and sufficiently high resistive and Nottingham heating to reach $>10^7\text{A/cm}^2$ current densities during the explosive consumption of these microemitters. Whether the explosive action associated with cathode spots is an auxiliary effect that applies solely to the vaporization of the emitting microprotrusion, or an integral emission and vaporization explosive process, it does not appear that it

- 70 -

can be restricted to high-field VAD Type II cathode spots, given that it can be equally made to occur with the low field PAGD hybrid cathode spot, and be macroscopically observed. Indeed, in the plate diode configuration, it is easy to
5 visualize the metallic particle explosions that surround and accompany the plasma jets, near to upper current limit conditions for PAGD operation. However, if we are to assume that any of these models apply to the emission mechanism, we would, in all likelihood, have to conclude that the PAGD
10 initial emission sites must be submicroscopic (100 to 10 nm), rather than microscopic. Resolution limits to our own metallographic examination of the smoothing action of the PAGD discharge on the collector would thus have precluded us from detecting formation of such submicroscopic protrusions,
15 as well as their presence in a 'soft' cathode- and thus infer their disappearance from a pitted, hardened cathode; but if the disappearance of such submicroprotuberances were responsible for the observed alteration of cathode work function, one would also thereby have to postulate the
20 existence of a mechanism for microroughness regeneration (eg. tip growth) at the anode, in order to explain the observed increased emission upon cathode re-reversal. Furthermore, this regeneration would have to be actively promoted by operation with reversed polarity, and this is problematic.
25 Focusing of the distorted or magnified field upon alumina inclusions on pure iron electrodes has been demonstrated to degrade breakdown voltage for field emission, but the effect was greater for larger microscopic particles. If we were to apply this concept to our work, it would require the
30 existence of unmistakably abundant microscopic heterogeneities in the quasi-homogeneous electrode surfaces employed, which we did not observe; on the contrary, their absence suggests that either the microroughness responsible for the low field PAGD emission is submicroscopic, or that
35 the field distortion responsible for eliciting the PAGD is independent of the presence of these protuberances. This last possibility must be taken all the more seriously, in

- 71 -

light of the fact that PAGD functioning is able to cover with craters the entire surface of an emitter.

Whereas the discharge potentials observed in the PAGD have been shown to be relatively independent of the kind of gas present, there is a gas effect in the PAGD phenomenon, particularly in what concerns its frequency, observed when the same 'run down' cathode was capable of much higher emission rates when exposed to argon, than to air. Utilizing the technique of bias sputtering, it has been demonstrated that the number of charge symmetric collisions (dependent upon sheath thickness d and the ion mean free path) in the plasma sheath, which are responsible for lower energy secondary peaks in ion energy distribution $N(E)$, at pressures of 0.2 Torr, is substantially greater in argon than in argon-nitrogen mixtures, and thus that, under these conditions, mostly Ar^+ and Ar^{++} ions impact the negatively biased electrode. In non-equilibrium RF discharges, greater ion densities have also been attained with argon, than with air. With respect to field emissions, one would expect a gas effect only with regards to changes on surface conditions, though such studies have shown contradictory effects of argon upon cathode work function. In light of the foregoing, and given that the PAGD is an emission discharge and not a sputtering discharge per se, in the strict sense, we can conceive of the role of inert gas atoms in increasing, as compared to air or nitrogen, the ion energy density distribution at the PAGD cathode spot interface with the cathode surface emitter, and thus elicit increased emission rates from the cathode, by pulling electrons from the metal via the field effect. While this is consistent with the concept of focused distortions of space-charge field fluctuations inducing localization of the emission foci, the argon effect can be observed in the PAGD regime over the entire range of the Paschen low vacuum curve, and into Cooke's mid to high vacuum curve, at low fields and without negative biasing. Thus, it is not simply a high pressure

- 72 -

(nor a gas conditioning) effect, even if the gas effect in question applies to the description of a local pressure rise at the emission site/cathode spot interface, which may play a role in enhancing the local field.

5 Considered together, the PAGD emission-derived sputtering, the observed metallic plating of the anode and the explosive aspect of the discharge, suggest the presence of a jet of metallic vapor present in the discharge and running, contrary to the normal flow of positive ions, from
10 the cathode to the anode. This jet appears to have properties similar to the high speed vapor ejected from the cathode in a VAD, as first detected by Tanberg with his field emission pendulum (Tanberg, R (1930), "On the cathode of an arc drawn in vacuum", Phys. Rev., 35:1080). In fact, the VAD
15 high field emission process is known to release, from the cathode spot, neutral atoms with energies much greater than the thermal energy of the emission discharge. This anomalous phenomenon brings into play the role of the reported cathode reaction forces detected in vacuum arc discharges (Tanberg,
20 as above, also Kobel, E (1930), "Pressure and high vapour jets at the cathodes of a mercury vacuum arc", Phys. Rev., 36:1636), which were thought to be due to the counterflow of neutral metallic atoms, from the cathode onto the anode (ions are normally expected to target the cathode). In absolute
25 units of current, this current quadrature phenomenon has been shown to reach, in the VAD regime, proportions of the order of $100 \cdot I^2$ (see also the Aspden papers referenced below). Early interpretations attributed this to the cathode rebounding <2% of positive ions hitting it and being charge
30 neutralized in the process, but having kept most of their thermal energy. Tanberg held instead that the counterflow of neutral particles responsible for the cathode reaction force was cathode derived, and effectively, that it constituted a longitudinal interaction acting in the direction of the
35 metallic arc jet flow cathod to anode. However, even though secondary high energy distributions of neutral atoms

- 73 -

emanating from the cathode do not have thermal energies, their modal distribution does (Davis, W.D. and Miller, H.C. (1969) J. Appl. Phys., 40:2212); furthermore, the major anomalous atomic counterflow that accompanies the high energy
5 electron flow toward the anode, was shown mass spectrographically to consist predominantly of multiply ionized, positively charged ions of cathode metal, rather than neutral atoms. If this made it easier to abandon the primacy of the rebounding model, it was now more difficult
10 for field emission theorists to accept and explain the observed high energies (ion voltages in excess of the discharge voltage drops) and the high ionization multiplicity associated with these counterflowing positive ions. This field of investigation has indeed been one of the mounting
15 sources of evidence suggesting that there is something amiss in the present laws of electrodynamics. The anomalous acceleration of counterflowing ions, and the energy transfer mechanisms between high speed or 'relativistic' electrons and ions in a plasma (Sethian, J.D. et al, "Anomalous Electron-
20 Ion Energy Transfer in a Relativistic-Electron-Beam-Heated Plasma" Phys. Rev. Letters, Vol. 40, No. 7, pages 451-454), in these and other experiments, has been brilliantly addressed by the work of the British physicist and mathematician, H. Aspden, who first proposed a novel
25 formulation of the general law of electrodynamics capable of accounting for the effect of the mass ratio factor (M/m') in the parallel (and reverse) motion of charges with different masses, (Aspden, H. (1969) "The law of electrodynamics", J. Franklin Inst., 287:179; Aspden, H. (1980) "Physics Unified",
30 Sabberton Publications, Southampton, England). The anomalous forces acting on the counterflowing metallic ions would stem from their out of balance interaction with the emitted high speed electrons, as predicated by the electrodynamic importance of their mass differential. This results in a
35 fundamental asymmetry of the plasma flow between electrodes, localized onto the discontinuous interfaces of the plasma with the electrodes, namely, in the cathode dark space and in

- 74 -

the anodic sheath: on the cathode side, electrons act upon ions, as the emitted electrons having less than zero initial velocities, drift against the incoming ion flux and in parallel with the ion and neutral counterflows; on the anode

5 side of the discharge, positive ions flowing toward the cathode confront mainly the incoming counterflow of positive ions and neutral atoms, as the high speed electrons have abnormally transferred their energy to counterflowing, high speed, cathodic metal ions. An out of balance reaction force

10 thus results at the cathode, to which the leaving metallic atoms impart a force of equal momentum but opposite direction, a force which is added to the cathode momentum generated by impacting, normal flowing positive ions. Moreover, Aspden confirmed theoretically the fundamental

15 contention of Tanberg's experimental findings that an electrodynamic force will manifest itself along the direction of the discharge current flow. Aspden further demonstrated that this asymmetry of plasma discharges does not imply any violation of the principles of conservation of energy and

20 charge equivalence, given that there will be no out-of-balance force when such anomalous forces are considered in the context of the whole system of charge which must, perforce, include the local electromagnetic frame itself. Such discharges must be viewed as open energy

25 systems, in balance with their electromagnetic environment: their apparatuses may constitute materially closed or limited systems, but they are physically and energetically open systems. Current work on Aspden's formulation of Ampere's Law indicates that both classical electromagnetism and

30 special relativity ignore precisely, in circuits or in plasma, the longitudinal interactions that coexist with transverse ones. Standing longitudinal pressure waves, of a non-electromagnetic nature, have been previously shown in plasma electrons, which did not conform to the Bohm and Gross

35 plasma oscillation mechanism (Pappas, P.T. (1983) "The original Ampere force and Bio-Savart and Lorentz forces", *Il Nuovo Cimento*, 76B:189; Looney, D.H. and Brown, S.C. (1954)

- 75 -

"The excitation of plasma oscillations", Phys. Rev. 93:965).

The present theoretical approach to the novel regime of electrical discharge which we have isolated in specially designed devices, and to its mixed glow-arc characteristics, suggests that a similar, out-of balance current quadrature phenomenon occurs in the discharge plasma during the low field, autoelectronic emission-triggered PAGD, and is responsible for the observed surplus of energy in the experimental system described in this application. Clearly, all the evidence we have adduced indicates that there is a powerful longitudinal component to the emission-triggered PAGD, ie that the discharge pulses characteristic of this pre-VAD regime are longitudinally propelled jets of cathode-ejected high speed electrons and high speed ions. We have performed experiments, in the PAGD regime of operation, with very thin axial members that bend easily when placed in the path of the discharge, or with Crooke radiometer-type paddle-wheels, and both show the presence of a net longitudinal force in the plasma discharge acting in the direction of the anode, which confirms the magnitude of the atomic counterflow (ionized and neutral) present during the PAGD, very much like Tanberg's pendulum did for the VAD. These observations also tally with the explosive action of the emission mechanism, such as we have examined it above. In this context, two aspects of the PAGD are remarkable: the fact that a phenomenon akin to field emission occurs at low field values, for large area electrodes across large gaps, and the conclusion that the PAGD must deploy an excessively large counterflow of, in all probability, both ionized and neutral cathodic particles. The observation of ion current contributions to the cathode current in the order of 8 to 10%, in VADs, can hardly apply to the PAGD mechanism responsible for the anomalous currents and counterflows observed. Hence, we should further expect that the characteristically intermittent, or chopped current regime of the PAGD, is a major factor in the generation of

- 76 -

disproportionately high energy longitudinal pulses and in allowing our system to capture most of the electrical energy output from the device. In all probability, field collapse at the end of discharge favours the nearly integral
5 collection of the plasma charge, and ensures the transduction of most of the plasma energy of the pulse (blocked, as it is, from flowing back through the input port to the drive pack) to the output port, through the parallel, asymmetric capacitance bridge that interfaces with the charge recovery
10 reservoir (the charge pack). Collapse of the field of the discharge may also be a contributing factor to the anomalous acceleration of ions, and to the observed anode plating effect. It is equally possible that such abnormally large longitudinal pulses may never be observable, for a given
15 arrangement and scale, above threshold frequencies of the oscillation; we have, in this sense, presented data that indicates that for a given geometry, above specific PAGD frequencies, the capture of surplus energy decreases steadily in efficiency until it ceases altogether, for a given
20 arrangement. The point at which this surplus begins to decrease coincides with the setting in of frequency-dependent irregularities in the discharge sequence and, most importantly, it coincides with a reduction of the peak pulse current for each PAGD pulse. We have further remarked that
25 increasing the PAGD frequency above the zero surplus point, for a given arrangement, by manipulating any of the frequency control parameters, provokes the slippage of the PAGD into a full fledged VAD regime, while input currents greatly increase and output peak currents greatly decrease (to
30 comparable peak input levels of 10 to 15A). The transition between the two modes of emission-triggered discharge, PAGD and VAD, thus appears to be tied in to adjustable thresholds in the frequency of the emission discontinuities; in this sense, it is rather likely that the plasma field collapse
35 plays a major role in regularizing and optimizing the anomalous energies of field emissions, as in the PAGD regime. At low frequencies of low field emission, the emission regime

- 77 -

is highly discontinuous, diachronic and regular, for it has time to fully extinguish the discharge; hence the PAGD singularity, in which the phases of each discharge pulse are well defined and sequential. Above a given high frequency, when ion and electron recombination will happen more often, before each can be collected at the electrodes, the stream of emitted discontinuities merges into a noisy, randomized continuum, where simultaneous emissions and partial plasma reignitions become possible, and the plasma field no longer has time to collapse and fully resolve the longitudinal pulses. Any anomalous energy generated is then minimized and trapped in the plasma body and, in these conditions, the VAD regime eventually sets in. Such model would easily explain why the high field VAD experiments performed to date have never detected such extraordinarily large anomalous forces as those observed by us in the PAGD regime.

The plating observed at the anode most likely results from the impact of counterflowing ions (and possibly neutral atoms), whereas the pitting of the (locally molten) cathode results from the emission of vaporized metallic material and electrons, as well as, secondarily, from bombardment by incident positive ions. The first action smooths the surface by mirroring it (deposition of cathode-derived atoms) and abrading it, whereas the latter smooths it in places by rounding concavities and by forming molten droplets upon local cooling, while simultaneously roughening it on the crater peripheries. One might think that this cathode roughening should lower the work function and facilitate the discharge, but the facts indicate that just the opposite must be happening in view of changes in the PAGD according to the nature and state of the cathode surface. The observed alterations of electrode work function for PAGD low field emission must thus be related to the molecular and charge effects of these different actions at the two electrodes. It appears that for large parallel plate electrodes, the PAGD low field emission is modulated by the

- 78 -

nature and, most likely, by the molecular structure of the metallic surface layer of the emitter.

We have thus devised a system for the capture as electricity of the energy of anomalously energetic
5 longitudinal pulses sequentially triggered by spontaneous emissions of high speed electrons and ions generated from low work function cathodes, during the low field PAGD regime of electrical discharge in vacuo. To confirm the above
10 interpretation of the anomalous flux in the observed PAGD phenomenon, the cathode jet composition, as well as time- and usage-dependent changes occurring in the tubes, with diverse sealed negative pressures and after submission to prolonged PAGD operation, must be analyzed mass spectroscopically. In
15 any event, the excess energy present in the anomalous counterflowing force appears to stem from a discharge mechanism that effectively pulls high speed electrons and constituent atoms out of a metal surface, at low fields and with high current densities, and is modulated by a complex
20 multiplicity of parameters. The system described appears to transduce efficiently the observed nonlinear longitudinal pulse discontinuities of the plasma field, under conditions of current saturation of the cathode, because the self-extinguishing and self-limiting properties of the
25 discharge allows the energy from the collapse of the discharge to be captured. The particular design of the circuitry, which couples a rectification bridge to the asymmetric bridge quadrature of large capacitances, placed at the output of the PAGD generator, permits effective capture
30 (the most immediate effect of increasing the capacitance of all bridge members is to increase the current charging the charge pack). Our findings constitute striking evidence for Aspden's contention of a need to revise our present electrodynamic concepts. The dual ported PAGD discharge tube
35 systems we know of which permit effective exploitation of anomalous cathode reaction forces and allow for the recovery

- 79 -

of electrical energy from systems exhibiting this effect. Any apparent imbalance in the electrical energy input to the system and withdrawn from the system by its operator must be considered in the context of the entire continuum in which
5 the system operates, within which it is anticipated that accepted principles of energy balance will be maintained.

Moreover, the energy conversion system of the invention has substantial utility as an electrical inverter accepting direct current, and providing one or more of a
10 direct current output at lower voltage and higher current, variable frequency input to alternating current motors, and, by suitable combinations of discharge tube systems, more flexible DC to DC conversion systems.

As an alternative to the batteries used in the
15 experiments described, a DC power supply may be utilized or, more advantageously from the viewpoint of entailing less transformation losses, a DC generator to provide the electrical energy input to the system. As a DC motor can be run directly from the rectified output of the circuit of
20 Figure 26 at E1-E2, in place of a battery charge pack, DC motor/generator sets of suitable characteristics (in terms of back E.M.F. and circuit loading) can be used to charge the batteries of the drive pack, utilizing the rectified PAGD output to drive the DC motor component of the set. This
25 provides a simple, one battery pack solution, where the PAGD input and output circuits are electrically separated by the DC motor/generator interface: the drive pack is simultaneously being discharged to drive PAGD production, and charged by the DC generator output which, in turn, is being
30 driven by the electromechanical transformation of the rectified PAGD output that would typically accrue to a charge pack in the experiments already described. The main limitations to such an arrangement lie in the efficiency of the motor and generator transformations utilized.

- 80 -

A pulsed DC source could be used to provide input to the circuit if suitably synchronized, but care is needed not to interfere unduly with the autoelectronic mechanism of the field induced cathode emissions. In fact, externally
5 pulsing an abnormal glow discharge does not mimic the autogenous PAGD regime, because it precludes the emission mechanism responsible for triggering the PAGD.

While the invention has so far been described with reference to exploitation of the PAGD regime, because of the
10 advantages inherent in its endogenous pulsation, the larger currents attainable in a VAD may justify the difficulty and extra complication inherent in externally switching on and off a VAD, to achieve repeated complete VAD extinctions and re-ignitions.

15 The requirement for a minimum current to support the cathode spot of a vacuum arc discharge, as supposed by modern field-emission and smooth surface theories of the cathode spot (Ecker, G (1980) 'Theoretical aspects of the vacuum', in 'Vacuum arcs, Theory and application', Lafferty
20 JM, ed, p.228 &f, J.Wiley &sons, NY, NY, p. 310), leads directly to the prediction of a current chopping phenomenon at the extinction of the arc discharge. This is observed for both high pressure arc discharges (HPAD) and vacuum arc
25 discharges (VAD), though the magnitude of chopping currents and the arc re-ignition by the high voltage transients generated are more pronounced in the VAD regime, given the residual ionization present in HPAD gaps and the fast recovery of the dielectric strength of the vacuum gap. When
30 one considers a single cathode spot in a VAD, the decrease over time of the total discharge current leads to a situation where extinction of the discharge will occur unless the applied voltage can be raised further or the transient voltages are high and rapid enough to re-ignite the gap (as
35 with the current chopping of a resistive circuit). In the latter instance, and essentially under low current

- 81 -

conditions, rapid re-ignitions of the gap prevent full extinction, and the VAD lifetime is extended. This is typically avoided by increasing the capacitance placed in parallel with the cold-cathode vacuum arc gap, to suppress transient voltage rises and diminish the probability of arc re-ignition (Farrall, GA (1980) 'Current zero phenomena', in 'Vacuum arcs, Theory and application', Lafferty JM, ed, p.184 &f, J.Wiley &sons, NY, NY, p.193-194). Increasing the parallel capacitance also raises the level of the chopping current. With inductive circuits, even small inductances such as those associated with lead wires, can generate high transient voltages across the gap upon extinction, but re-ignition is unlikely given the slow rise rate of these voltages. These considerations have led to the formulation of a predictive model for the current-voltage characteristic (an "existence diagram") of a single cathode spot, that explains how below a certain critical current the vacuum arc discharge does not necessarily extinguish because of a steep rise in voltage drop (Ecker, G (1980) 'Theoretical aspects of the vacuum', in 'Vacuum arcs, Theory and application', Lafferty JM, ed, p.228 &f, J.Wiley &sons, NY, NY, p. 310). The value of the extinction currents expected might thus be lower than that predicted from the value of the critical current. One may thus suppose that given the applicability of the existence diagram for the quasi-stationary single cathode spot, the extinction and re-ignition patterns of the auto-electronic emission-triggered PAGD regime might just be the result of a low current, single cathode spot VAD with a high cathode voltage drop and its frequency determined by random re-ignition due to unsuppressed transients. In practice, aside from the other characteristics of the discharge already examined, such as the PAGD positive slope in a Fowler-Nordheim plot and the involvement of the abnormal glow in the PAGD regime, the re-ignition frequency of the PAGD is a virtually regular phenomenon, which may be controlled at will by manipulation of operational and structural parameters (applied current, rise rate of applied

- 82 -

voltage, pressure, gap distance, plate area, etc). For a given set of conditions, the PAGD frequency can be made to increase as a function of the augmenting current until, at very high applied currents (~3-5 DCA) and ignition frequencies, a vacuum arc discharge sets in and replaces the PAGD regime. As the frequency increases and the pressure is kept constant, the duration of the PAGD emission jet decreases. This is the opposite of that found for VADs (Farrall, GA (1980) 'Electrical breakdown in vacuum', in 'Vacuum arcs, Theory and application', Lafferty JM, ed, p. 184 &f, J.Wiley &sons, NY, NY, p. 193), where the average lifetime of an arc increases with increasing current. However, if the PAGD frequency increase promoted by the current be compensated by a frequency decreasing parameter (still in conditions where no re-ignition occurs because of transients generated), then the current increase does augment the lifetime of the PAGD cathode jet (and the return pulse lasts longer). Within the PAGD range, the value of the extinction currents increases with increasing parallel capacitance (as in VADs), with increasing cathode voltage drop (opposite to the theoretical existence diagram of low current VADs) and with increasing applied direct current (in a range well beneath that considered necessary to establish a vacuum arc discharge across the large gaps of the pulse generator). While typically resonant frequencies may appear before extinction of each PAGD emitter (inductive characteristics of the circuit), and while the pulse extinction may be related to resonant modes of current decay specified by these transient frequencies present at the end of a pulse, the complete extinction characteristic of the PAGD regime appears to be a complex function of the gap distance, plate area (which affects the PAGD frequency and the electrical breakdown characteristics), the pressure and nature of the gas, the magnitude of the applied voltage and current, and the size of the parallel capacitance. However, unlike the dependence of decreasing VAD chopping currents upon increasing input current (for currents 10 to 100x

- 83 -

greater than those used for the PAGD input), the magnitude of the PAGD extinction currents increases with increasing peak currents measured at the collector (and which are much greater than the input current waveform, see Fig. 40). The
5 PAGD extinction currents also depend upon frequency, such that, when the increase in applied current results in a increase of PAGD frequency, and this is not counter-balanced by manipulation of a frequency decreasing factor (eg. pressure), the value of the extinction current rises until
10 the vacuum arc discharge sets in; for the frequency increases with the applied current, but the current increases with the pressure while the frequency, above certain pressure, does not. Indeed, the largest PAGD pulses in terms of input and peak output currents, as well as in terms of the largest
15 cathode voltage drops, occur at low frequencies and the lowest pressures possible.

The possible common trait of the PAGD and the VAD lies not in the mechanism of extinction (complete in the former and incomplete in the latter), but on that of the
20 initial plasma ignition: other than for the start-up ignition, the plasma re-ignition that maintains the VAD is an uninterrupted and cumulative process of partial re-ignition that precludes full relaxation of the plasma, whereas PAGD re-ignition is a regular process that entails complete plasma
25 relaxation; thus, what produces the anomalous large peak currents and voltages characteristic of the PAGD is the initial cathodic eruption that ignites the plasma and which is equally present at the start of a VAD. For the PAGD to achieve its characteristic large peak currents collected at
30 the output of any of the circuits described above, extinction of the previous discharge must be complete; only then can plasma re-ignition again generate large reaction forces. This is easily observed in the same circuit (Figure 23) utilized to produce the PAGD with aluminum plates, where VAD
35 production is carried out with zinc plates under the very same conditions. In the latter case, the very high parallel

- 84 -

capacitance (17,350 microfarads) did not prevent permanent re-ignition of the arc discharge, but the transients at re-ignition, upon partial extinction, were much smaller than the initial VAD transient current and voltage peaks, or the voltage and current peaks characteristic of the PAGD. Increase of the current did not affect the rate of the re-ignition. Conversely, PAGD production in the aluminum plates (as well as in zinc plates with different values) in the same circuit is characterized systematically by complete extinction of the emission current before re-ignition; moreover, this re-ignition is neither controlled nor determined by transients (mostly suppressed by the large parallel capacitance), but by all the other conditions affecting PAGD frequency. This then leads to the existence of (PAGD) field emissions at currents lower than the critical current of a single cathode spot for a vacuum arc discharge, and which have a current-voltage characteristic that, unlike the VAD existence diagram, has a positive U/I slope (where U is the magnitude of the cathode voltage drop and I the emission current) for chopping currents characteristic of the PAGD. These considerations thus lead us to have to assume that an externally switched on/off VAD discharge, being triggered at much higher currents than those required to support PAGD production, can be used to generate excess energy from charged metals 'in vacuo' in the same way and circuit as the PAGD regime, which does so on its own. The utilization of such externally pulsed or interrupted VADS has been experimentally confirmed by examining the oscilloscopic profile of the ignition start-up pulse for VADs: indeed, it has the same aspect as that of a PAGD, while any subsequent VAD re-ignitions do not, unless the VAD is interrupted and re-started.

The anomalous PAGD discharge also can be triggered by the physically external stimulation of a moving static charge, a moving magnetic field or a spark gap, upon an insulating gap stimulated with prebreakdown voltages. The

- 85 -

PAGD auto-electronic emissions produced with subcritical currents are thus functionally equivalent to electronic emission discharges whose extinction is provoked by an insufficient rise rate of the applied voltage or by an external switching off. However, in the absence of cathodic emission, as in flashing of the NGD or AGD, no such abnormal reaction forces are registered.

An example of the use of interrupted VADs achieved by an altered discharge tube or plasma reactor design is given in Figs. 35A and 35B. In Fig. 35A, seen from the anode side, an insulator disc 100 has two metallic sectors 102 diametrically opposed and well separated. Both present an extended surface area and greater width at the periphery than towards the center of disc, and are connected together as cathodes to the remainder of an energy converter circuit by two wires 104 buried in the body of the insulator disc and connected to a shaft 106 passing through a vacuum tight gland 108 in the envelope of the vacuum tube. This gland 108 serves both as a support for the cathode disc 100 and as the common electrical feeder to the cathode sectors 102 via wires 104. The shaft is joined externally to a control motor that rotates the cathode disc assembly at the desired speed. A rectangular anode 110 is located at the bottom of a side well 112 of the envelope 114 (see Fig. 35B) that occupies about 25% of the envelope's side wall area, and is mounted on a shaft 116 which passes through gland 118 to allow adjustment of the discharge gap. The envelope of the vacuum device, seen in cross-section in Fig. 35B, is shaped so as to prevent the arc, once established, from propagating beyond the raised lip of the envelope wall surrounding the anode on the side of the anode wall closest to the center of the device. For the remaining 75% of the side wall area of the envelope adjacent the cathode disc assembly, the envelope is as shallow as possible. Assuming rotation of the cathode disc assembly in one or other direction, arc initiation will occur shortly after a field is established between the anode and a cathode

- 86 -

segment entering the well at one of its corners, assuming an appropriate gap distance and suitable conditions of excitation (which may involve an external trigger, e.g. a neighbouring spark gap). The arc will tend to travel with
5 the axial motion of the cathode segment until interrupted by the cathode segment leaving the well. Extinction of the discharge is thus mechanically achieved by moving the cathode away from the anode. The timing from onset to extinction of the VAD is determined by the effective gap distance, the
10 effective anode area and the rotational speed of the disc. When the plasma reactor of Figs. 35A and 35B is driven at 120 RPM, four VADs per second with a maximum duration of 125 msec each may be produced. There is no limit to the number of metallic cathode segments affixed onto the disc, but an
15 increase in their number will require smaller anode areas, which may be compensated by increasing the diameter of the cathode disc assembly and multiplying both the number of anodes and their associated wells. The rotational speed of the disc assembly is determined by the desired parameters of
20 operation for any given size of energy converter system. The polarity of the electrode members of this device can be transposed, but for any given set of conditions, this will reduce the range of operation for clearly demarcated VADs.

As an alternative to physical commutation being
25 built into the plasma reactor itself, electrical or mechanical commutation of the power input to the device may be used, as soon after ignition as the VAD ceases to output charge through output ports to the secondary arm of the circuit. The result of turning off the arc discharge shortly
30 after ignition is to externally force the VAD to pulse between on and off states, thereby simulating the cycling between charge and discharge characteristic of the PAGD regime.

The circuit of Figure 41 is generally similar to
35 that of Figure 26 except for the provision of mechanical

- 87 -

switches S7, S8 at the inputs to the discharge tube and associated arc suppression circuits across the switch contacts formed by R5, R6, C9, C10, and D9, D10 in order to protect the switching and prevent atmospheric arcs from debasing the action of the circuit. The arc suppression circuits shown across the mechanical switches are well known in the art of arc suppression in relay contacts. The mechanical switches are operated simultaneously by a mechanical device (a lever, a motor with a mechanical commutator, or the like, not shown) or electronically (eg by a digital controller operating an electromagnetic switcher) to produce a desired frequency of low frequency intermittent arc discharges.

A preferred method of control is however to use electronic switches and thereby avoid the mechanical and arcing problems of a circuit such as that of Fig. 41. One amongst several possible examples is shown in Fig. 42, and utilizes two insulated bipolar transistors IGBT1 and IGBT2 to switch on and off the inputs to the discharge tube. DR1 and DR2 are manufacturer recommended driver and short-circuit protection circuits, triggered in synchrony at terminals T1 and T2 by pulses from an external clock and pulse generator, eg a digital controller. The same controller adjusts the potentiometer R1, which is digitally controlled, both to control the vacuum tube input current as well as to turn off the VAD in case one of the IGBTs or protecting diodes D12 or D13 fails. The controller preferably includes feedback control loops to detect VAD ignition (and also to detect turn off status, if several devices are fired sequentially and in parallel): upon formation of an arc, which may be detected optically by a photoelectric device or current sensing loop feeding back to the external controller, the controller turns the IGBTs off. Feedback control is preferred to fixed frequency switching because of the lag time between application of the electrical field and the initiation of the arc, which is greatly affected by the electrical breakdown

- 88 -

state of the gap, the dissipation of the plasma and the rise time of the applied potential across the electrodes. This emphasizes the need for carefully programmed controller timing with phases that are not so short as to frustrate
5 optimal conditions for full VAD ignition. However, this can be compensated by using external triggers to synchronize the discharge with the switching on of power. Utilizing such no-contact commutation methods has the distinct advantages of eliminating the maintenance and arcing associated with
10 mechanical commutation, while making possible self-regulation of the converter system and synchronization of the optimal switching action at both inputs and optionally the outputs from the plasma reactor.

The effect of physically or externally interrupting
15 a VAD to form pulses was investigated using the circuit of Figure 38 which is a modification of the circuit of Figure 26, to provide oscillographic comparison of the waveform voltage and current traces for both regimes of plasma discharge, PAGD and VAD, at terminals V1 and I1 monitoring
20 the drive pack outputs, at terminals V2 and I2 monitoring the discharge tube, and at terminals V3 and I3 monitoring the input to the charge pack. The circuit included resistors forming voltage dividers R10-11 and R13-14 having the same 1:100 ratio. Current monitoring resistors R9, R12 and R15
25 all had 1 ohm values. Two different tubes were utilized for observations of the two plasma discharge regimes: for the PAGD experiments, a vacuum tube having 128 cm² aluminum plates and a 5 cm gap, at argon pressure of 0.1 Torr, was employed, and for the VAD experiments a vacuum tube having 16 cm² zinc
30 plates and a 4 cm gap, at 0.8 Torr. The six waveforms appearing at terminals V1 to V3, and I1 to I3 for each plasma discharge regime are shown in Figs. 39 (PAGD voltages), 40 (PAGD currents), 41 (VAD voltages) and 42 (VAD currents). All waveforms were obtained at the same input voltage (560
35 VDC) and current (0.4 to 0.7A). It is apparent that both PAGD and VAD voltages (Figs. 39 and 41) are comparable at

- 89 -

ignition (zero on the time axis), but that the observed successive re-ignitions of the arc before dissipation of the plasma gap lead to the self-sustaining condition of the VAD regime, where the strong voltages developed at breakdown are absent (see V2 after about 150 msec, Fig. 39), and no potential greater than that of the charge pack (about 320V) forms at the outputs (see V3, after about 150 msec, Fig. 39). These repeated arc ignitions do not pulse the plasma gap, and present the typical vacuum arc discharge profile of randomized high frequency electronic emissions partially sustained by ionic bombardment of the cathode. Similar VAD discharges can be observed with aluminum devices at higher current and voltage inputs than those utilized for the condition of both PAGD (with aluminum cathodes) and VAD (with zinc cathodes) in these experiments.

Like the VAD, the PAGD discharge is self-starting and self-sustaining, but that is because, unlike the VAD, the PAGD discharge is self-extinguishing (see Fig. 39). This characteristic prevents the formation of a stable discharge channel such as it characterizes the VAD, while allowing the PAGD to repeatedly develop the abnormal discharge (V2) and charging potentials (V3). What is self-sustaining about the PAGD regime is its cycle of auto-electronically triggered plasma discharge and full plasma extinction that permits it to constantly drive surplus charge into the charge pack. This is apparent from a comparison of the observed current waveforms for the PAGD and VAD (Figs. 40 and 42, respectively). The current avalanches at ignition in both the PAGD (steep curve I2, Fig. 40) and the VAD (sustained curve I2 with flattened peak, Fig. 42) drive charging currents into the charge pack (I3 in Figs. 40 and 42), but as multiple VAD reignitions occur, I3 decreases to near zero (in about 50 to 75 msec for the values employed for capacitances C3 and C5, Fig. 42). As the arc stabilizes, both I2 and I3 current avalanches cease, while the arc current (I1) at the drive pack output and at the cathode (I3) remains constant

- 90 -

throughout. In contrast, the full extinction of the PAGD determines the repeated current avalanches observed, upon auto-electronic emission, at the cathode (I2) and the intermittently charging currents at the outputs of the conversion system (I3, Fig. 40). Finally, the magnitude and duration of the I3 currents registered for both the PAGD and for the VAD ignition profiles will decrease or increase (to a maximum) as the values of C3 and C5 are increased or decreased from that employed (0.035 F), without affecting the observed relationships.

One may thus think of the VAD as a discharge that initiates by resembling the PAGD, but completes the discharge channel to reach a different steady state than that of the PAGD: PAGD re-ignition is a quasi-regular phenomenon, and the regime is self-sustaining because the extinction of the discharge is complete; VAD re-ignition is a high-frequency process that sustains the discharge through successive partial extinctions and re-ignitions. The purpose of the physical and external (mechanical or electronic) commutators discussed is to arrest the VAD before it reaches this re-ignition steady state, and thus to make its intermittent regime mimic the PAGD. The practical purpose of so doing is that, in contrast to the PAGD regime, which is dependent upon an input current range lower than that needed to establish the VAD regime (for the same device, and with all other conditions being identical), the higher input currents needed for VAD initiation provoke, upon electrical breakdown of the vacuum by cathodic emission, surges of energy released from the cathode of greater magnitude than are possible with PAGD under otherwise similar conditions. An energy conversion system such as that proposed can thus utilize power inputs greater than those permitted by the PAGD regime, and generate larger power outputs per ignition than for the PAGD, for as long as it utilizes an interrupted vacuum arc discharge which is commutated as described above.

- 91 -

The various circuits described above utilizing electric motors in the energy recovery arm have not included circuits suitable for driving three phase motors. Figure 43 illustrates how the circuit of Figure 42 can be adapted and
5 triplicated to power a three phase motor rather than a battery charging circuit. The charge pack DP and immediately associated components are common to all three circuits, whilst the diode bridge V1, charge pack CP and intermediate components are replaced by a three phase motor M with one
10 phase winding connected across the output capacitors C3, C5 of each circuit, the references for the indicated components of each circuit being suffixed A, B or C as the case may be. The capacitors C3A, C3B and C3C are connected to the common ground point of the motor. Phasing of the operation of the
15 three discharge tubes is readily achieved by suitable timing of control signals applied to the drives DR1A, B & C and DR2A, B & C.

TABLE 1

Results for the ballast resistance (and current) dependent PAGD frequency utilizing an H34 aluminum pulse generator with 128cm² plates at 5.5cm distance, in the triode configuration, at a pressure of 0.8 Torr. The circuit employed is that of the present invention, as described in the third Results Section. DCV=560.

R in ohms	Regime of Discharge	Pulse Rate >100V
5,000	NGD (Cold Cathode)	0
600	PAGD	10 PPS
300	PAGD	40 PPS
150	PAGD	180 PPS
100	VAD	0
50	VAD	0

TABLE 2

RESIDUAL GAS EFFECT

pressure in Torr	in AIR	PPS in ARGON
0.45	ND	10
0.5	1.8 \pm 0.3	ND
0.55	4.8 \pm 0.9	16.7 \pm 1.8
1.0	11.4 \pm 0.8	448 \pm 27.4
1.25	214.5 \pm 14.3	ND
2.0	36.2 \pm 2.6	206 \pm 19.6 158.7 \pm 24
2.5	1.36 \pm 0.3	0

TABLE 3

Charge pack No. of cells	PPS	PAGD
36	0	-
31	1	+
29	10	+

TABLE 4- part 1

1	2	3	4	5	6	7	8	9
Expt. No.	Battery Pack	Position	Open Voltage	V/cell	%total rel.cpty.	Max. hr. left	%rel. cpty gained lost	Total kWh
1	Charge	start	348	12.0	40	8		0.835
	Charge	end	366	12.62	83	16.6	43	1.823
	Driver	start	576	12.52	77	15.4		2.660
	Driver	end	572	12.43	70	14	7	2.402
2	C	b	331	11.41	2	0.4		0.040
	C	a	351	12.1	47.5	9.5	45.5	1.002
	D	b	553	12.02	40	8		1.327
	D	a	546	11.9	33	6.6	7	1.081
3	C	b	345	11.9	32.5	6.5		0.673
	C	a	361	12.45	72.5	14.4	40	1.559
	D	b	559	12.15	51	10.2		1.710
	D	a	552	12.0	40	8	11	1.324
4	C	b	360	12.41	70	14		1.512
	C	a	373	12.86	103	>20	33	2.238
	D	b	562	12.22	54.5	10.9		1.838
	D	a	557	12.11	48	9.6	6.5	1.604
5	C	b	340	11.7	20	4		0.408
	C	a	365	12.59	83	16.6	63	1.818
	D	b	527	11.45	3.2	0.6		0.101
	D	a	517	11.24	1.8	0.4	0.2	0.056
6	C	b	340	11.72	21.5	4.3		0.438
	C	a	367	12.66	87.5	17.5	66	1.927
	D	b	589	12.8	100	20		3.530
	D	a	564	12.26	58.5	11.7	41.5	1.979
7	C	b	318	10.97	1.2	0.24		0.023
	C	a	359	12.38	67.5	13.5	66.3	1.454
	D	b	575	12.5	77	15.4		2.656
	D	a	567	12.32	63.5	12.7	13.5	2.160
8	C	b	328	11.71	20	4		0.393
	C	a	350	12.5	76.5	15.3	56.5	1.606
	D	b	582	12.65	87.5	17.5		3.055
	D	a	579.5	12.60	84	16.8	3.5	2.921

TABLE 4- part 3

1 9	2 0	2 1	2 2	2 3	2 4	2 5	2 6	2 7	2 8	2 9
Plate	R1 ohm	C3/C5 mfd	C7a/C7b mfd	Motor arm	Pressure	Gap cm	OV rlx. time	C4 mfd	R4 ohms	Motor rpm
H34	300	20,700	3,300	off	0.8Torr	5.5	30'	NA	NA	NA
H34	300	20,700	3,300	off	0.8Torr	5.5	30'	NA	NA	NA
H34	300	20,700	3,300	off	0.7Torr	5.5	15'	NA	NA	NA
H220	300	34,700	5,500	off	0.2Torr	5.5	30'	NA	NA	NA
H34	150	34,700	3,300	on	0.8Torr	5.5	15'	8	500	1,200
H34	300	20,700	3,300	on	0.8Torr	5.5	15'	16	0	2,000
H34	600	34,700	3,300	off	0.8Torr	4	30'	NA	NA	NA
H34	600	34,700	5,500	off	0.8Torr	4	30'	NA	NA	NA

TABLE 5- part 1

1	2	3	4	5	6	7	8	9	10	11	12	13
Expt. No.	Config.	Pressure Torr	Tube	DP DCV	Plates DCV	DP DCA	DP Watts	PAGD Volts	PAGD V/cm	CP DCV	CP DCA	CP Watts
1	dd	0.8	A29	562	350	0.65	137.8	212	77.1	375	1.25	468.8
2	dd	0.09	A29	562	402	0.60	96	160	58.2	378	0.70	264.6
3	dd	0.8	A29	560	371	0.59	111.5	189	68.7	374	0.65	243.1
4	dd	0.09	A29	563	409	0.49	75.9	154	56	379	0.76	288
5	t	1.5	A28	561	439	0.41	49.9	122	22.2†	377	0.58	219
6	t	1.5	A28	560	425	0.51	68.9	135	24.5†	375	0.69	259
7	t	1.0	A28	556	398	0.48	75	158	28.7†	376.5	0.57	213.1
8	t	0.5	A28	559.5	398	0.68	109.8	161.5	29.4†	377.5	0.67	252.9
9	t	0.5	A28	563	390	0.75	112.45	173	31.5†	373	0.65	280
10	sd	0.5	A28	565	422	0.47	67.2	143	26	376	1.03	387.3
11	sd	0.5	A28	561.5	415	0.50	73	146.5	26.6	380	0.73	277.4
12	sd	0.5	A28	562	413.5	0.55	81.7	148.5	27	380	0.71	269.8
13	dd	0.25	A28	553	438	0.35	40	115	41.8	381.5	0.59	225.1
14	dd	0.25	A28	549	325	0.70	156.8	224	81.5	263	1.36	357.7

† These field values for the triode configuration, only take into account the distance separating the axial member (functioning as auxiliary cathode) and the anode or the rarer discharges from the main plate cathode to the axial member, which have the same gap distance; discharges from the main cathode to the anode have double this distance.

TABLE 5- part 2

14	15	16	17	18	19	20
Total Resistance	Breakeven Efficiency	PPS	Bridge diode	Input diode	Motor status	Fig.3
326	340%	450	M860	HFR	off	+
270	276%	92	M860	HFR	off	
243	218%	500	HFR	HFR	off	
314	379%	77	HFR	HFR	off	
298	439%	52	HFR	HFR	off	
265	376%	100	M860	HFR	off	
329	284%	355	M860	HFR	off	
238	230%	92	HFR	HFR	off	
266	249%	118	M860	HFR	off	+
286	530%	25	M860	HFR	off	
293	379%	11	HFR	HFR	off	+
270	330%	10	HFR	HFR	on	+
329	563%	10	HFR	HFR	off	
320	228%	1	HFR	HFR	off	

TABLE 6 - part 1

1	2	3	4	5	6	7	8	9	10	11			
Expt. No.	Battery Pack	Position	Total Wh	Rel. Cap.	Torr	Limit in W	ΔkWh gain	loss	Exptl. time	abs. kWh/h gain	loss	net	BE
1	C	b	159	12%	0.8	90	269	32	21.5'	753	89	+664	846%
	C	a	428	32%									
	D	b	1764	85%									
	D	a	1732	84%									
2	C	b	118	9%	0.8	90	192	7.3	18'	640	24	+616	2,667%
	C	a	303.5	23%									
	D	b	542.3	26%									
	D	a	535	25.9%									
3	C	b	950.4	72%	0.2	90	210.9	6.5	70'	191.7	5.6	+186	3,485%
	C	a	1,161	88%									
	D	b	660	32%									
	D	a	654	32%									
4	C	b	15.8	1.2%	0.8	90	65	16	64.5'	60	14.7'	+53.7	406%
	C	a	81.9	6%									
	D	b	181	8.7%									
	D	a	165	8%									
5	C	b	34.5	2.6%	0.8	90	104.3	24	28.5'	219.6	50.5	+169.1	436%
	C	a	138.8	10.5%									
	D	b	1,114	54%									
	D	a	1,089	53%									
6	C	b	55.4	4.2%	0.8	90	182.2	37.7	74'	148	30.6	+117	483%
	C	a	237.6	18%									
	D	b	669.3	32%									
	D	a	631.7	30.6%									

SUBSTITUTE SHEET

TABLE 6 - part 2

12	13	14	15	16	17	18	19	20	21	22
Config.	Tube	Cathode area	gap cm	PPS	PAGD seq. method	R1 ohms	Plate material		C3/C5 mfd	C7a/C7b mfd
Triode	A26	128cm ²	5.5	8	Continuous	300	H34		20,700	3,300
Triode	A26	128cm ²	5.5	61	Interrupted	300	H34		20,700	3,300
Triode	A28	128cm ²	5.5	32	Interrupted	300	H220		34,700	5,500
Triode	A46	64cm ²	4.0	5	Continuous	600	H34		34,700	5,500
Triode	A46	64cm ²	4.0	32	Interrupted	600	H34		34,700	5,500
Plate Diode	A29	128cm ²	5.5	8	Interrupted	300	H220		34,700	5,500

SUBSTITUTE SHEET

TABLE 7

Utilizing: Al H200, 128cm² plates
DP = 46 cells
CP = 23 cells

	PPS	CP Gain per pulse in mWh	Net Gain per pulse mWh	CP Gain per second mWh	Net Gain per second mWh	Pressure in Torr
#1	1.5	22.3	11.7	33.45	17.55	0.2
#2	8	5.6	4.4	44.8	35.2	0.8
#3	110	0.78	0.27	85.8	29.7	2.0

- 103 -

WE CLAIM:

1. Apparatus comprising a discharge tube and an electrical circuit containing said discharge tube and configured to operate the latter to provide pulsatory cold cathode autoelectronic emissions in the abnormal gas discharge or vacuum arc discharge regimes, the circuit being double ported with an input port connected to a source of direct current at a potential sufficient to initiate said emissions, and an output port connected to an external circuit providing a current sink effective to absorb at least a substantial portion of electrical energy released by said emissions.
2. Apparatus according to claim 1 configured so that the emissions occur in a pulsed abnormal glow discharge regime.
3. Apparatus according to claim 1 configured so that the emissions occur in a commutated vacuum arc discharge regime.
4. Apparatus according to claim 3, including switching means for commutating the input port.
5. Apparatus according to claim 4, wherein the switching means includes electronic switches.
6. Apparatus according to claim 2, wherein the input port includes components ensuring that the flow of current therein is unidirectional, and incorporating impedance sufficient to limit the flow of current therein.
7. Apparatus according to claim 1, including capacitors connected to the discharge tube, the input port and the output port, which provide charge storage and direct current isolation between the input and output ports.

8. Apparatus according to claim 7, wherein the output port comprises a rectifier having an input connected to said capacitors, reservoir capacitance connected to the output of said rectifier, and reverse current blocking devices connected between said reservoir capacitance and the current sink.

9. Apparatus according to claim 8, wherein the rectifier is a bridge rectifier, and the reservoir capacitance is provided by a capacitor bridge having ends connected to outputs of the bridge rectifier, and an intermediate point connected to one input of the bridge.

10. Apparatus according to claim 7, further including an alternating current motor and a capacitor in series, connected between the connections of said capacitors to the output port.

11. Apparatus according to claim 1, wherein the current sink comprises a secondary battery.

12. Apparatus according to claim 1, wherein the current sink comprises an electric motor.

13. Apparatus according to claim 1, wherein the current source comprises a secondary battery.

14. Apparatus according to claim 1, wherein the current source is a DC generator.

15. Apparatus according to claim 12, wherein the motor is a DC motor.

16. Apparatus according to claim 13, including a circuit for charging from the output port a battery to be used as the current source.

- 105 -

17. Apparatus according to claim 1, wherein the current source is a rectified AC source.
18. Apparatus according to claim 1, wherein the discharge tube is connected as a single diode.
19. Apparatus according to claim 1, wherein the discharge tube is connected as a multiple diode with plates connected as cathodes and an intermediate electrode connected as an anode.
20. Apparatus according to claim 1, wherein the discharge tube is connected as a triode, with an intermediate electrode functioning as an auxiliary cathode.
21. Apparatus according to claim 1, wherein a first potential is applied to the input port by the source of direct current to induce emission, a back EMF is applied to the output port by the current sink, and an extinction potential of the emissions is greater than the back EMF.
22. A method of energy conversion, comprising initiating repeated plasma eruptions from the cathode of a discharge tube operating in a pulsed abnormal glow discharge or an interrupted vacuum arc discharge regime utilizing electrical energy from a source in a first circuit connected to said discharge tube, and capturing electrical energy generated by such eruptions in a second circuit connected to said discharge tube.
23. A method according to claim 22, wherein the operating regime of the tube is an endogenous pulsed abnormal glow discharge.
24. A method according to claim 22, wherein the operating regime of the tube is a commutated discontinuous vacuum arc discharge.

- 106 -

25. A method according to claim 23, wherein current flowing into the discharge tube during said eruptions is at least 50 ma.

26. A method according to claim 23, wherein current flowing into the discharge tube during said eruptions is at least 500 ma.

27. A method according to claim 23, in which charge carriers within the plasma outputs are accelerated through at least one of an electric and magnetic field.

28. A method of energy conversion, comprising inducing endogenous pulsatory low-field, large-area cold-cathode autoelectronic emissions from the cathode of a discharge tube capable of sustaining such emissions, utilizing electrical energy from a source in a first circuit connected to said discharge tube, and capturing electrical energy generated by the collapse of such emissions in a second circuit connected to said discharge tube.

29. A direct current power transducer comprising a cold cathode vacuum discharge tube having an anode and a cathode and capable of autoelectronic emissions under abnormal glow discharge conditions, which emissions have an extinction potential substantially higher than the sustaining potential of a vacuum arc discharge in the same tube, and an external circuit including a direct current source connected between the anode and the cathode, the external circuit having a first energy input arm being capable of developing a potential sufficient to initiate said autoelectronic emissions, and an impedance sufficient that, as autoelectronic emissions are established, potential between the anode and the cathode collapses below said extinction potential before a vacuum arc is established, thus setting up an endogenous cyclical pulsed abnormal glow discharge, and a second energy recovery arm for recovering energy released by

said discharge.

30. Apparatus according to claim 1, wherein the external circuit comprises an electromechanical arm in parallel with the discharge tube and presenting a capacitance across the tube, said electromechanical arm including an electromechanical transducer device dependent on the application of cyclical power pulses for its operation.

31. Apparatus according to claim 30, wherein the electromechanical transducer device comprises a rotary electric motor having a stator converting cyclical power pulses into a rotating magnetic field and a rotor rotating in that field.

32. Apparatus according to claim 1, the discharge tube including at least one auxiliary electrode influencing emissions within the tube.

33. Apparatus according to claim 1, including a connection between said auxiliary electrode and said external circuit to affect an operational parameter of the transducer.

34. Apparatus according to claim 30, including at least one auxiliary electrode influencing emissions within the tube, and a connection between that auxiliary electrode and a point within the electromechanical arm selected to increase a cycling rate of the pulsed abnormal glow discharge.

35. Apparatus according to claim 31, wherein the motor is a synchronous motor.

36. Apparatus according to claim 31, wherein the motor is an asynchronous induction motor.

37. Apparatus according to claim 31, including electric motors connected in tandem.

- 108 -

38. Apparatus according to claim 31, including plural discharge tubes connected in tandem.

39. Apparatus according to claim 1, wherein the external circuit includes an arm in parallel with the discharge tube and presenting a capacitance across the tube, said arm including a transformer.

40. Apparatus according to claim 1, wherein the tube contains multiple cathodes and a common anode, and the external circuit is configured to develop a potential sufficient to initiate autoelectronic emissions between the anode and each cathode in turn to produce multiple endogenous cyclical pulsed abnormal discharges, the effects of which are combined in the external circuit.

41. Apparatus according to claim 40, wherein the tube contains two cathodes and the external circuit provides both capacitance between each cathode and the anode and inductances coupled in antiphase between the cathodes.

42. Apparatus according to claim 30, wherein the electromechanical arm includes a synchro-transmission system providing a remote output.

1/31

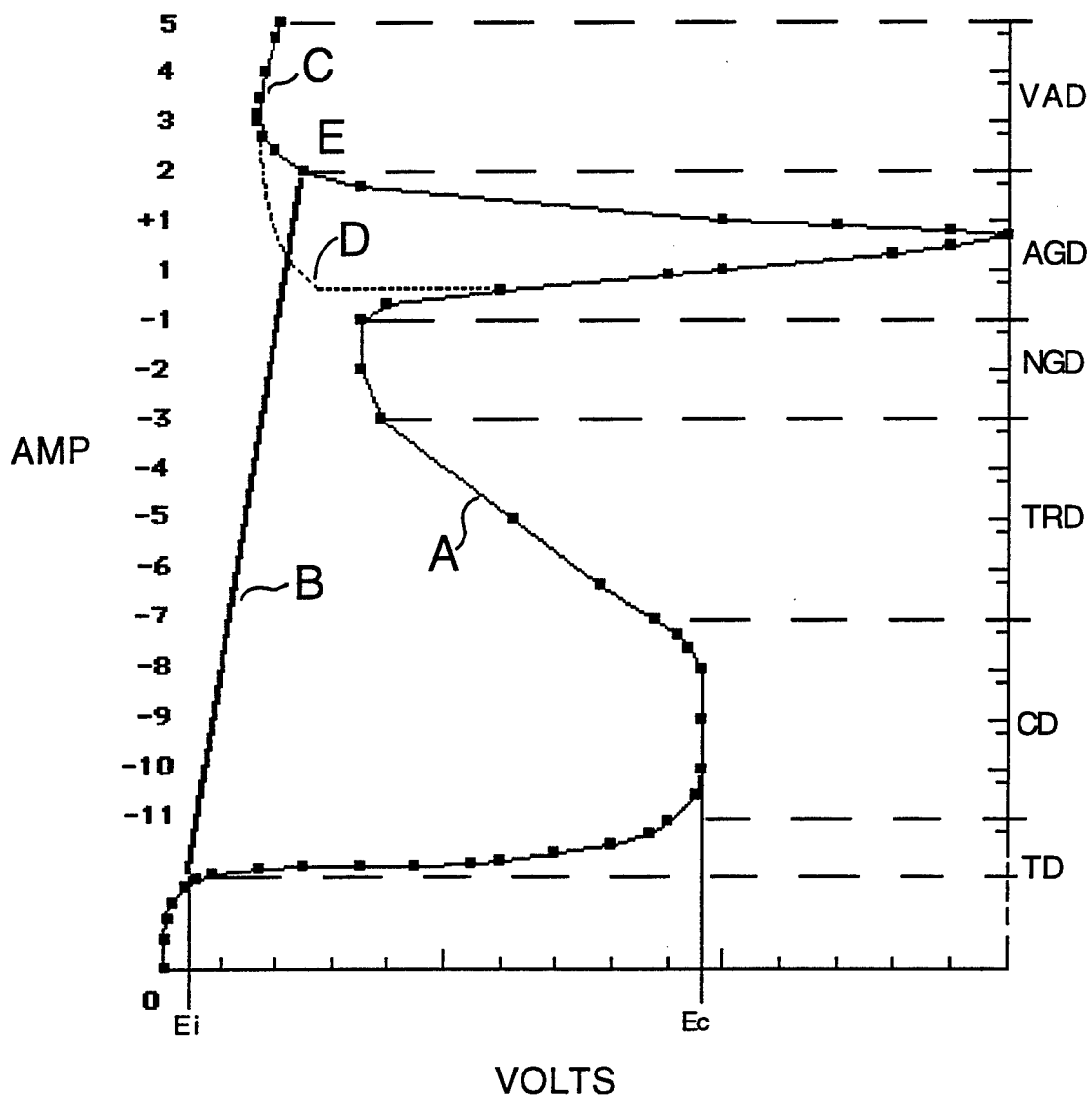


Fig. 1

SUBSTITUTE SHEET

2/31

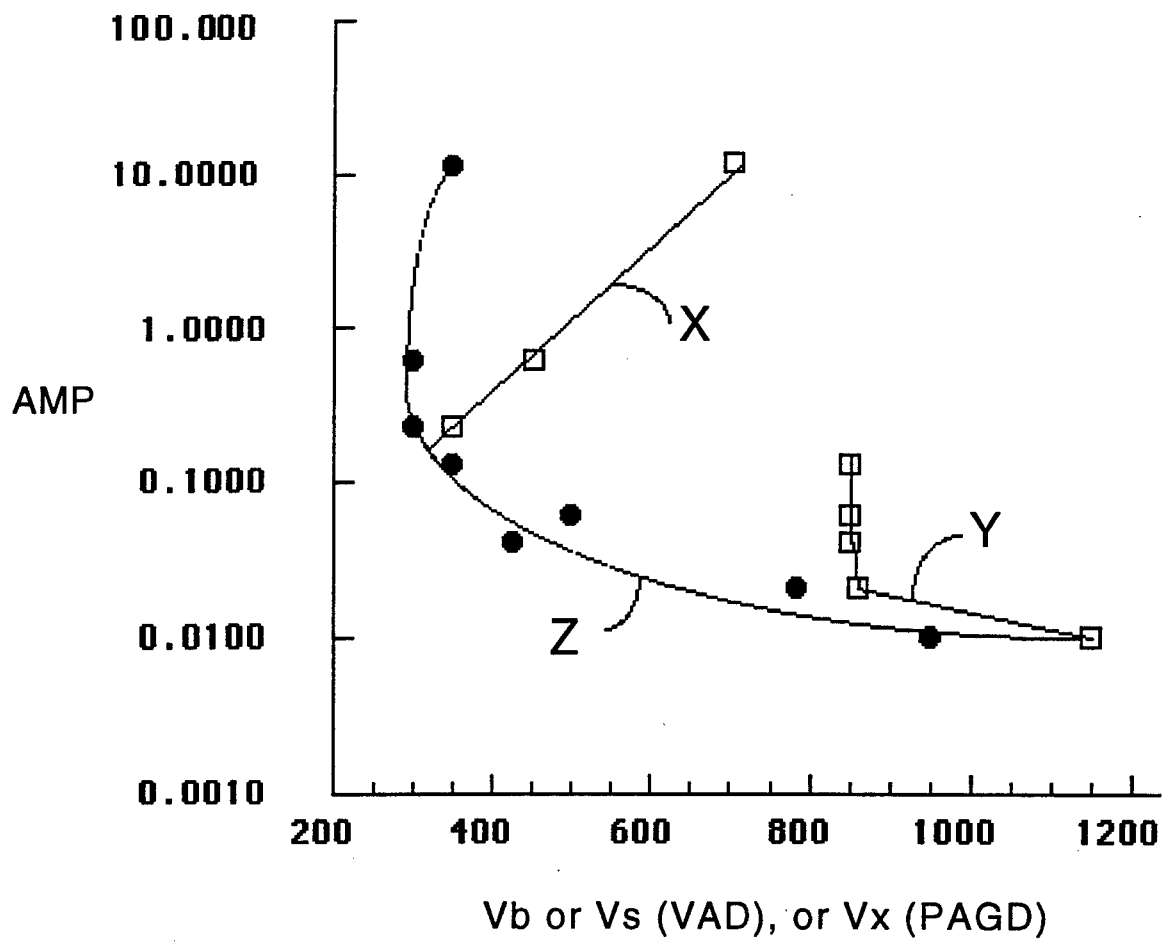


Fig. 2

SUBSTITUTE SHEET

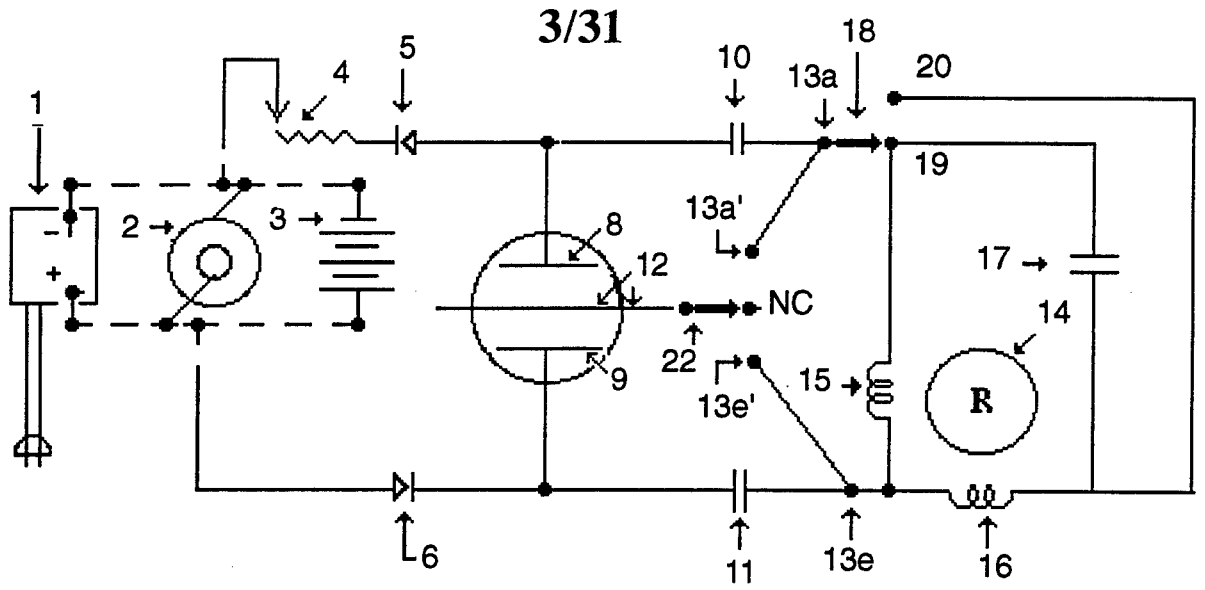


Fig. 3

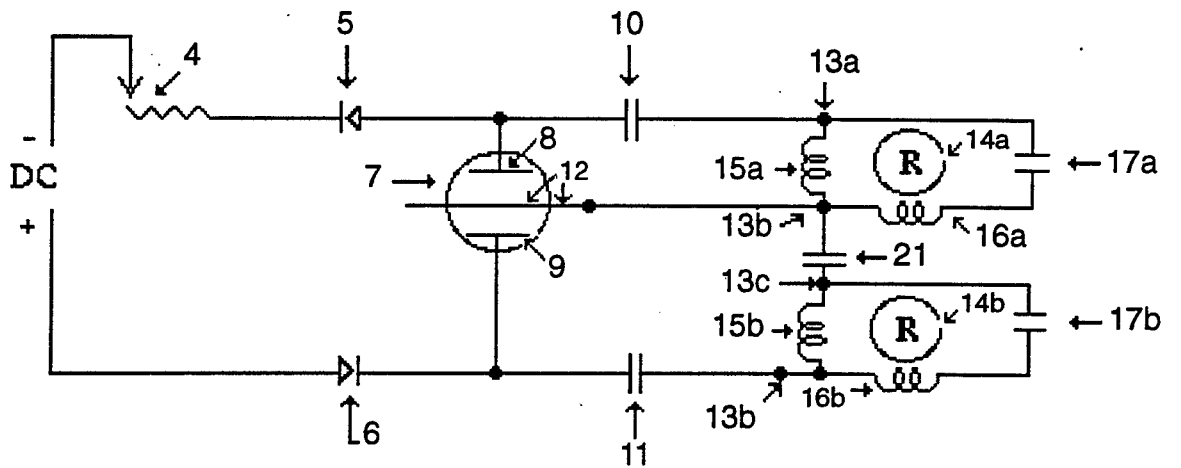


Fig. 4

4/31

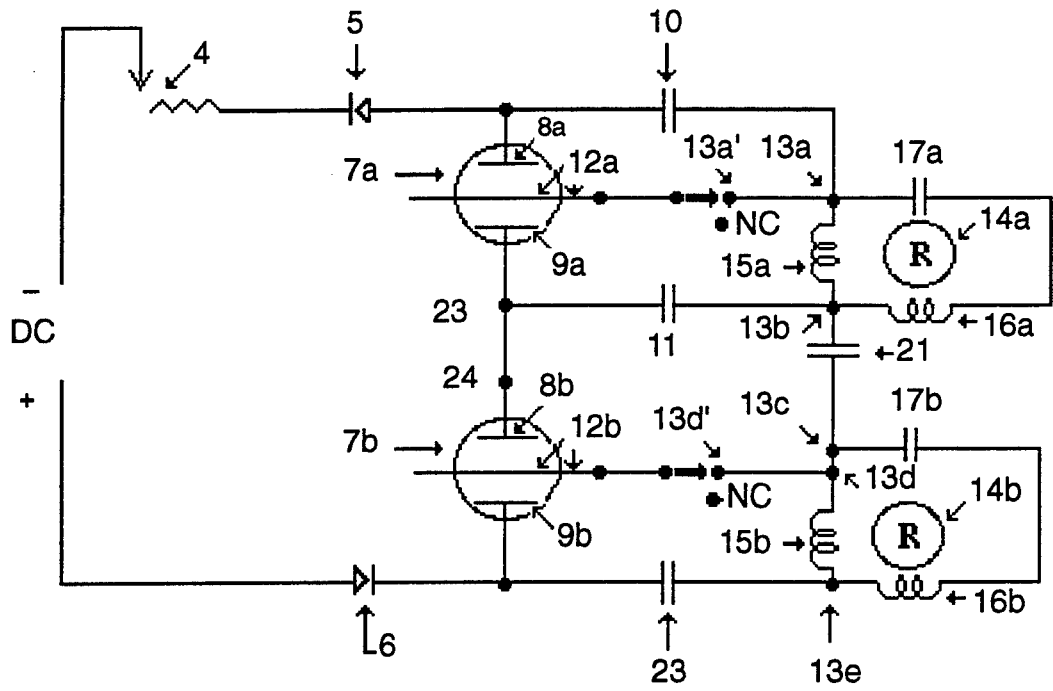


Fig. 5

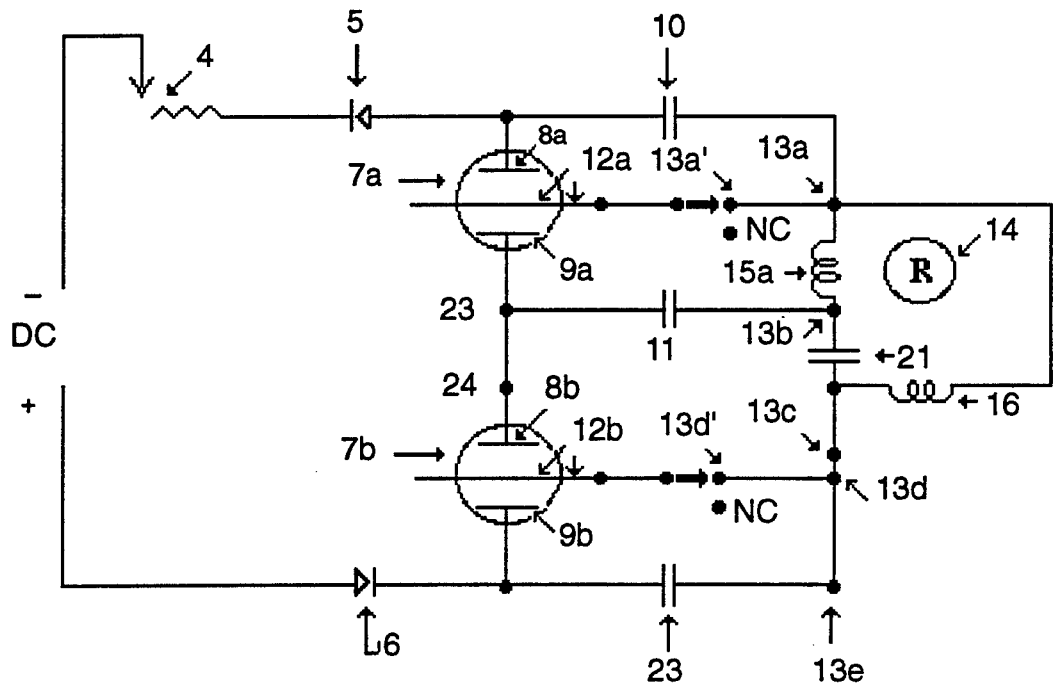


Fig. 6
SUBSTITUTE SHEET

5/31

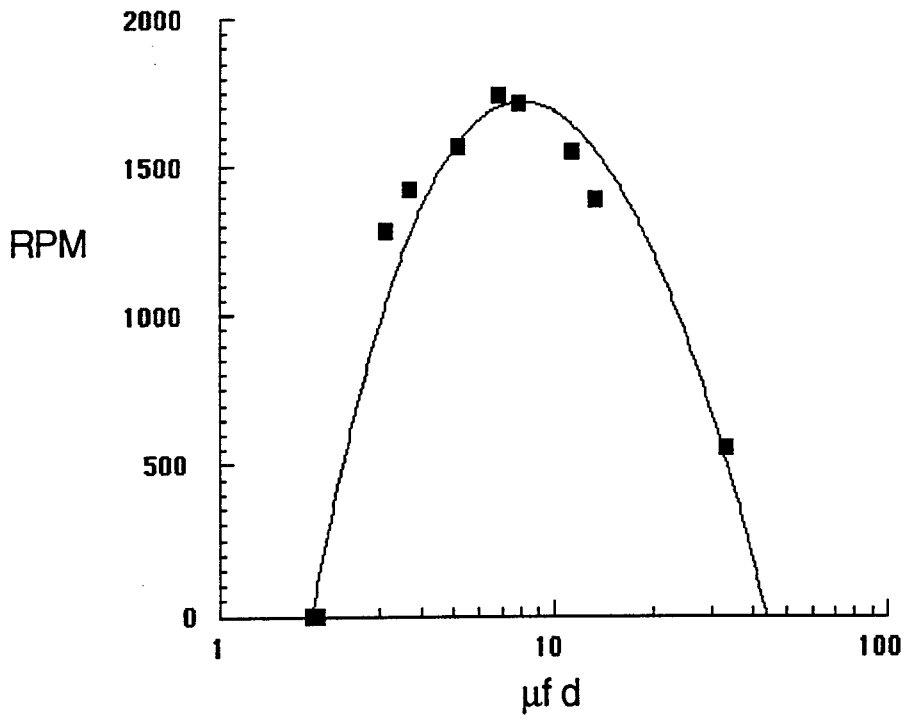


Fig. 7

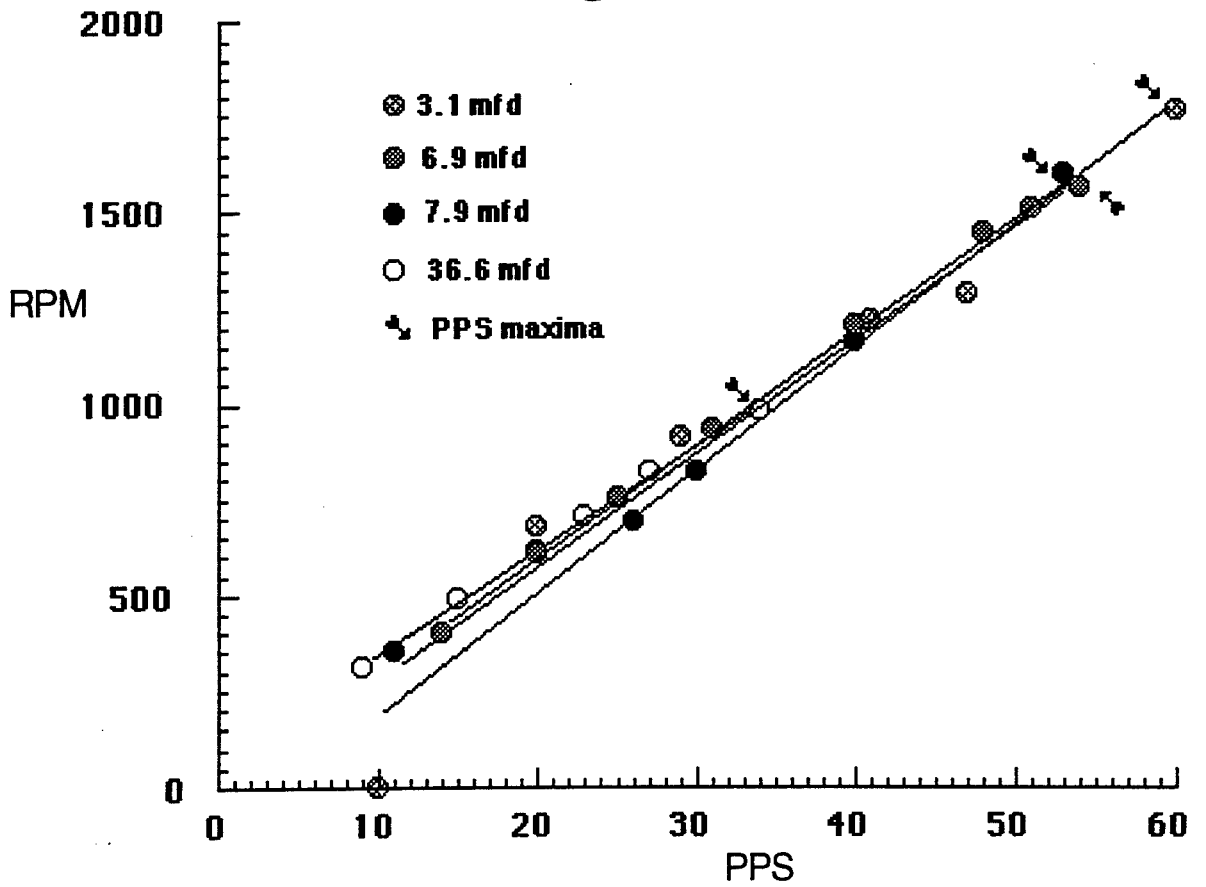


Fig. 8

SUBSTITUTE SHEET

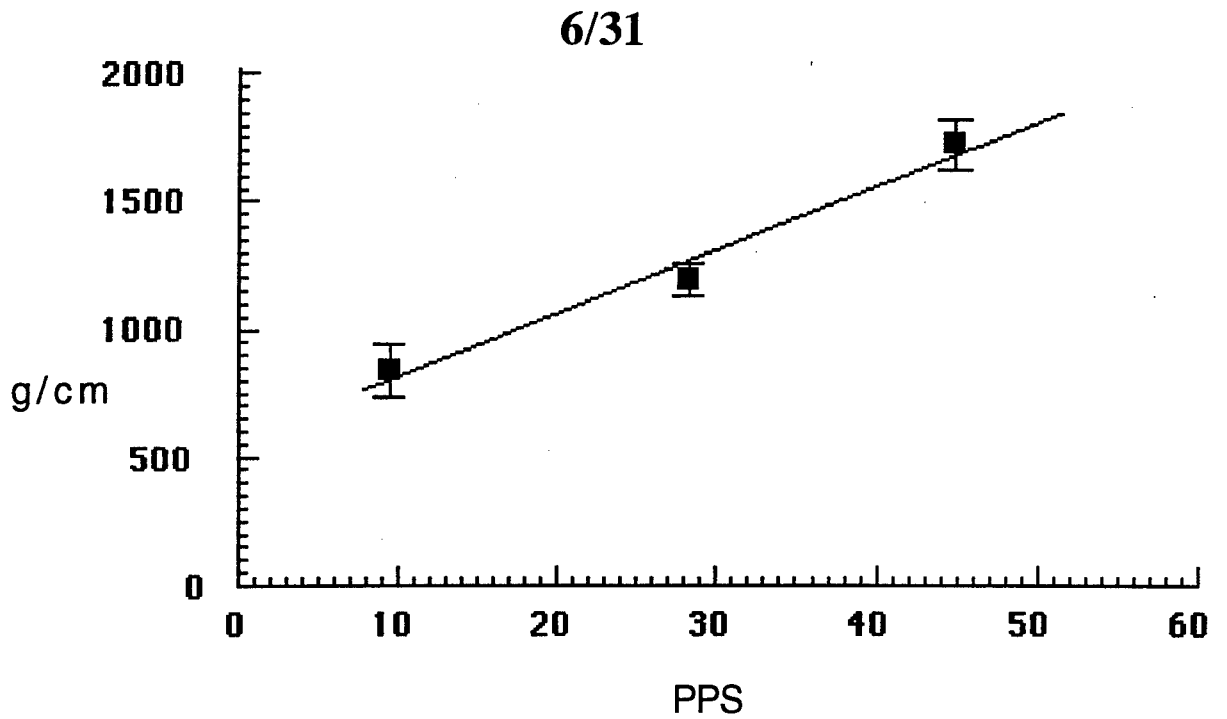


Fig. 9

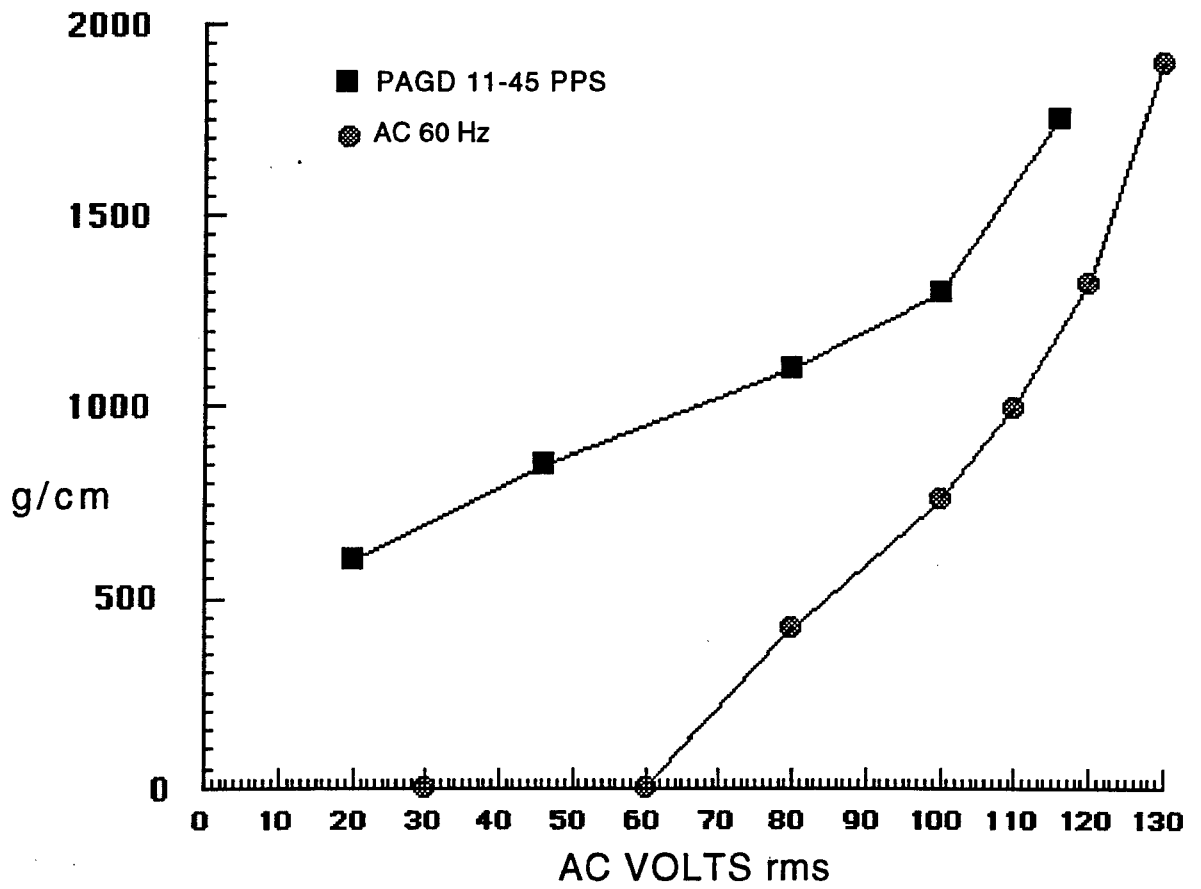


Fig. 10

SUBSTITUTE SHEET

7/31

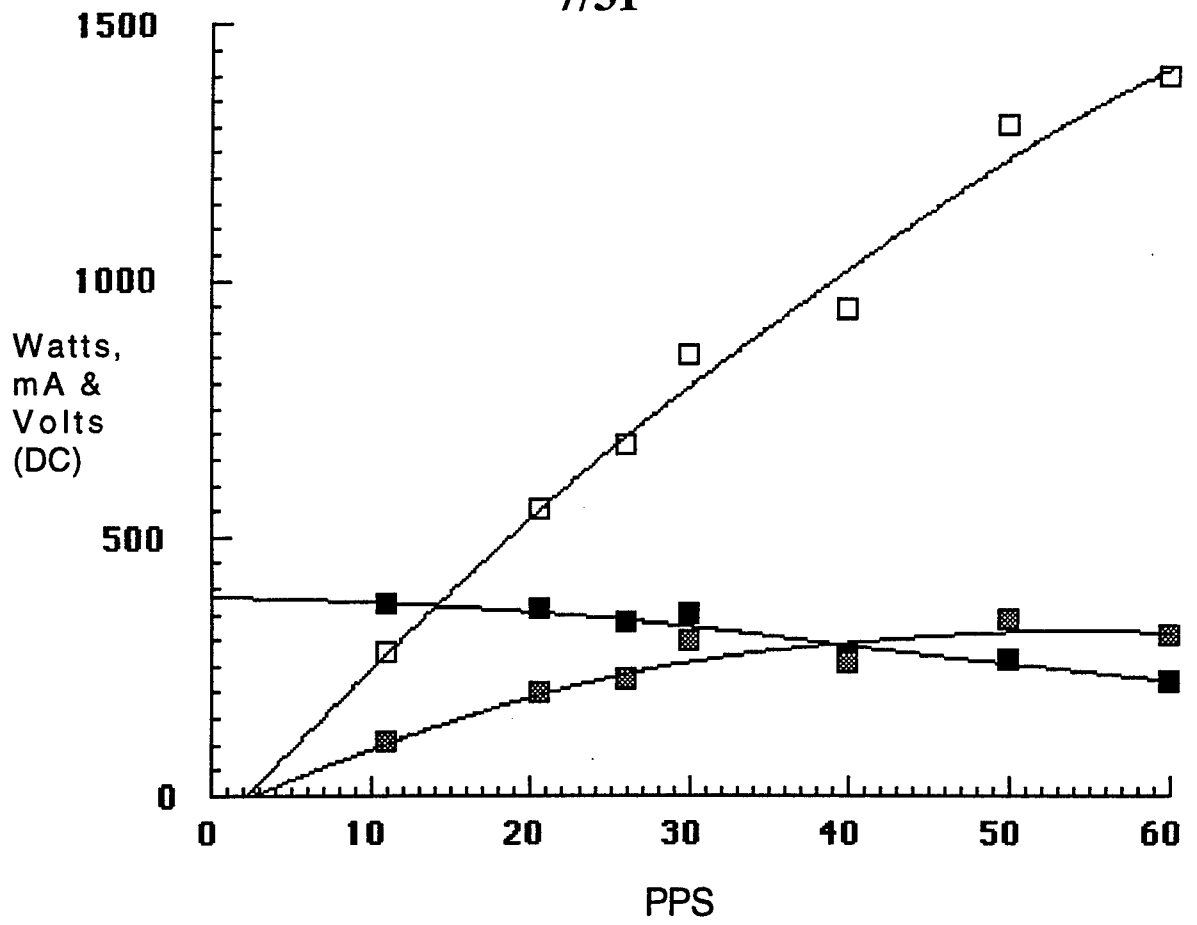


Fig. 11

SUBSTITUTE SHEET

8/31

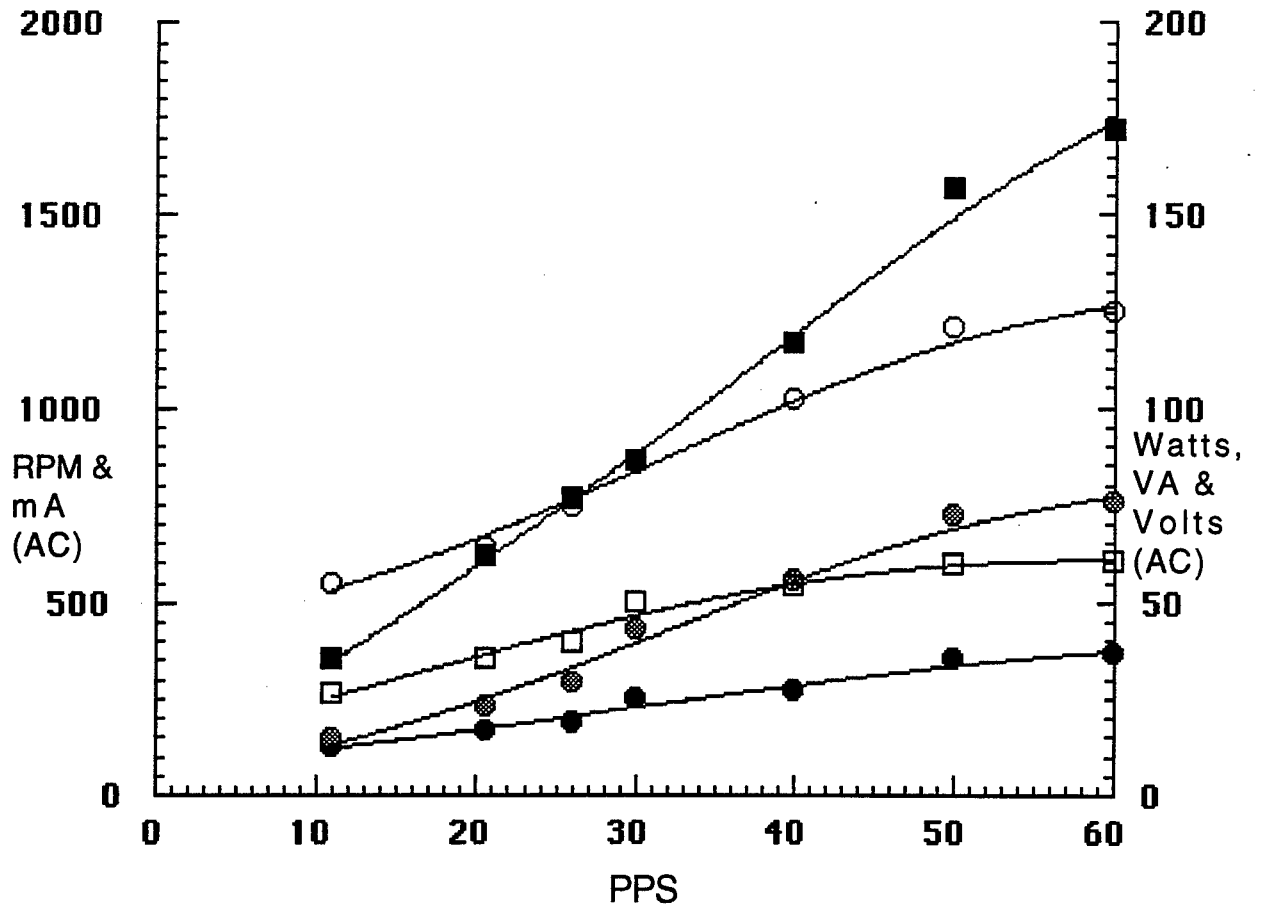


Fig. 12

SUBSTITUTE SHEET

9/31

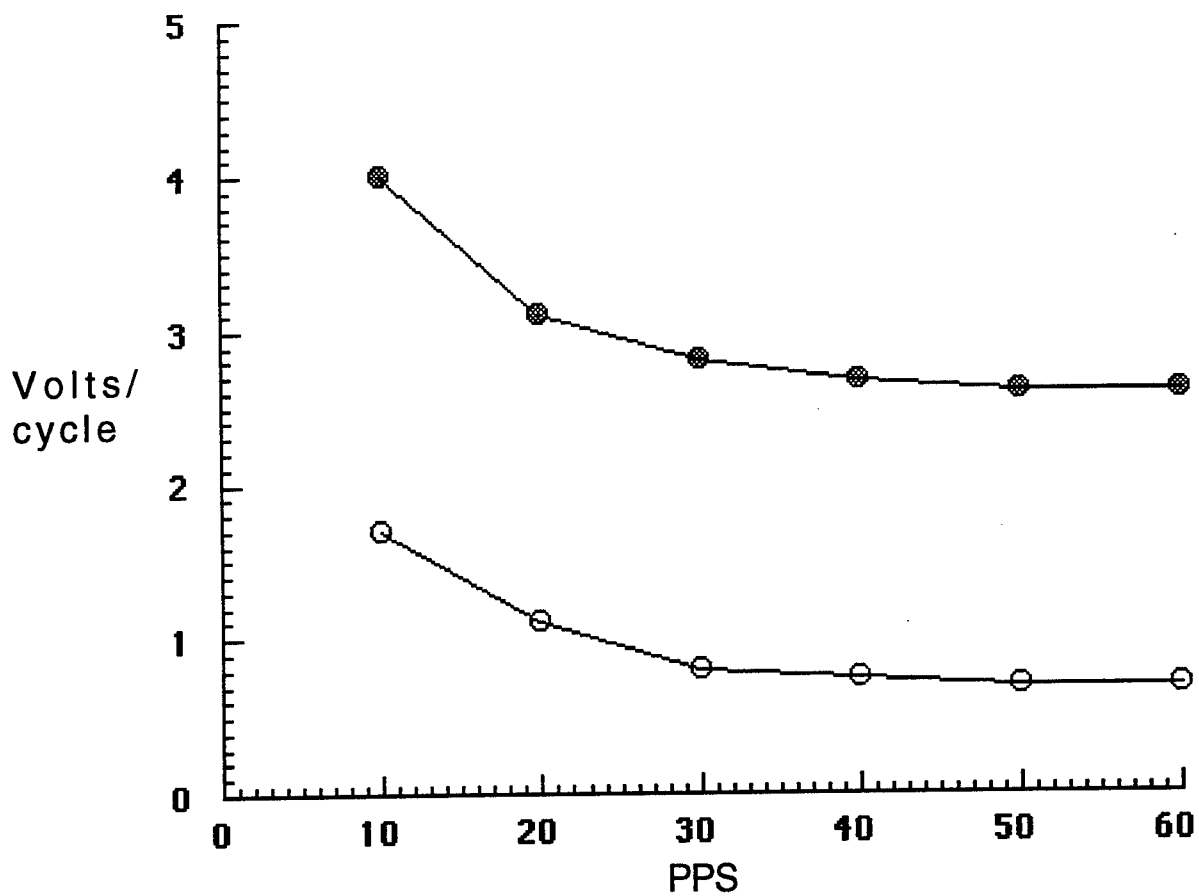


Fig. 13

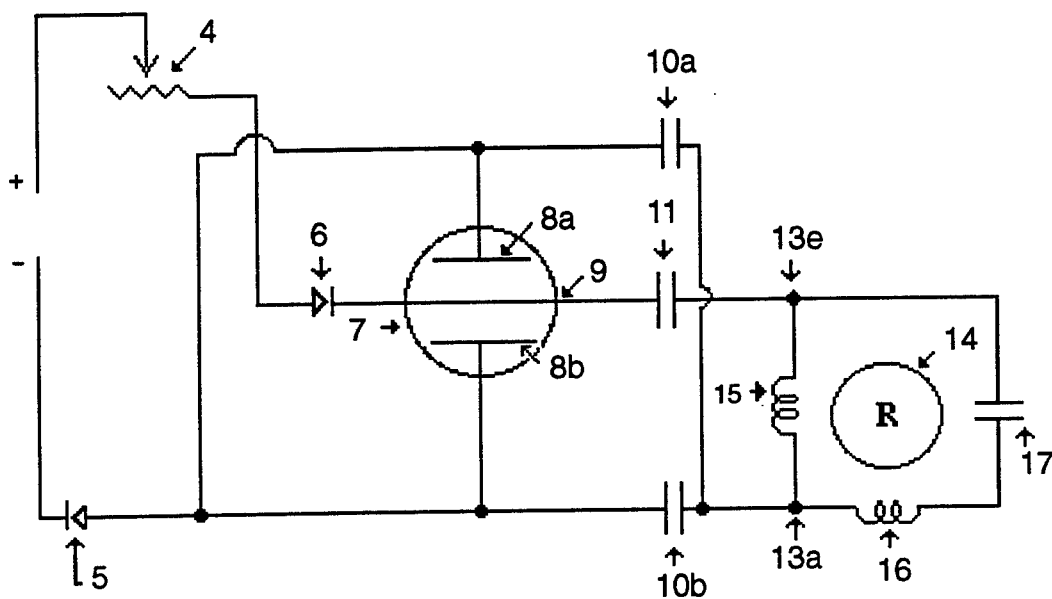


Fig. 14

SUBSTITUTE SHEET

10/31

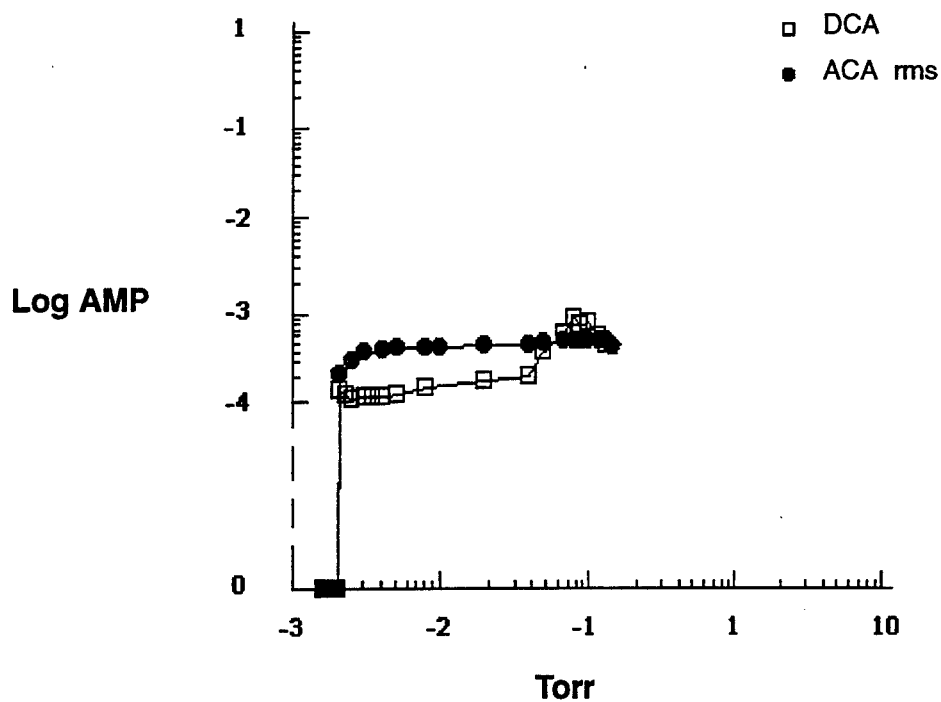


Fig. 15

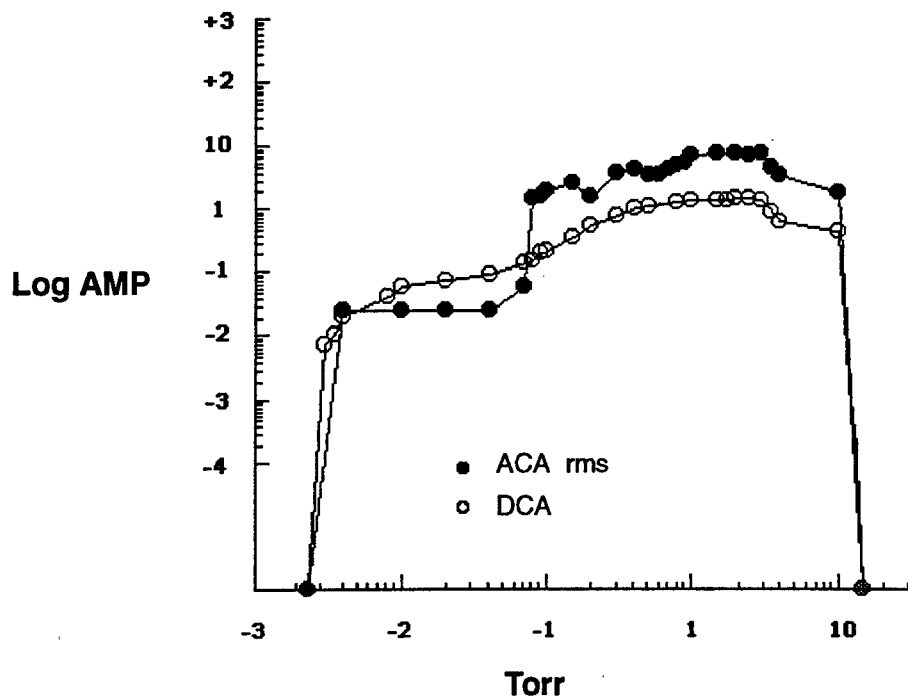


Fig. 16

SUBSTITUTE SHEET

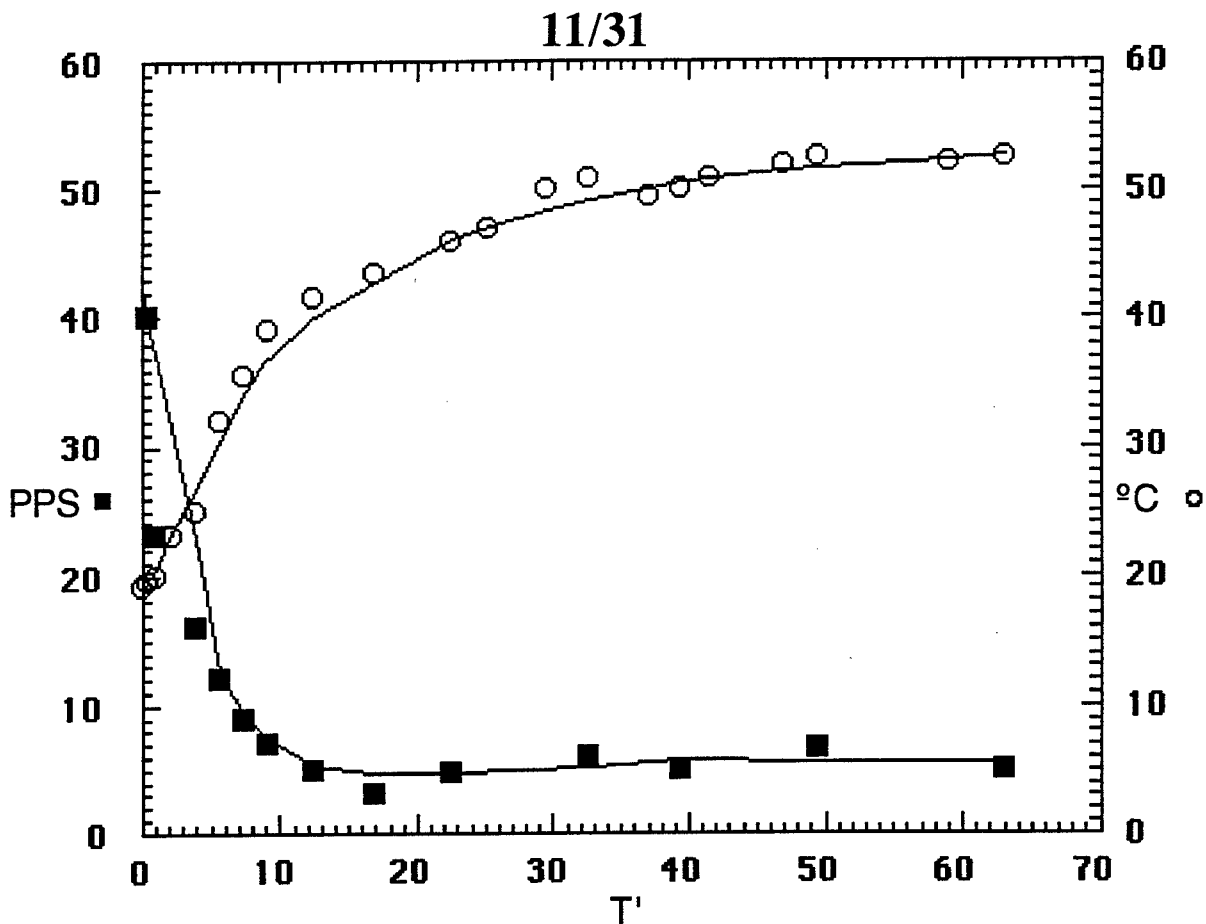


Fig. 17

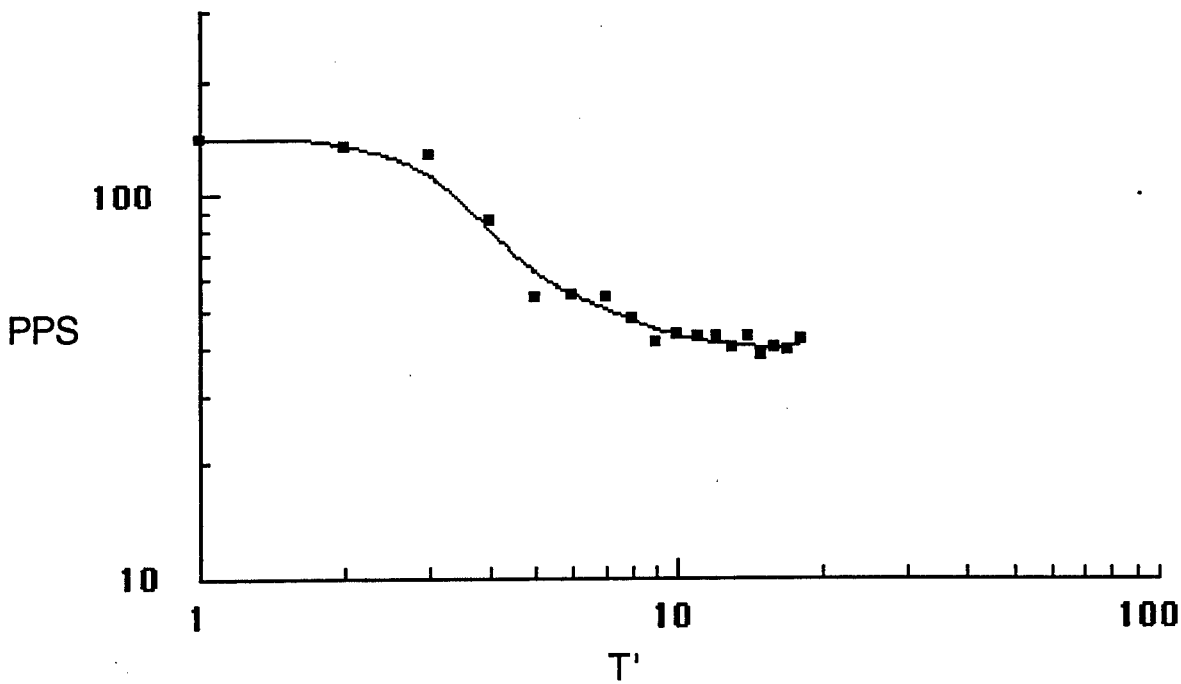


Fig. 18

12/31

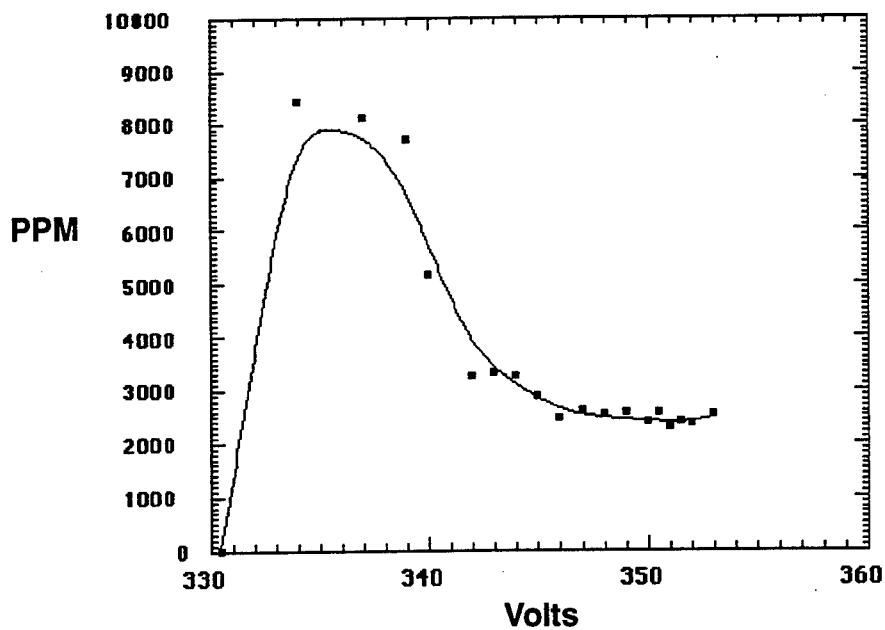


Fig. 19

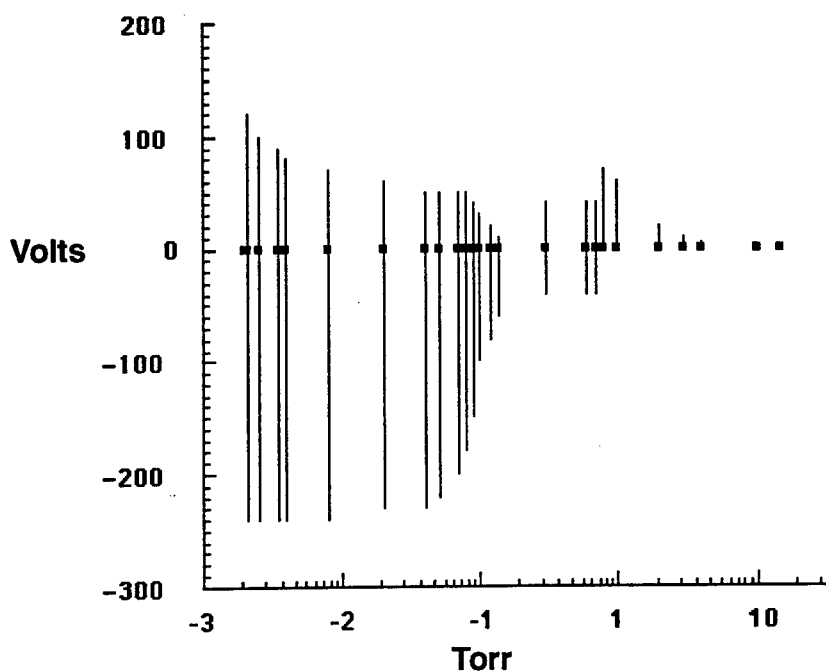


Fig. 20

SUBSTITUTE SHEET

13/31

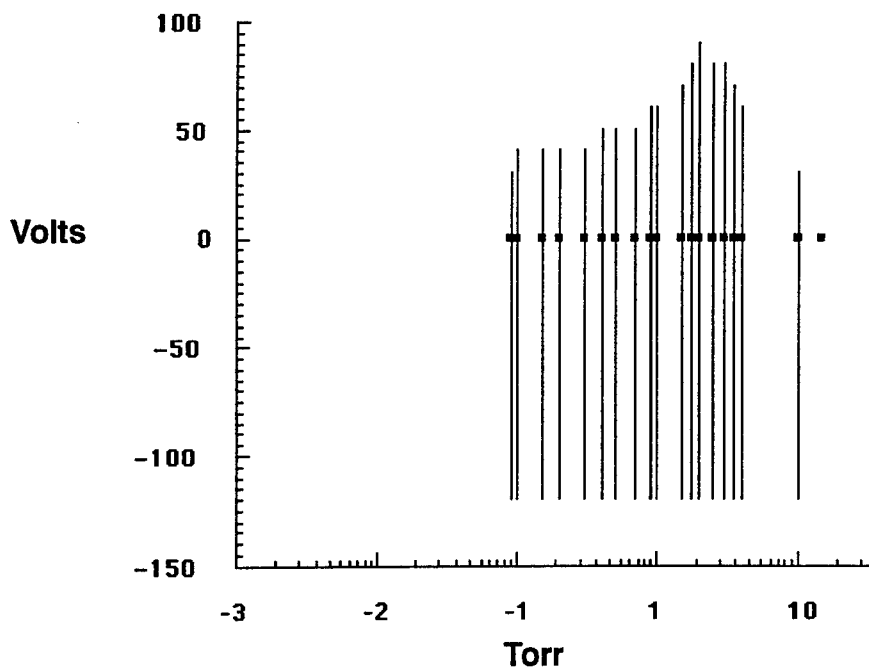


Fig. 21

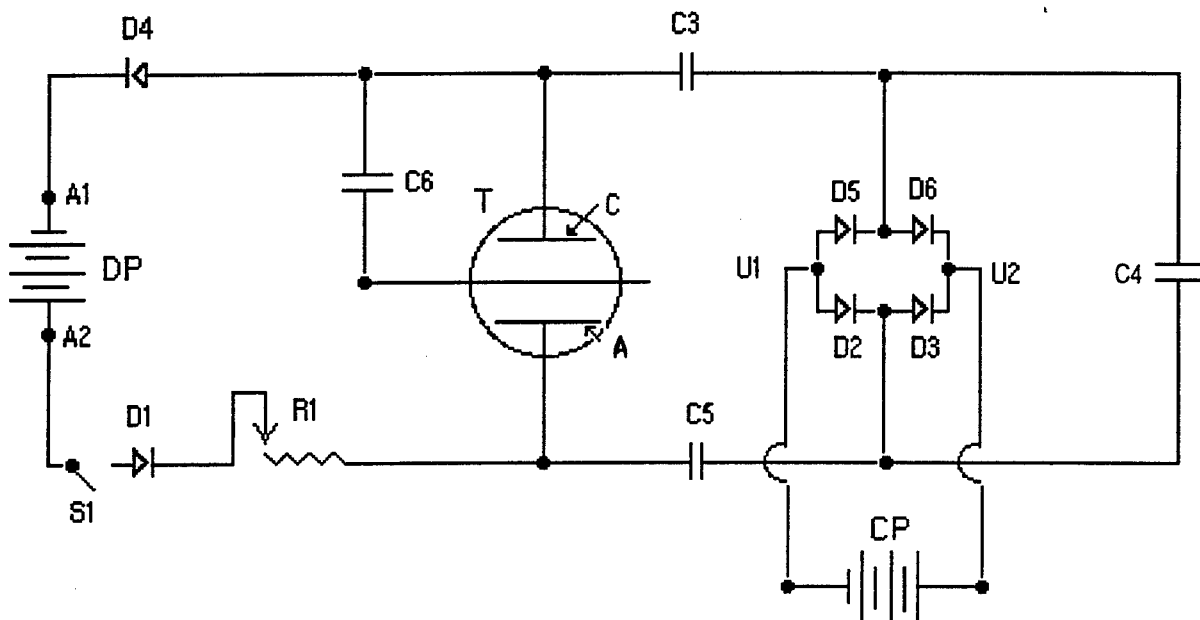


Fig. 22

SUBSTITUTE SHEET

14/31

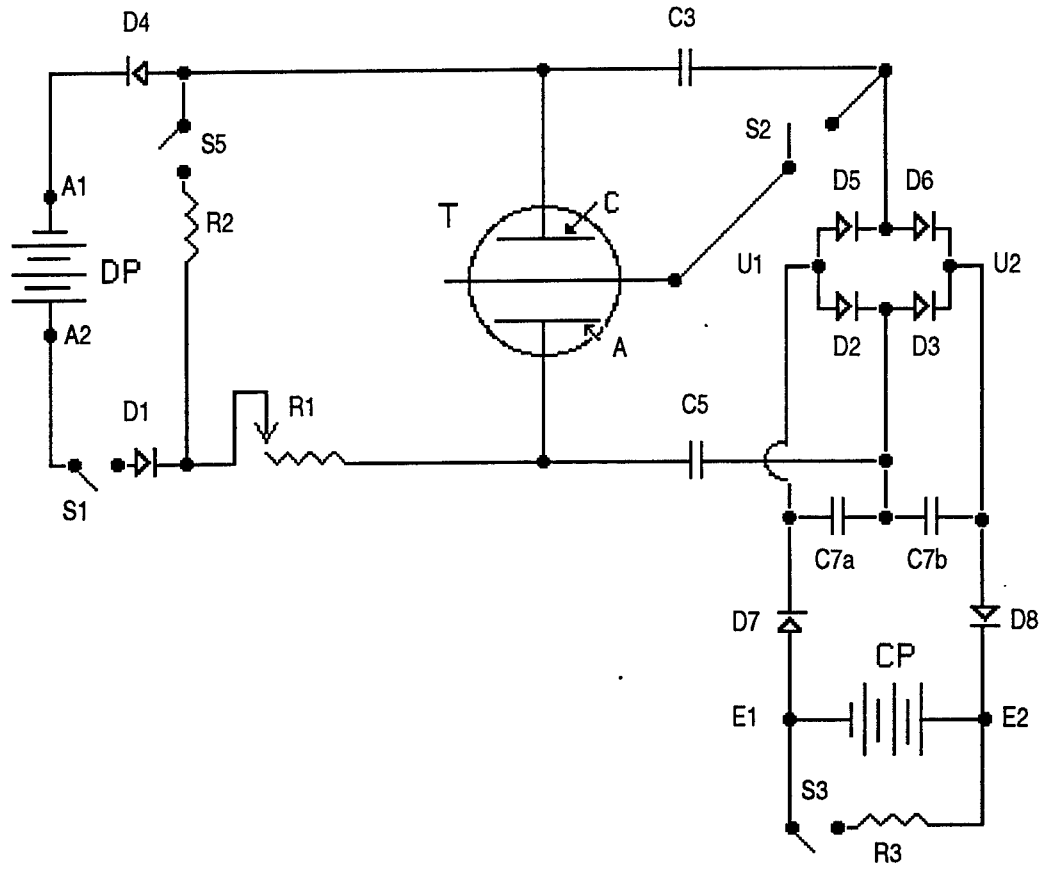


Fig. 23

SUBSTITUTE SHEET

15/31

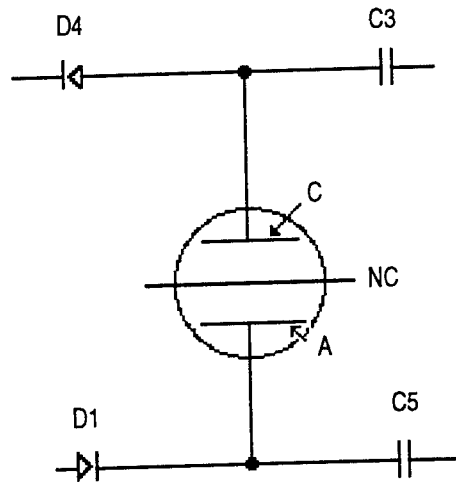


Fig. 24A

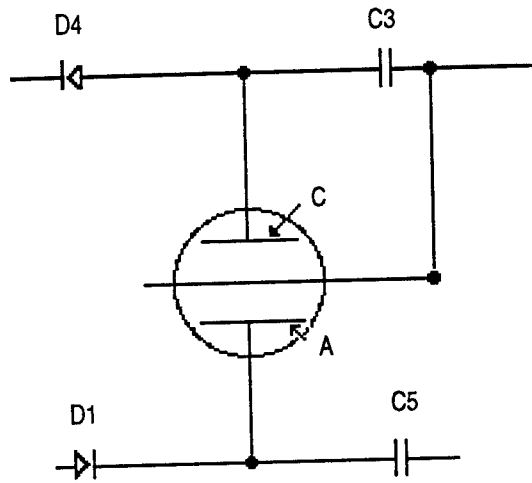


Fig. 24B

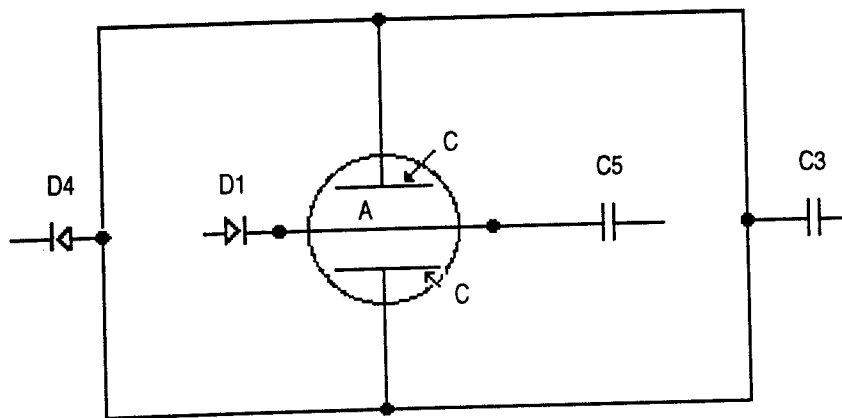


Fig. 24C

SUBSTITUTE SHEET

16/31

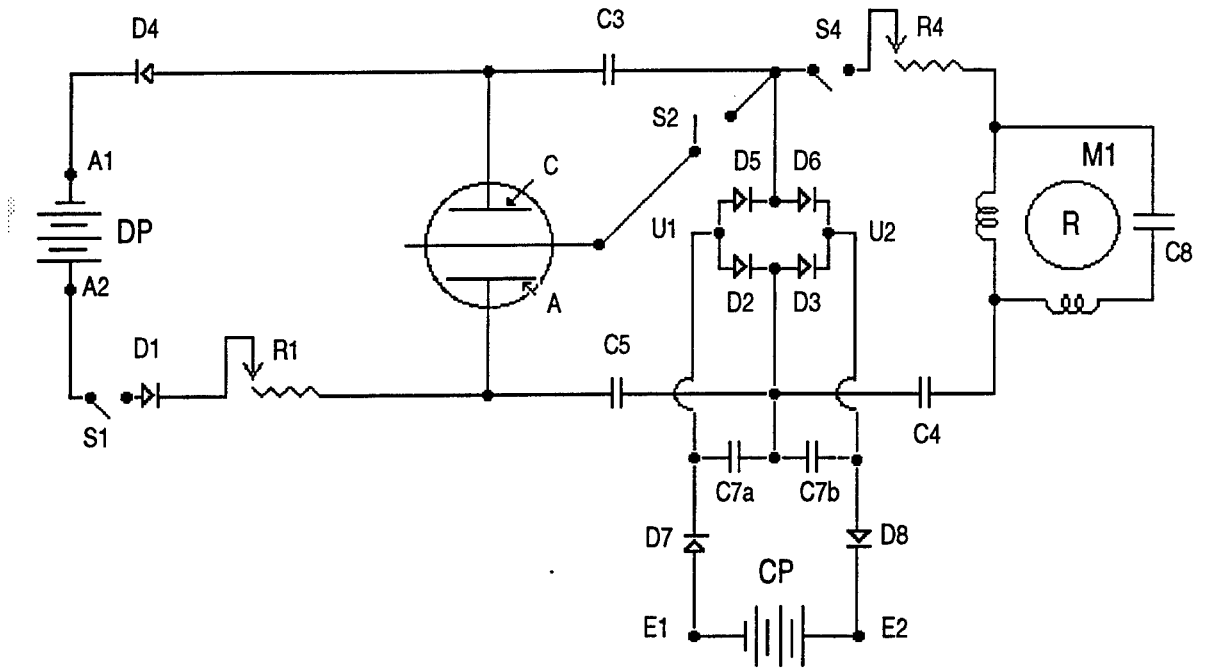


Fig. 25

SUBSTITUTE SHEET

17/31

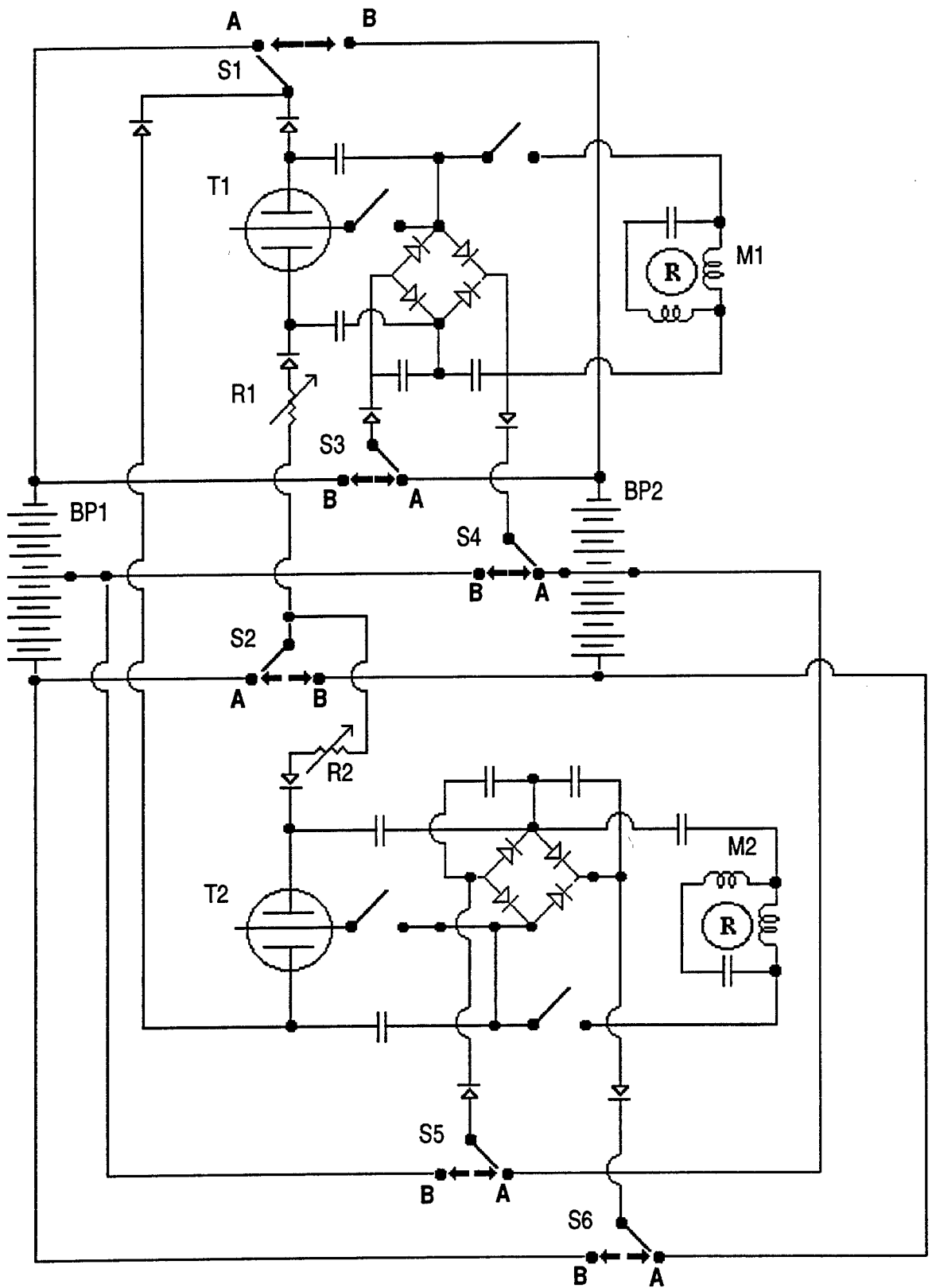


Fig. 26
SUBSTITUTE SHEET

18/31

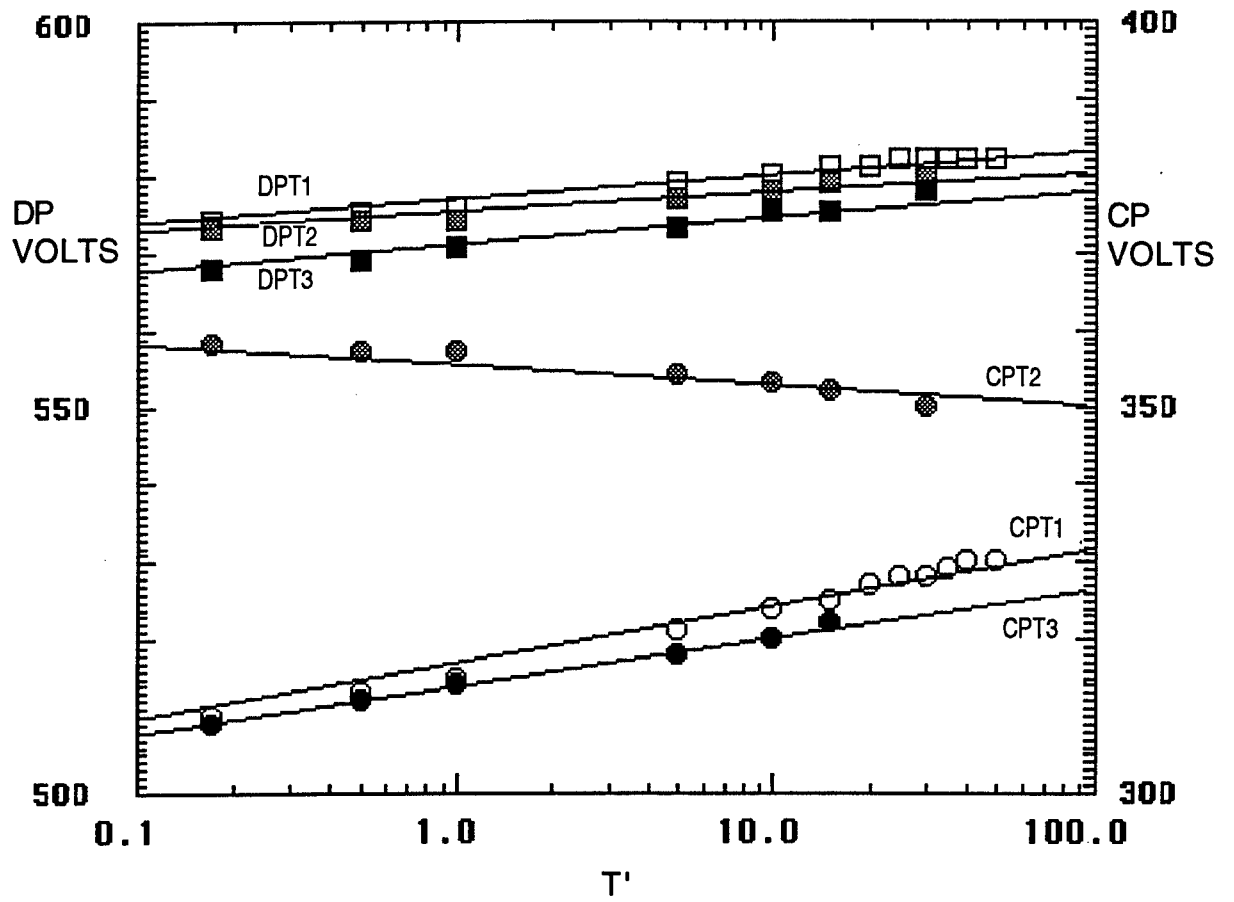


Fig. 27

SUBSTITUTE SHEET

19/31

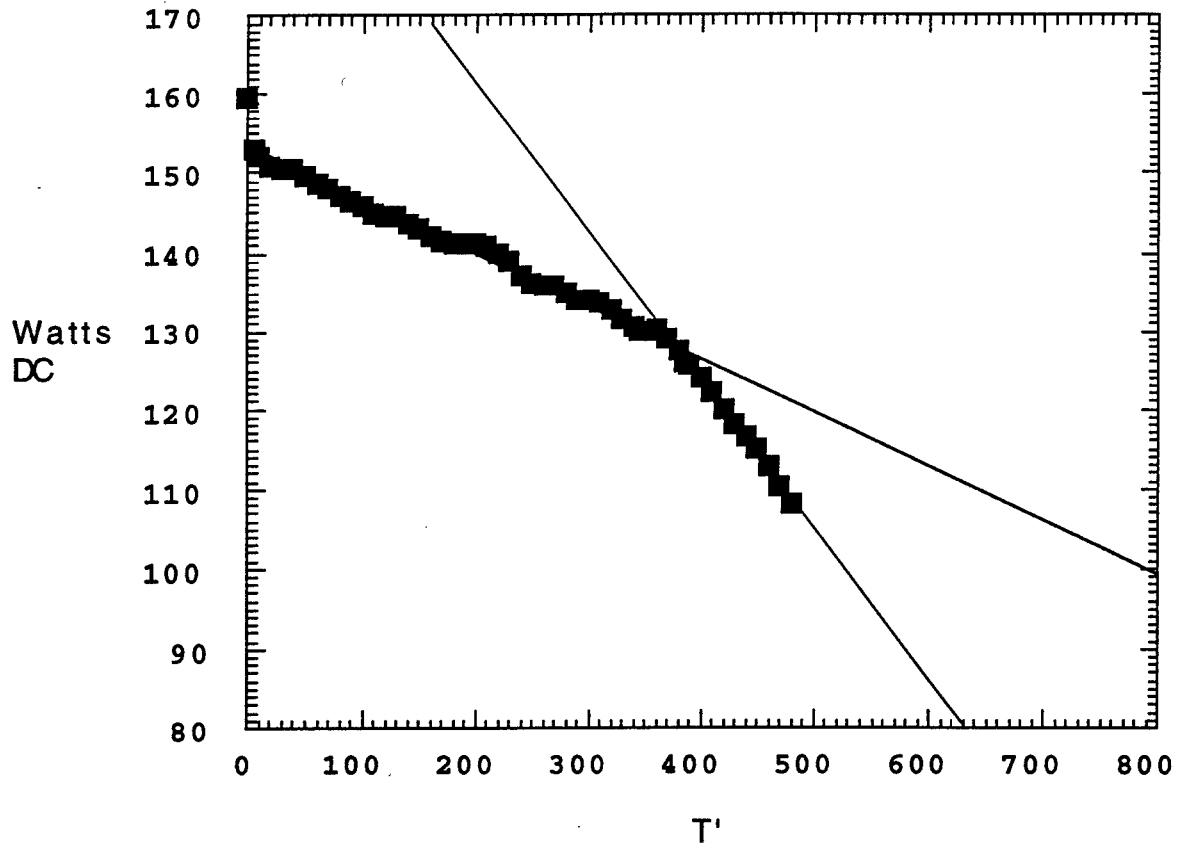


Fig. 28A

SUBSTITUTE SHEET

20/31

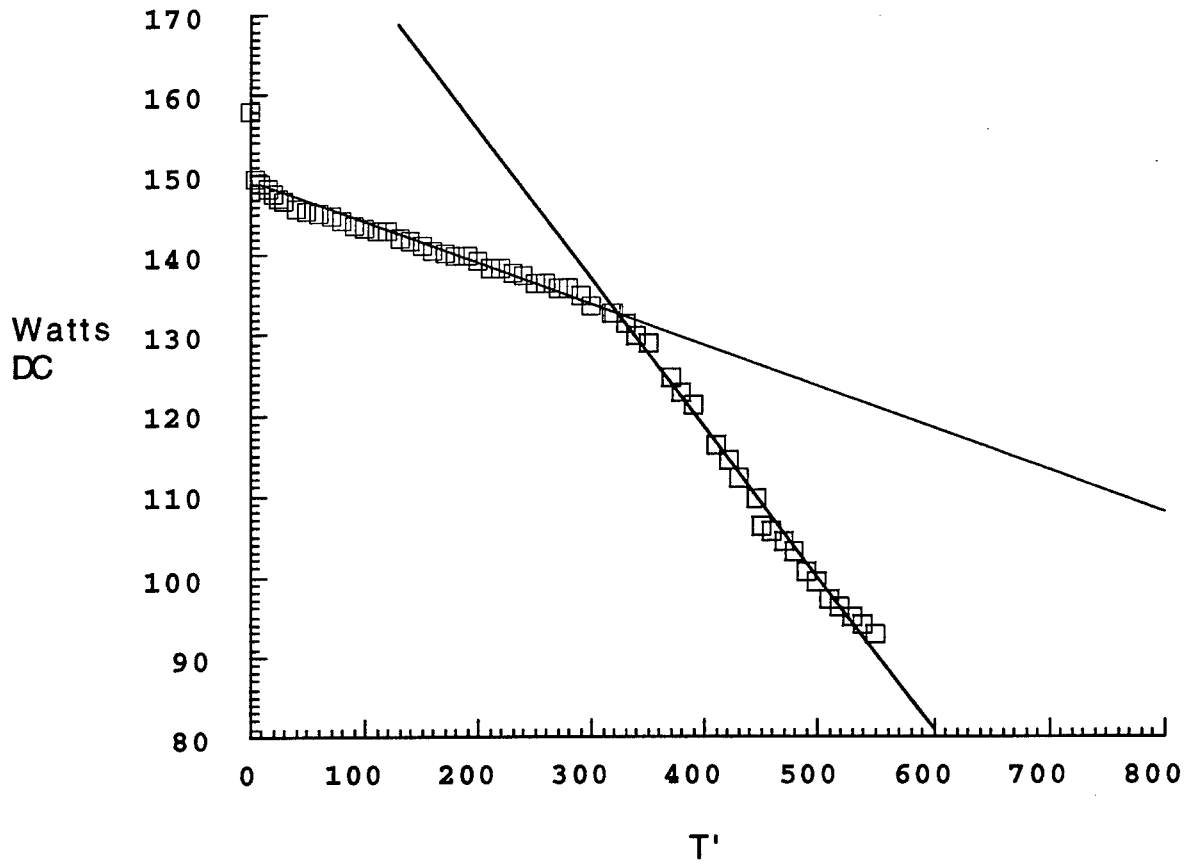


Fig. 28B

SUBSTITUTE SHEET

21/31

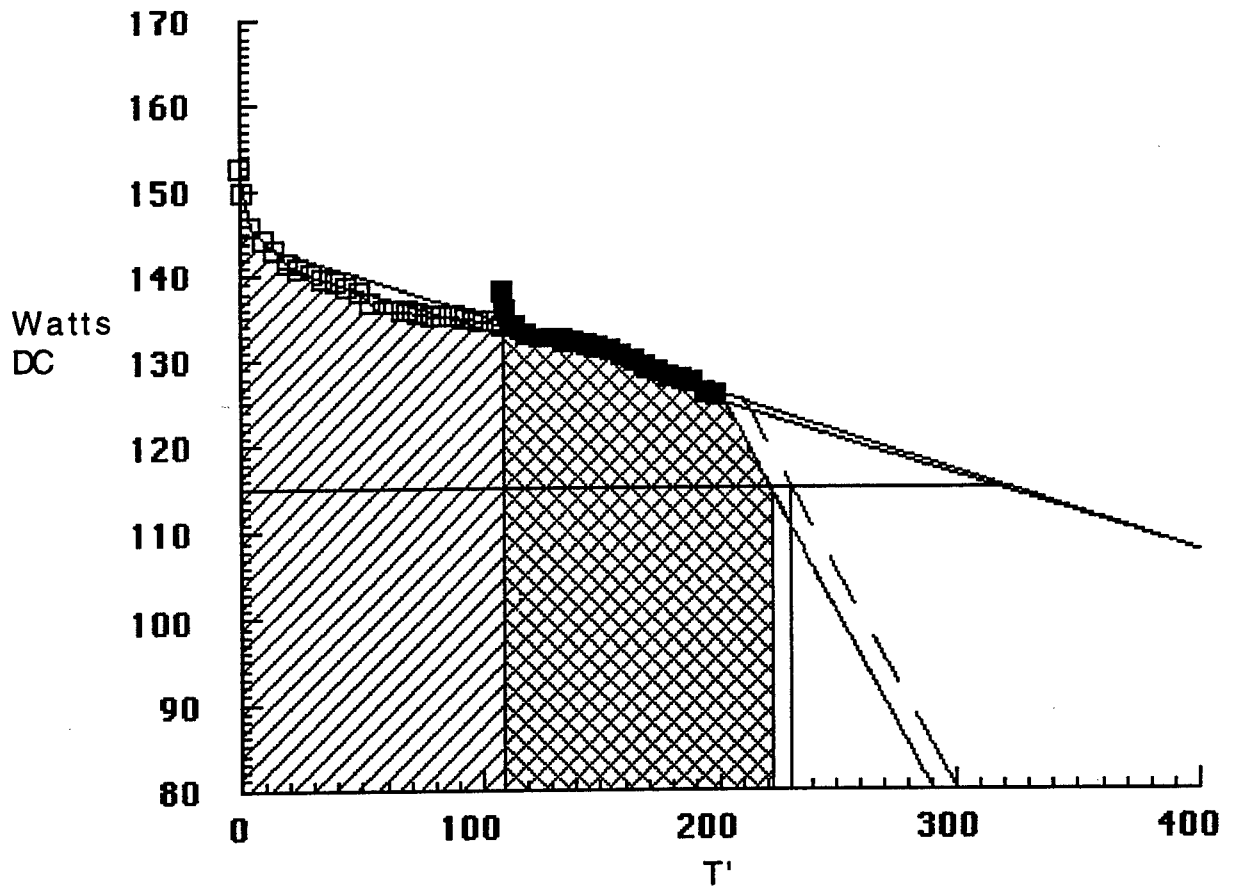


Fig. 29

SUBSTITUTE SHEET.

22/31

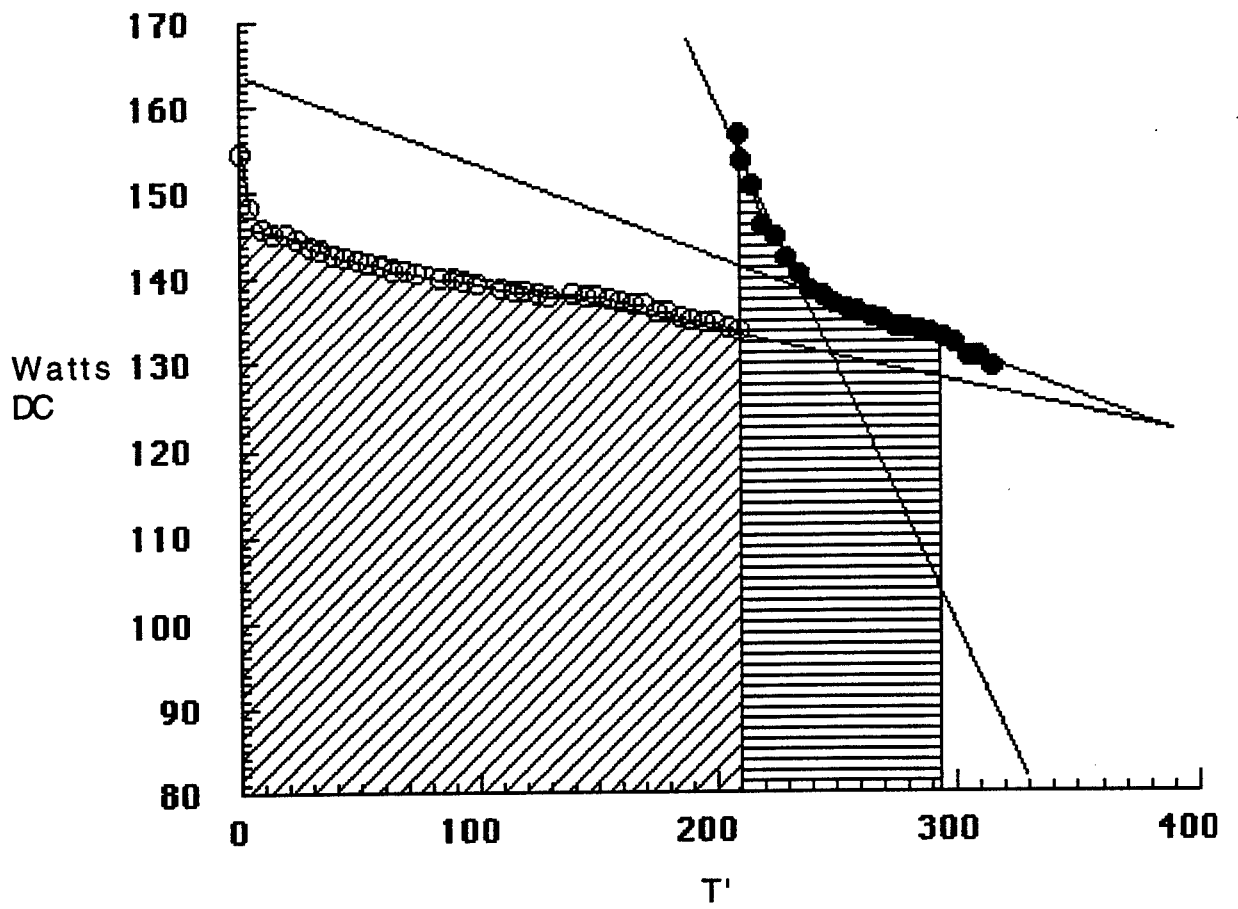


Fig. 30

SUBSTITUTE SHEET.

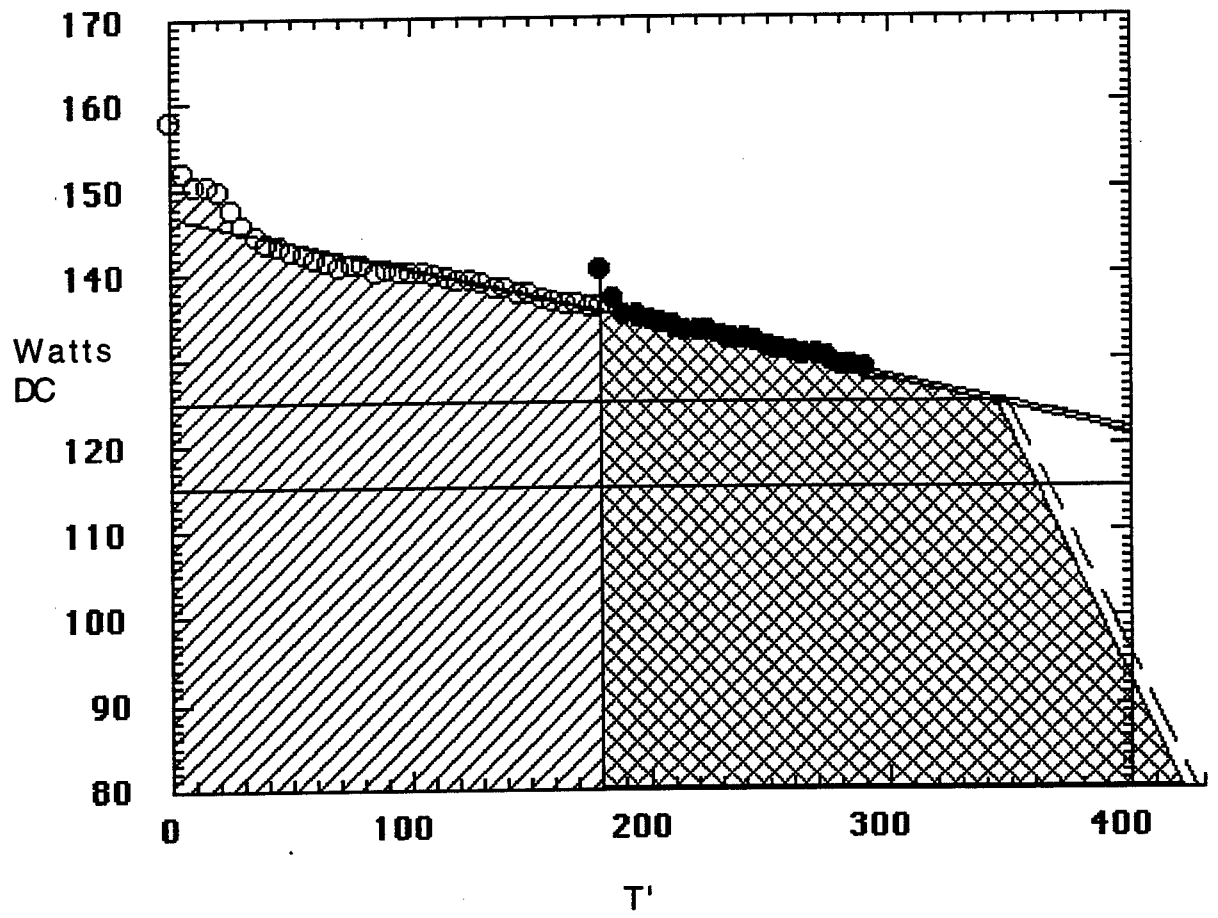


Fig. 31

SUBSTITUTE SHEET.

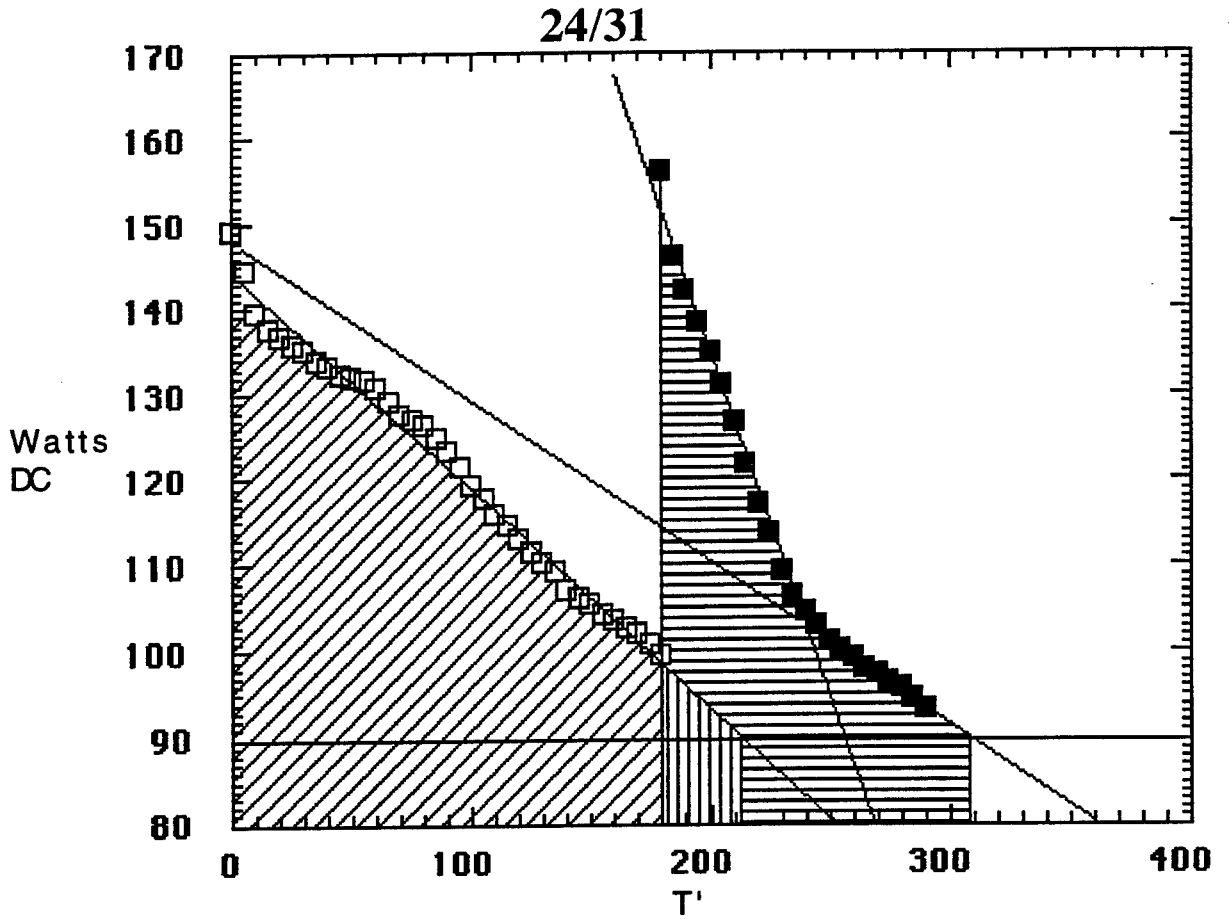


Fig. 32

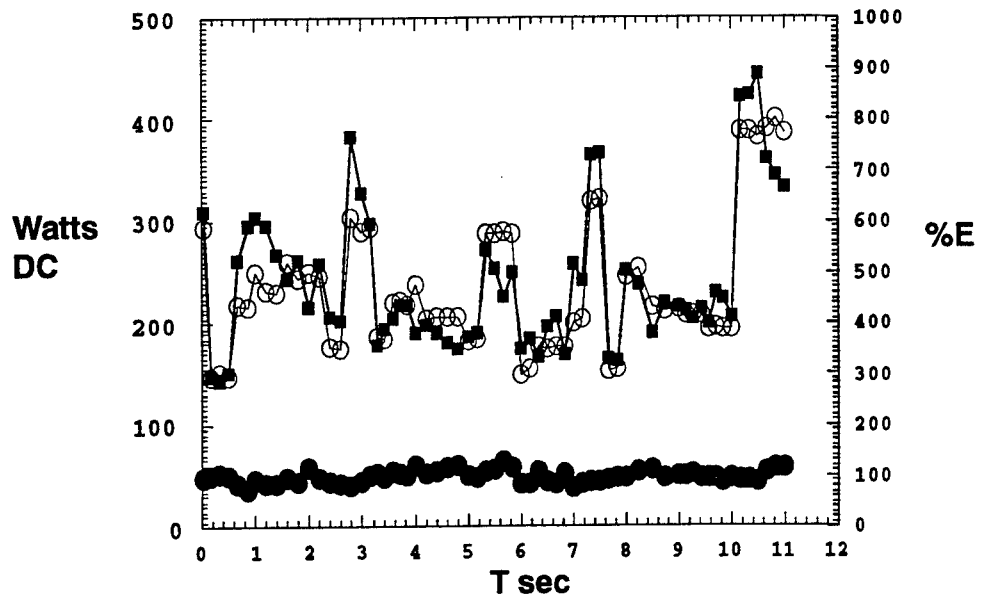


Fig. 33

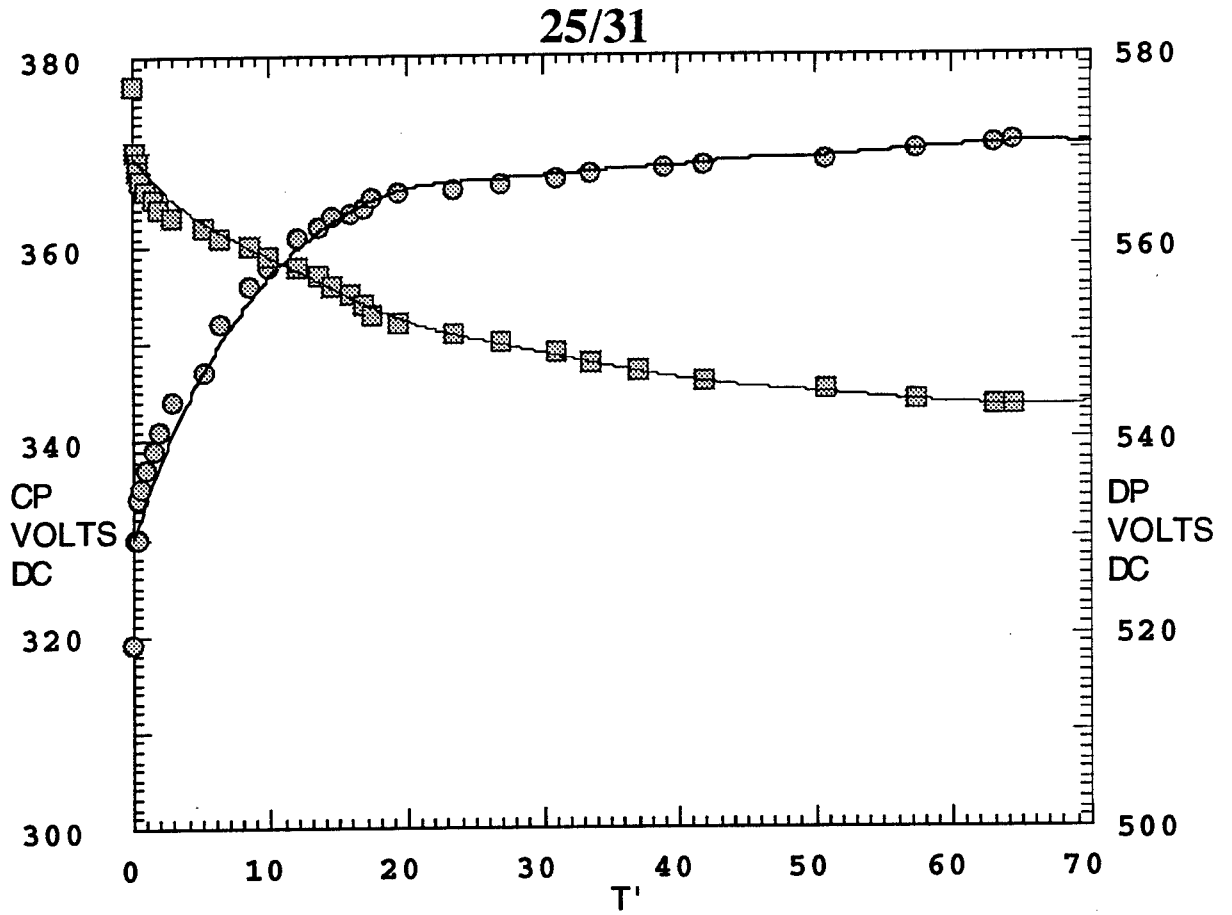


Fig. 34

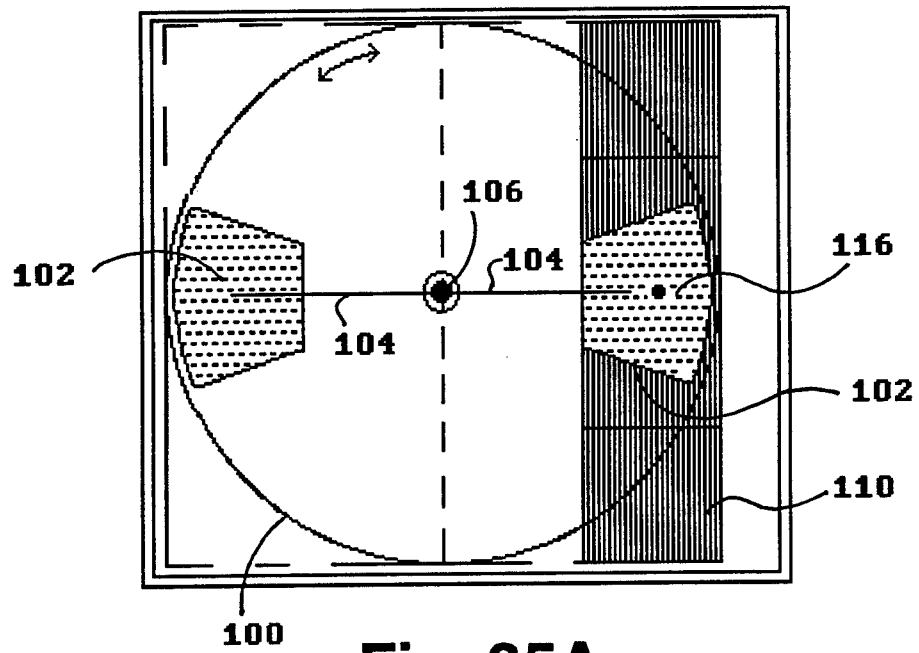


Fig. 35A
SUBSTITUTE SHEET

26/31

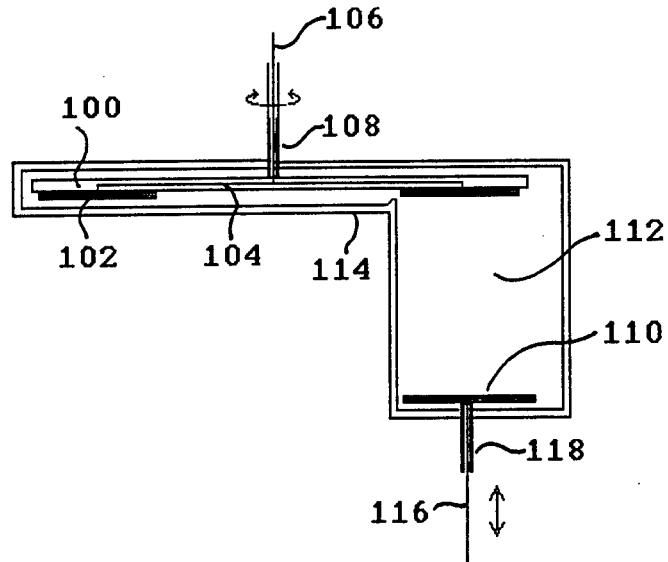


Fig. 35B

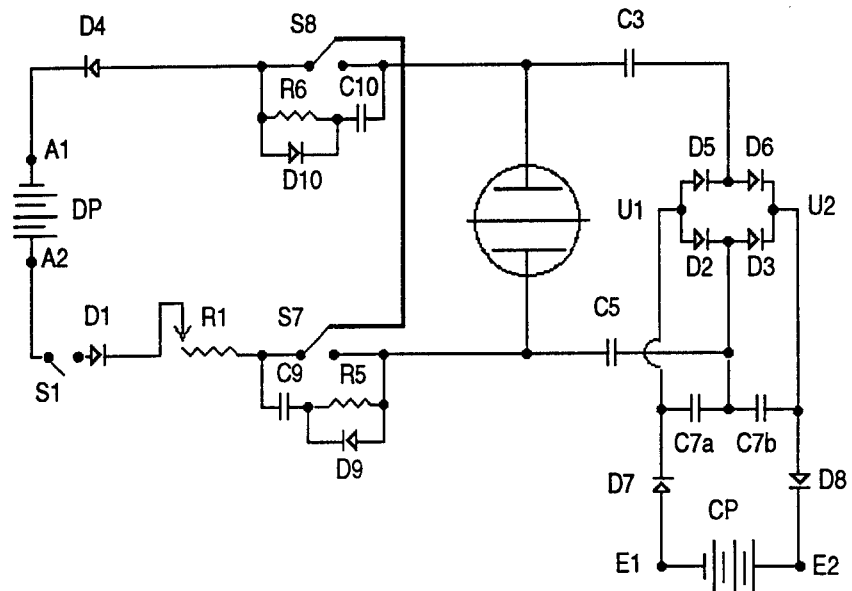


Fig. 36

27/31

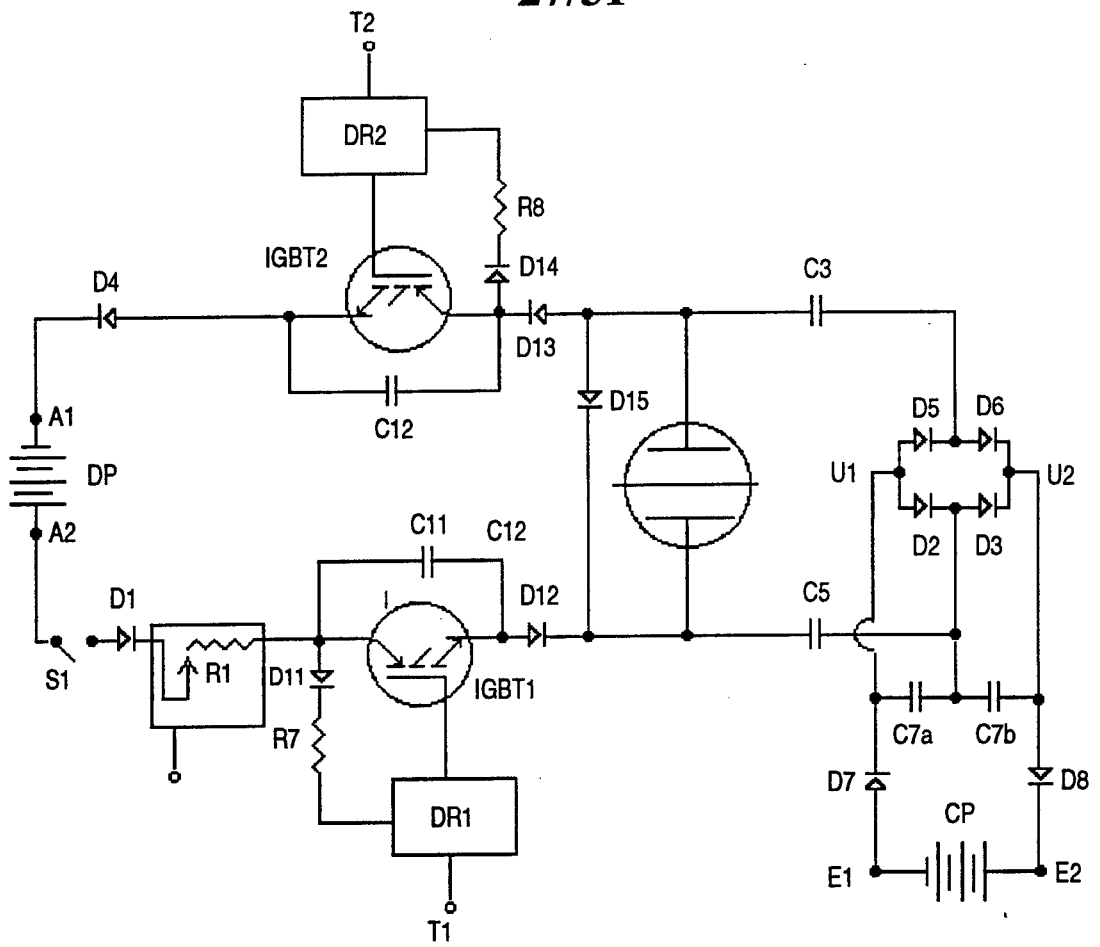


Fig. 37

SUBSTITUTE SHEET

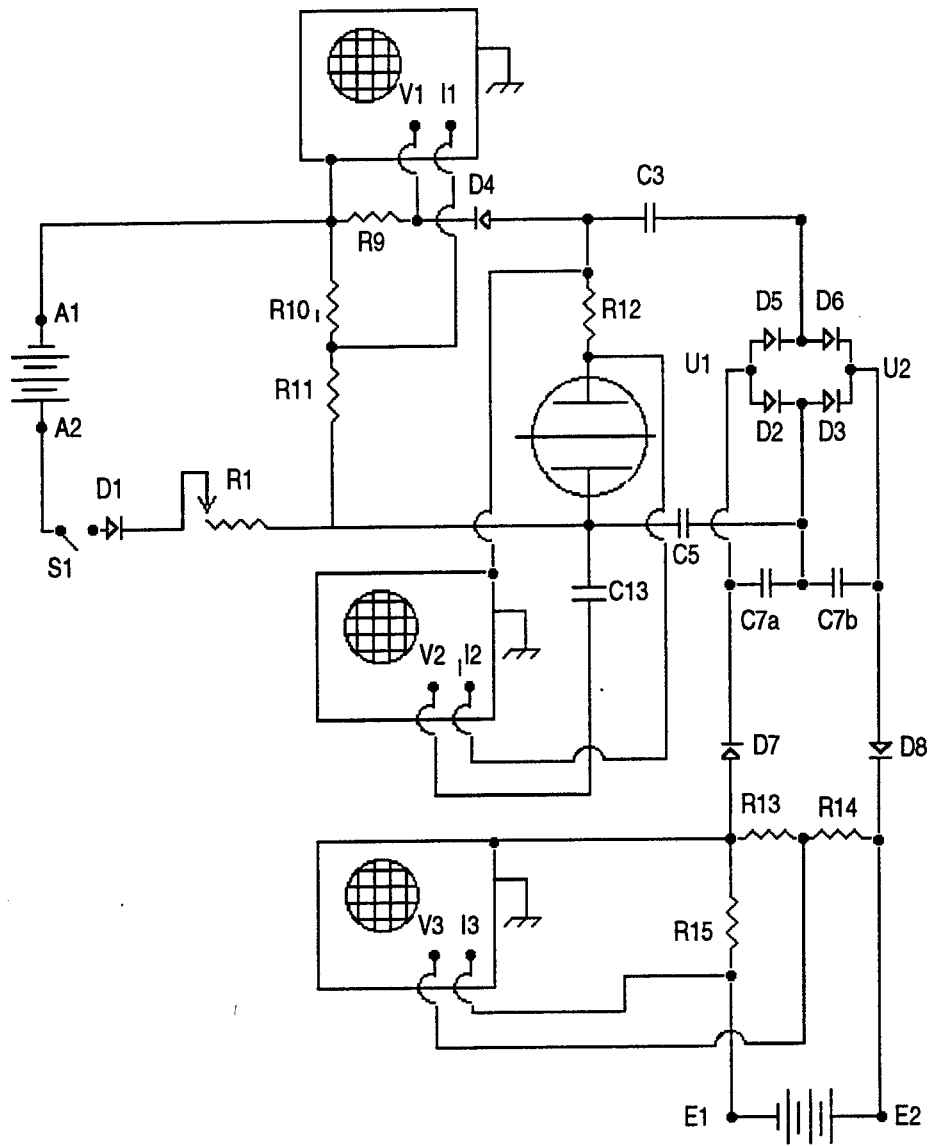


Fig. 38

SUBSTITUTE SHEET

29/31

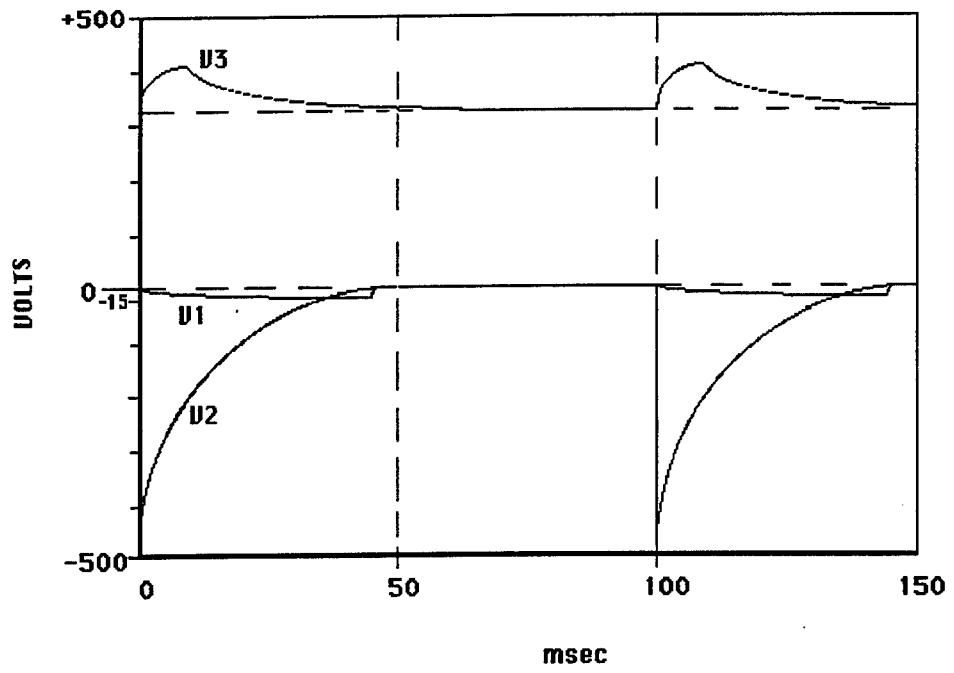


Fig. 39

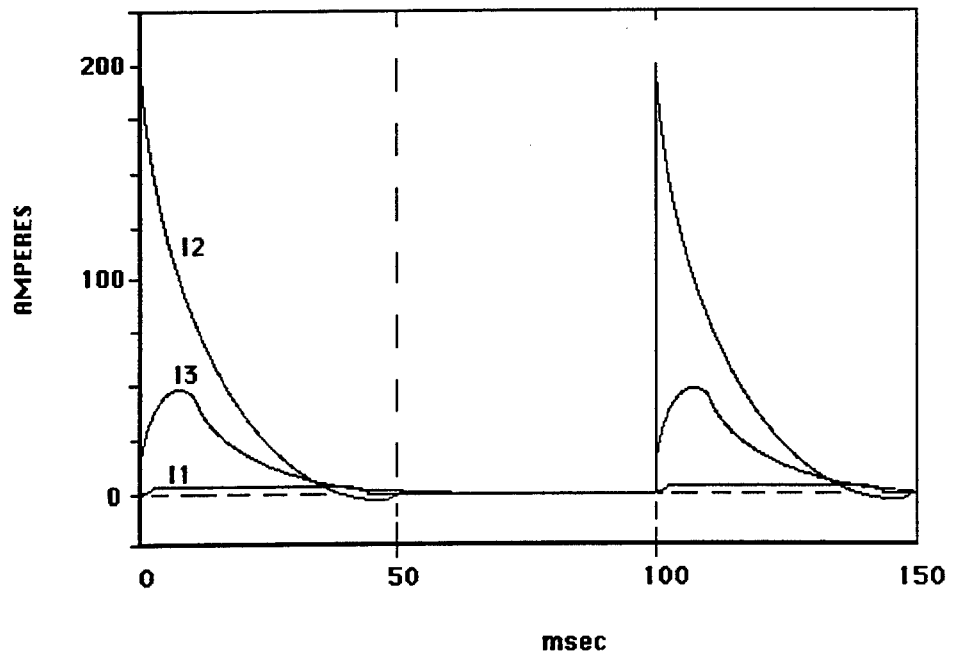


Fig. 40

SUBSTITUTE SHEET

30/31

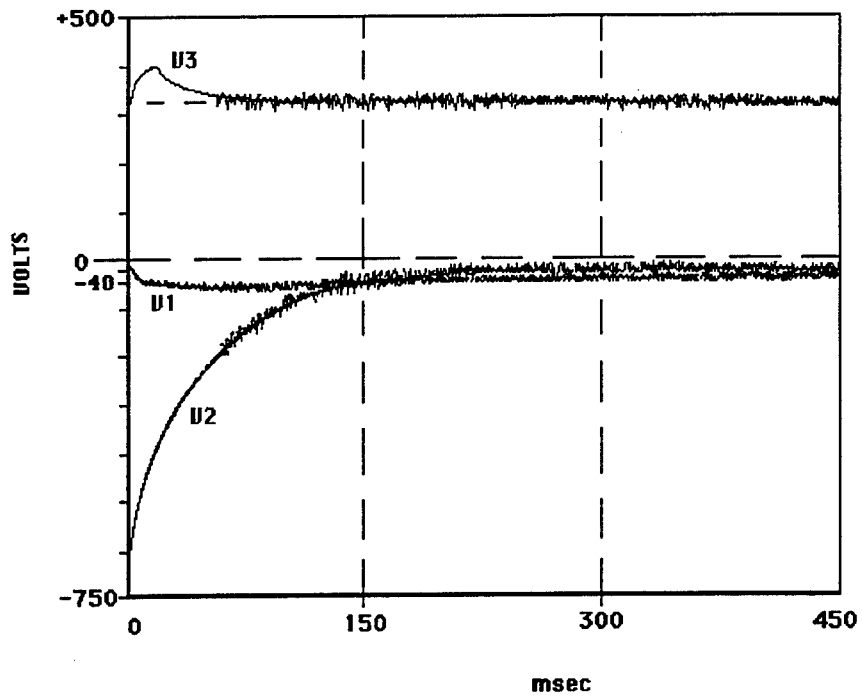


Fig. 41

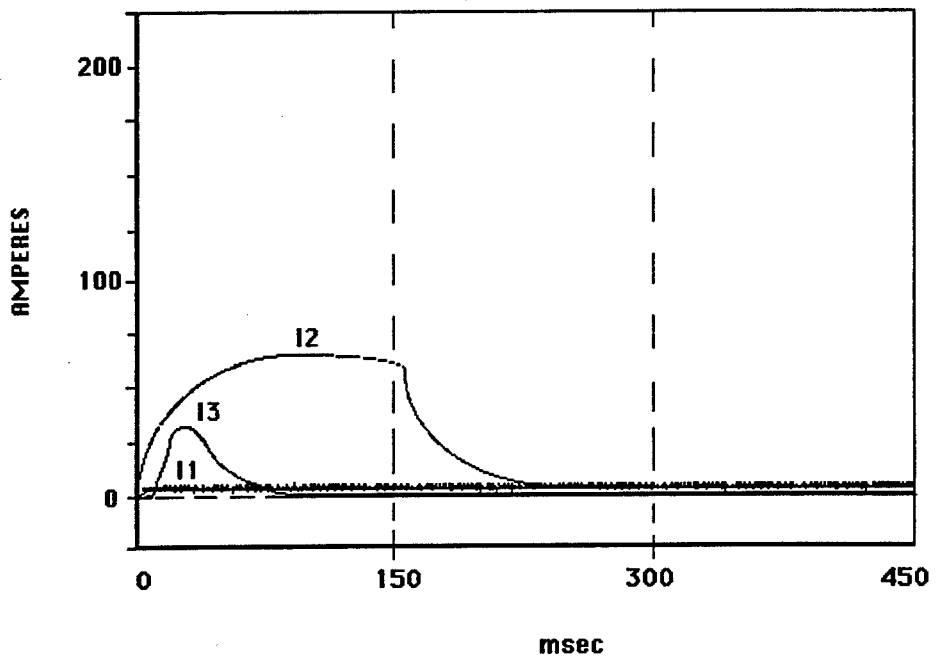


Fig. 42

SUBSTITUTE SHEET

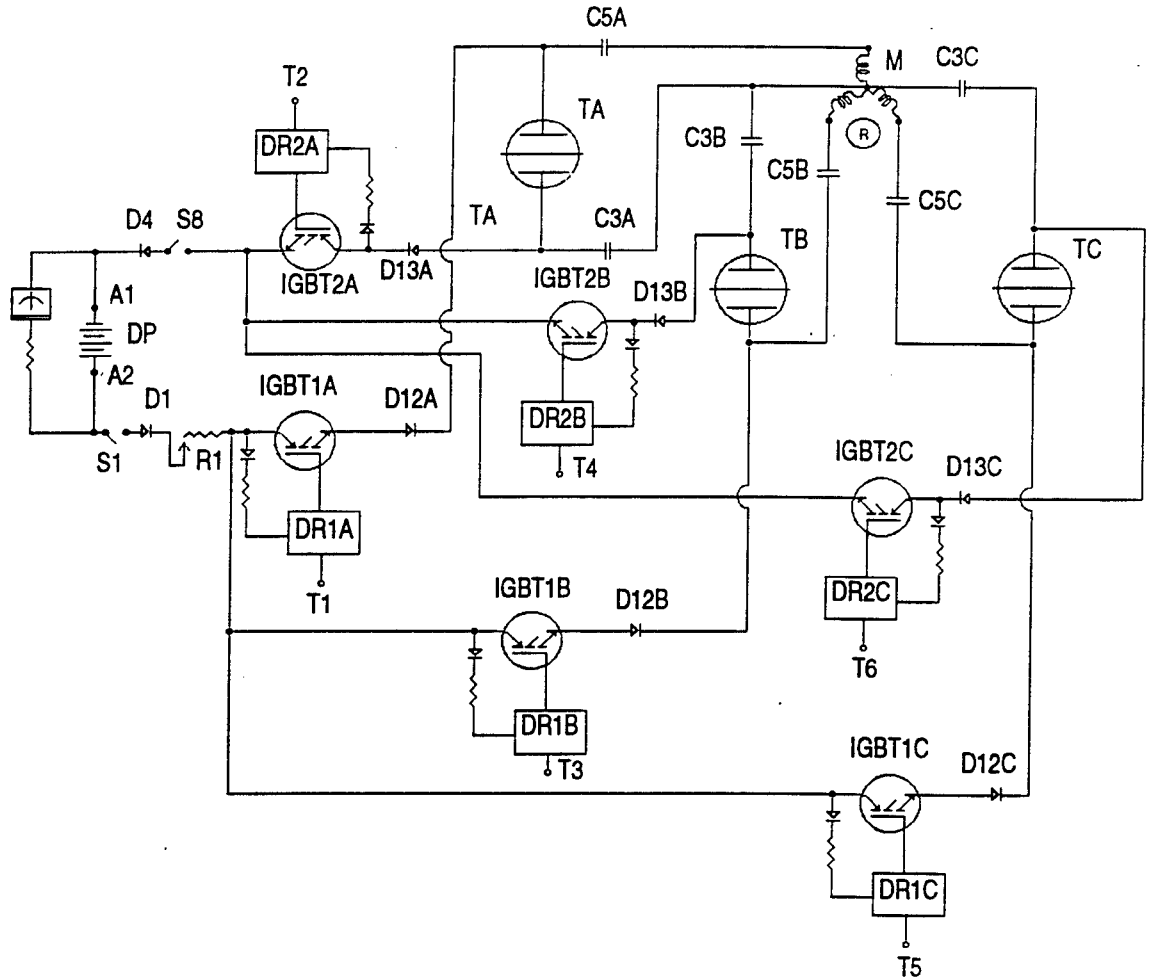


Fig. 43

SUBSTITUTE SHEET

INTERNATIONAL SEARCH REPORT

International Application No

PCT/CA 93/00430

I. CLASSIFICATION OF SUBJECT MATTER (if several classification symbols apply, indicate all) ⁶				
According to International Patent Classification (IPC) or to both National Classification and IPC				
IPC ⁵ : H 02 M 7/48, H 03 K 3/04, H 02 P 7/26				
II. FIELDS SEARCHED				
Minimum Documentation Searched ⁷				
Classification System	Classification Symbols			
IPC ⁵	B 05 B, H 01 J, H 03 M, H 02 P, H 03 B, H 03 K			
Documentation Searched other than Minimum Documentation to the Extent that such Documents are Included in the Fields Searched ⁸				
III. DOCUMENTS CONSIDERED TO BE RELEVANT ⁹				
Category ⁹	Citation of Document, ¹¹ with indication, where appropriate, of the relevant passages ¹²	Relevant to Claim No. ¹³		
A	DE, C2, 2 843 733 (THOMSON-CSF) 15 April 1982 (15.04.82), column 3, line 51 - column 4, line 34; fig. 2; claims 1,2. --	1, 6, 22		
A	SOVIET INVENTIONS ILLUSTRATED, EI sections, week C47, issued 07 January 1981 DERWENT PUBLICATIONS LTD, London, SU-725-194 --	1, 5, 6, 22		
A	US, A, 4 194 239 (JAYARAM et al.) 18 March 1980 (18.03.90), column 1, lines 25-43; fig. 1; claim 1. --	1		
A	US, A, 4 131 826 (HARRIS) 26 December 1978	1, 5		
<table style="width: 100%; border: none;"> <tr> <td style="width: 50%; border: none; vertical-align: top;"> <ul style="list-style-type: none"> * Special categories of cited documents: ¹⁴ "A" document defining the general state of the art which is not considered to be of particular relevance "E" earlier document but published on or after the International filing date "L" document which may throw doubts on priority claim(s) or which is cited to establish the publication date of another citation or other special reason (as specified) "O" document referring to an oral disclosure, use, exhibition or other means "P" document published prior to the International filing date but later than the priority date claimed </td> <td style="width: 50%; border: none; vertical-align: top;"> <ul style="list-style-type: none"> "T" later document published after the International filing date or priority date and not in conflict with the application but cited to understand the principle or theory underlying the invention "X" document of particular relevance; the claimed invention cannot be considered novel or cannot be considered to involve an inventive step "Y" document of particular relevance; the claimed invention cannot be considered to involve an inventive step when the document is combined with one or more other such documents, such combination being obvious to a person skilled in the art. "Z" document member of the same patent family </td> </tr> </table>			<ul style="list-style-type: none"> * Special categories of cited documents: ¹⁴ "A" document defining the general state of the art which is not considered to be of particular relevance "E" earlier document but published on or after the International filing date "L" document which may throw doubts on priority claim(s) or which is cited to establish the publication date of another citation or other special reason (as specified) "O" document referring to an oral disclosure, use, exhibition or other means "P" document published prior to the International filing date but later than the priority date claimed 	<ul style="list-style-type: none"> "T" later document published after the International filing date or priority date and not in conflict with the application but cited to understand the principle or theory underlying the invention "X" document of particular relevance; the claimed invention cannot be considered novel or cannot be considered to involve an inventive step "Y" document of particular relevance; the claimed invention cannot be considered to involve an inventive step when the document is combined with one or more other such documents, such combination being obvious to a person skilled in the art. "Z" document member of the same patent family
<ul style="list-style-type: none"> * Special categories of cited documents: ¹⁴ "A" document defining the general state of the art which is not considered to be of particular relevance "E" earlier document but published on or after the International filing date "L" document which may throw doubts on priority claim(s) or which is cited to establish the publication date of another citation or other special reason (as specified) "O" document referring to an oral disclosure, use, exhibition or other means "P" document published prior to the International filing date but later than the priority date claimed 	<ul style="list-style-type: none"> "T" later document published after the International filing date or priority date and not in conflict with the application but cited to understand the principle or theory underlying the invention "X" document of particular relevance; the claimed invention cannot be considered novel or cannot be considered to involve an inventive step "Y" document of particular relevance; the claimed invention cannot be considered to involve an inventive step when the document is combined with one or more other such documents, such combination being obvious to a person skilled in the art. "Z" document member of the same patent family 			
IV. CERTIFICATION				
Date of the Actual Completion of the International Search	Date of Mailing of this International Search Report			
14 January 1994	28.01.94			
International Searching Authority	Signature of Authorized Officer			
EUROPEAN PATENT OFFICE	MEHLMAUER e.h.			

III. DOCUMENTS CONSIDERED TO BE RELEVANT (CONTINUED FROM THE SECOND SHEET)		
Category *	Citation of Document, ** with indication, where appropriate, of the relevant passages	Relevant to Claim No.
A	(26.12.78), column 2, lines 1-14; claims 1,3,5. -- US, A, 3 471 316 (ERNESTO H. MANUEL) 07 October 1969 (07.10.69), column 2, lines 25-49; claim 1. -----	22

ANHANG

zum internationalen Recherchenbericht über die internationale Patentanmeldung Nr.

ANNEX

to the International Search Report to the International Patent Application No.

ANNEXE

au rapport de recherche international relatif à la demande de brevet international n°

PCT/CA 93/00430 SAE 80226

In diesem Anhang sind die Mitglieder der Patentfamilien der im obengenannten internationalen Recherchenbericht angeführten Patentdokumente angegeben. Diese Angaben dienen nur zur Unterrichtung und erfolgen ohne Gewähr.

This Annex lists the patent family members relating to the patent documents cited in the above-mentioned international search report. The Office is in no way liable for these particulars which are given merely for the purpose of information.

La présente annexe indique les membres de la famille de brevets relatifs aux documents de brevets cités dans le rapport de recherche international visé ci-dessus. Les renseignements fournis sont donnés à titre indicatif et n'engagent pas la responsabilité de l'Office.

Im Recherchenbericht angeführtes Patentdokument Patent document cited in search report Document de brevet cité dans le rapport de recherche	Datum der Veröffentlichung Publication date Date de publication	Mitglied(er) der Patentfamilie Patent family member(s) Membre(s) de la famille de brevets	Datum der Veröffentlichung Publication date Date de publication
DE C2 2843733	15-04-82	DE A1 2843733 FR A1 2405554 FR B1 2405554 GB A1 2005940 GB B2 2005940	12-04-79 04-05-79 04-04-80 25-04-79 10-03-82
US A 4194239	18-03-80	keine - none - rien	
US A 4131826	26-12-78	keine - none - rien	
US A 3471316	07-10-69	keine - none - rien	